GULF GENERAL ATOMIC
P.O. BOX 608, SAN DIEGO, CALIFORNIA 92112

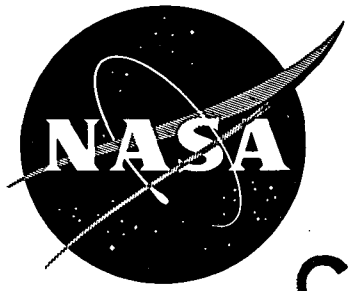

NASA-CR-120995

Gulf-GA-A12237

EXAMINATION OF UC-ZrC AFTER LONG TERM IRRADIATION AT THERMIONIC TEMPERATURE

Sponsored by
National Aeronautics and Space Administration
Lewis Research Center

Technical Management
NASA-Lewis Research Center
Nuclear Systems Division
J. R. Smith

Project: 0184
Contract: NAS 3-15323

Issued: December 21, 1972

NOTICE

This report was prepared as an account of Government sponsored work. Neither the United States, nor the National Aeronautics and Space Administration (NASA), nor any person acting on behalf of NASA:

A. Makes any warranty or representation, expressed or implied, with respect to the accuracy, completeness, or usefulness of the information contained in this report, or that the use of any information, apparatus, method, or process disclosed in this report may not infringe privately owned rights; or

B. Assumes any liabilities with respect to the use of, or for damages resulting from the use of any information, apparatus, method or process disclosed in this report.

As used above, "person acting on behalf of NASA" includes any employee or contractor of NASA, or employee of such contractor, to the extent that such employee or contractor of NASA, or employee of such contractor prepares, disseminates, or provides access to, any information pursuant to his employment or contract with NASA, or his employment with such contractor.

Requests for copies of this report should be referred to:

National Aeronautics and Space Administration
Office of Scientific and Technical Information
Attention: AFSS-A
Washington, D. C. 20546

1. Report No.	2. Government Accession No.	3. Recipient's Catalog No.
NASA CR-120995		

4. Title and Subtitle	5. Report Date
EXAMINATION OF UC-ZrC AFTER LONG TERM IRRADIATION AT THERMIONIC TEMPERATURE	December 21, 1972
	6. Performing Organization Code
7. Author(s)	8. Performing Organization Report No.
L. Yang and H. O. Johnson	Gulf-GA-A12237
	10. Work Unit No.
9. Performing Organization Name and Address	
Gulf General Atomic Company San Diego, California	11. Contract or Grant No. NAS 3-15323
	13. Type of Report and Period Covered
12. Sponsoring Agency Name and Address	Contractor Report
National Aeronautics and Space Administration Washington, D. C. 20546	14. Sponsoring Agency Code

15. Supplementary Notes

Technical Management, John R. Smith, Nuclear Systems Division, NASA Lewis Research Center, Cleveland, Ohio

16. Abstract

Two 1mm (40 mil) fluoride tungsten* clad UC-ZrC fueled capsules, designated as V-2C and V-2D, were examined in Gulf General Atomic hot cell after irradiation in NASA Plum Brook Reactor at a maximum cladding temperature of 1930°K for 11,089 and 12,031 hours to burnups of 3.0×10^{20} and 2.1×10^{20} fission/c.c. respectively. Percentage of fission gas release from the fuel material was measured by radiochemical means. Cladding deformation, fuel-cladding interaction and microstructures of fuel, cladding, and fuel-cladding interface were studied metallographically. Compositions of dispersions in fuel, fuel matrix and fuel-cladding interaction layer were analyzed by electron microprobe techniques. Axial and radial distributions of burnup were determined by gamma-scan, autoradiography and isotopic burnup analysis. The results are presented and discussed in conjunction with the requirements of thermionic fuel elements for space power application.

*Tungsten formed by hydrogen reduction of WF_6.

17. Key Words (Suggested by Author(s))	18. Distribution Statement
Carbide Fuel Irradiation Study Thermionic Fuel Material	Unclassified - unlimited

19. Security Classif. (of this report)	20. Security Classif. (of this page)	21. No. of Pages	22. Price*
Unclassified	Unclassified	150	$3.00

* For sale by the National Technical Information Service, Springfield, Virginia 22151

PREVIOUS REPORTS

Contract NAS 5-1253	GA-3523, Final Report for the Period Ending August 31, 1962. (U)
Contract NAS 3-2301	GA-3642, Final Report for the Period Ending August 31, 1962. (U)
Contract NAS 3-2532	GA-4769, Final Report for the Period Ending August 31, 1963. Part I (U). Part II (C/RD).
Contract NAS 3-4165	NASA CR-54322, GA-5665, Summary Report for the Period September 1, 1963 through August 31, 1964. (C/RD)
Contract NAS 3-6471	NASA CR-54980, GA-6860, Summary Report for the Period September 1, 1964 through November 23, 1965. (C/RD)
Contract NAS 3-8504	NASA CR-72315, GA-7682, Summary Report for the Period November 23, 1965 through January 31, 1967. (C/RD)
Contract NAS 3-8504	NASA CR-72327, GA-7745, Semi-Annual Report for the Period February 1, 1967 through July 31, 1967. (C/RD)
Contract NAS 3-6471	NASA CR-72517, GA-8974, Summary Report for the Period November 23, 1965 through September 30, 1968. (C/RD)
Contract NAS 3-8504	NASA CR-72627, GA-8956, Summary Report for the Period February 1, 1967 through July 31, 1969. (C/RD)
Contract NAS 3-8504	NASA CR-72947, Gulf-GA-11035, Summary Report for the Period August 1, 1969 through December 7, 1970. (C/RD)
Contract NAS 3-11822	NASA CR-120839, Gulf-GA-A11049, Summary Report for the Period June 1, 1968 through January 31, 1971. (C/RD)
Contract NAS 3-13471	NASA CR-120945, Gulf-GA-A12121, Fabrication of (U, Zr) C-Fueled/Tungsten-Clad Specimens for Irradiation in the Plum Brook Reactor Facility, Issued July 12, 1972. (U)

CONTENTS

CONTENTS (Continued)

FIGURES

FIGURES (Continued)

FIGURES (Continued)

FIGURES (Continued)

TABLES

This page intentionally left blank

SUMMARY

Two 1mm (40 mil) fluoride tungsten* clad UC-ZrC fueled capsules, designated as V-2C and V-2D, were examined in Gulf General Atomic hot cell after irradiation in NASA Plum Brook Reactor at a maximum cladding temperature of 1930°K for 11,089 and 12,031 hours to burnups of 3.0×10^{20} and 2.1×10^{20} fission/c.c. respectively. Percentage of fission gas release from the fuel material was measured by radiochemical means. Cladding deformation, fuel-cladding interaction, and microstructures of fuel, cladding, and fuel-cladding interface were studied metallographically. Compositions of dispersions in fuel, fuel matrix and fuel-cladding interaction layer were analyzed by electron microprobe techniques. Axial and radial distributions of burnup were determined by gamma-scan, autoradiography and isotopic burnup analysis. The results are presented and discussed in conjunction with the requirements of thermionic fuel elements for space power application.

*Tungsten formed by hydrogen reduction of WF_6.

1. INTRODUCTION

In the development of a thermionic fuel element for space power application, one of the most challenging aspects is the selection of a fuel-cladding combination for meeting system life and performance requirements. Considerable amount of effort has been made during the last several years under NASA sponsorship* to develop UC-ZrC fuel and tungsten cladding for nuclear thermionic application. Long-term irradiation study, however, remains to be carried out in order to assess the behaviors of such materials in a reactor environment. Two capsules, designated as V-2C and V-2D, were designed and fabricated in 1968 under Contract NAS 3-6471 for the evaluation of the long-term dimensional stability and compatibility of CVD fluoride tungsten** clad 90UC-10ZrC (for V-2C) and 50UC-50ZrC (for V-2D) fuel bodies in NASA Plum Brook Reactor. Details on the design and fabrication of the capsule components were given in the Summary Report of Contract NAS 3-6471 for the period November 23, 1965 through September 30, 1968.[1] The irradiation experiment was designated as 62-13-R2. Figure 1 shows the configurations of the carbide fuel pellets irradiated in these capsules. Figures 2(a) and (b) describe the arrangements, characteristics, and temperatures

*A list of previous reports on NASA sponsored thermionic material development work at Gulf General Atomic is given on the page next to the title page of this report.

**Tungsten prepared by chemical vapor deposition from a gaseous mixture of $H_2 + WF_6$.

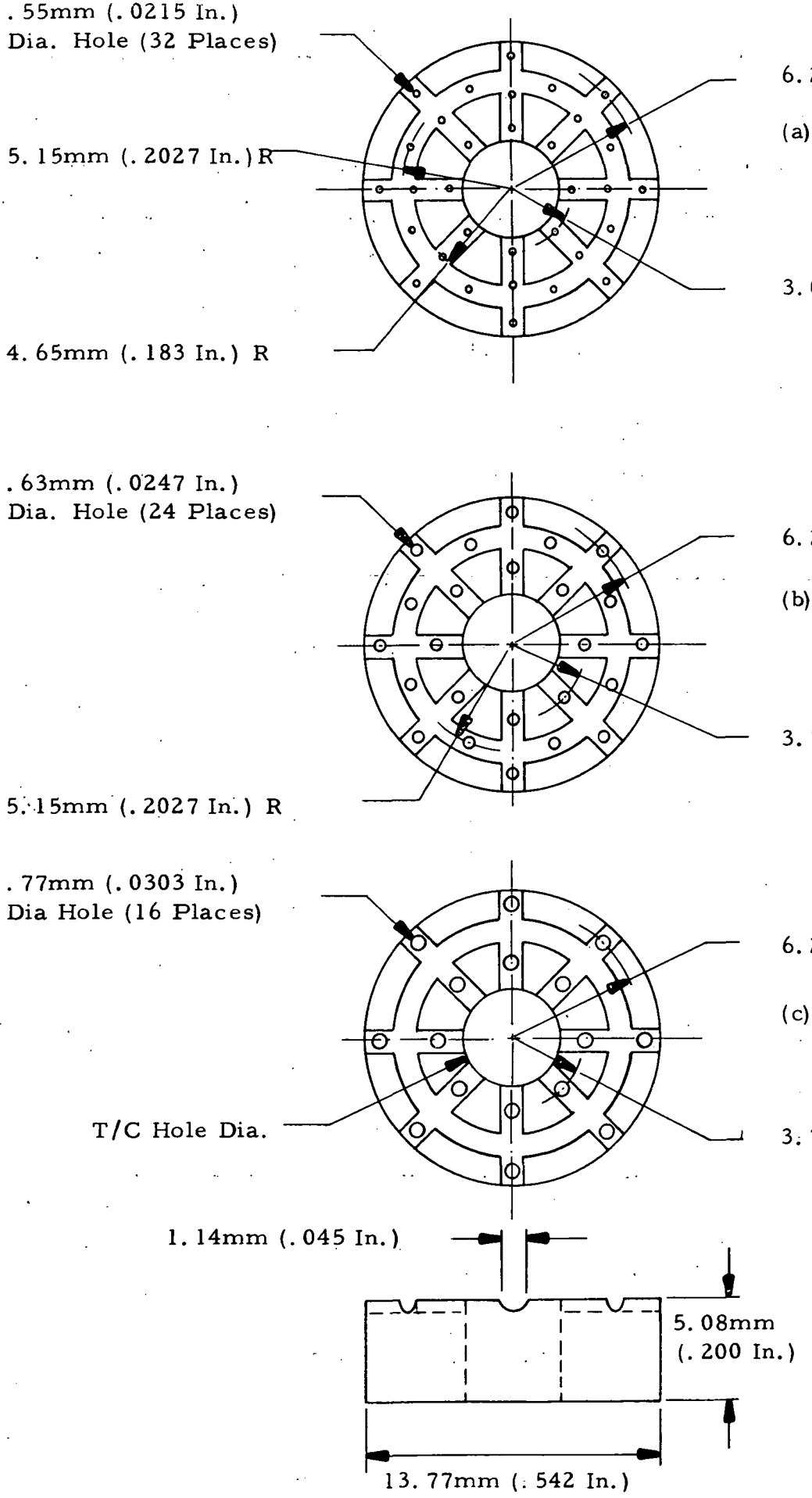

Fig. 1. Fuel configurations for V-2C and V-2D capsules

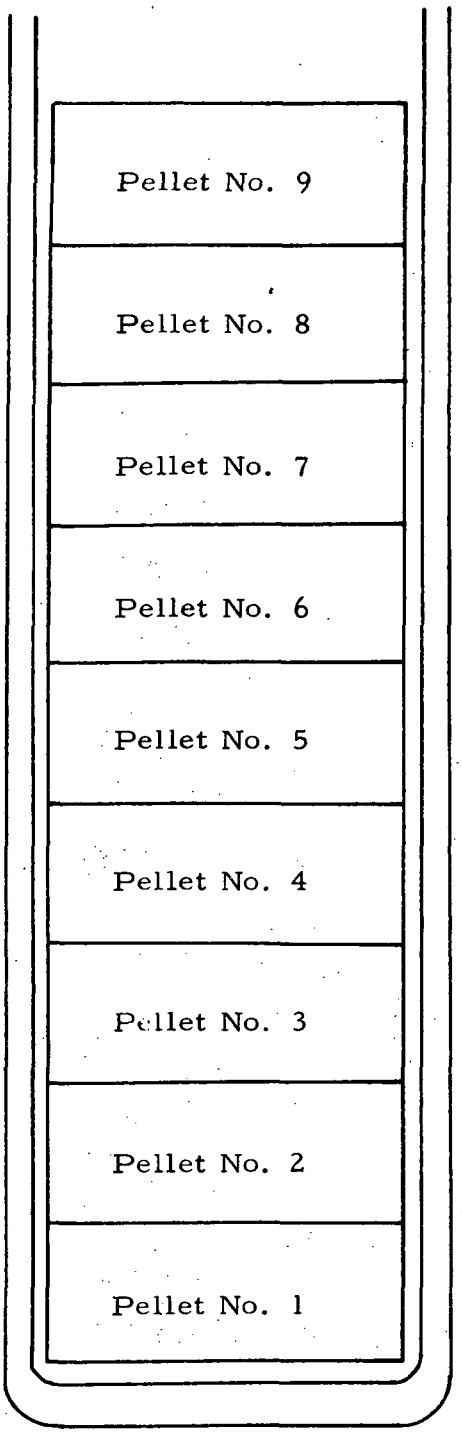

Fuel Pellet No.	Fuel Configuration (see Fig. 1)	Fuel Density (% Theoretical)	Fuel Stoichiometry (C/U Atom Ratio)	Fuel True Surface to Geometric Area Ratio	Fuel I. D. Temperature	
					Design (^{o}K)	Operating (^{o}K)
9	(a)	75.1	1.04	198	1760	1780
8	(a)	75.1	1.04	198	1844	1860
7	(a)	75.1	1.04	198	1903	1925
6	(a)	79.0	1.035	162	1940	1995
5	(a)	79.0	1.35	162	1962	2020
4	(b)	76.5	1.04	161	1973	2035
3	(b)	76.5	1.04	161	1973	2035
2	(c)	76.0	1.05	176	1960	2020
1	(c)	76.0	1.05	176	1934	1985

Cladding: CVD fluoride tungsten. F = 12 ppm, Wall thickness = 1.0 mm (40 mils) Bottom thickness = 1.5 mm (60 mils)

Fuel Composition: 90UC-10ZrC + 4 wt% W nominal. See p. 152 of Ref. (1) for exact composition of each pellet.

Fuel Enrichment: 30 atom percent of total uranium content

Fig. 2(a). Arrangement and characteristics of carbide fuel pellets in tungsten fuel pin of V-2C capsule

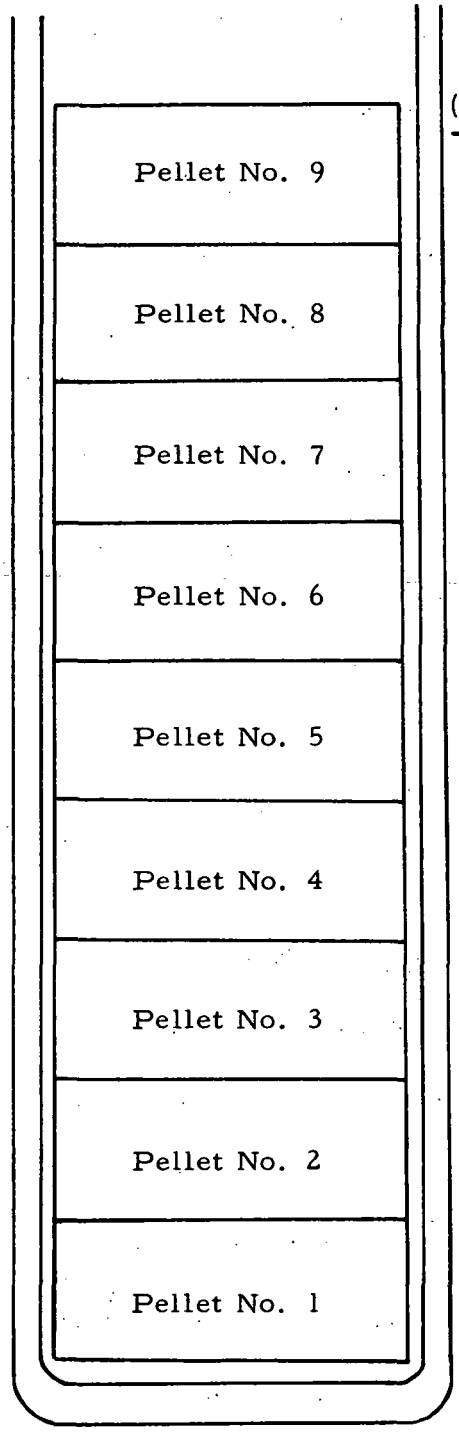

Fuel Pellet	Fuel Configuration (see Fig. 1)	Fuel Density (% Theoretical)	Fuel Stoichiometry (C/U Atom Ratio	Fuel True Surface to Geometric Area Ratio	Fuel I. D. Temperature	
					Design (°K)	Operating (°K)
Pellet No. 9	(a)	75.5	1.03	237	1761	1710
Pellet No. 8	(a)	75.5	1.03	237	1844	1805
Pellet No. 7	(a)	75.5	1.03	237	1903	1870
Pellet No. 6	(a)	80.0	1.045	185	1940	1925
Pellet No. 5	(a)	80.0	1.045	185	1962	1960
Pellet No. 4	(b)	78.0	1.04	>200	1973	1985
Pellet No. 3	(b)	78.0	1.04	>200	1973	1995
Pellet No. 2	(c)	79.9	1.04	>182	1960	1990
Pellet No. 1	(c)	79.9	1.04	>182	1934	1960

Cladding: CVD fluoride tungsten. F = 15 ppm, Wall thickness = 1.0 mm(40 mils) Bottom thickness = 1.5 mm(60 mils)

Fuel Composition: 50UC-50ZrC + 4 wt% W nominal. See p. 152 of Ref. (1) for exact composition of each pellet

Fuel Enrichment: 50 atom percent of total uranium content

Fig. 2(b). Arrangement and characteristics of carbide fuel pellets in tungsten fuel pin of V-2D capsule

(see Appendix A) of the carbide fuel pellets in the fuel pins of Capsules V-2C and V-2D respectively. Figures 3(a), (b), and (c) illustrate the arrangements of the components in the fuel containment, the Inconel primary containment and the stainless steel outer containment of these capsules respectively. Irradiation of Capsules V-2C and V-2D was continued between September 25, 1968 and September 28, 1970. Table 1 summarizes the test data. The tests were terminated because of the swelling of the fuel pins. Special design features and neutron radiograph results were presented at two previous Thermionic Specialist Conferences.[2],[3] This report describes the hot cell examination results.

2. CAPSULE DISASSEMBLY AND DETERMINATION OF FISSION GASES IN CONTAINMENT

2.1. Removal of Capsules V-2C and V-2D from Shipping Container

The capsules were shipped from Plum Brook Reactor Facility in a Schedule-40 steel container to Gulf General Atomic Hot Cell. The end of the container near the flexible instrument lead tubes of the capsules was cut off and the packing material around the tops of the tubes were removed by suctioning. The capsules could not be pulled out of the container because the packing material (Vermiculite) was tightly packed around the capsules, probably by vibration during shipping with the container held at an angle. Successive removal of short sections of the shipping container from the same end, followed by the removal of the end near the irradiated fuel sample, helped to loosen the packing and to free the capsules from the container. A

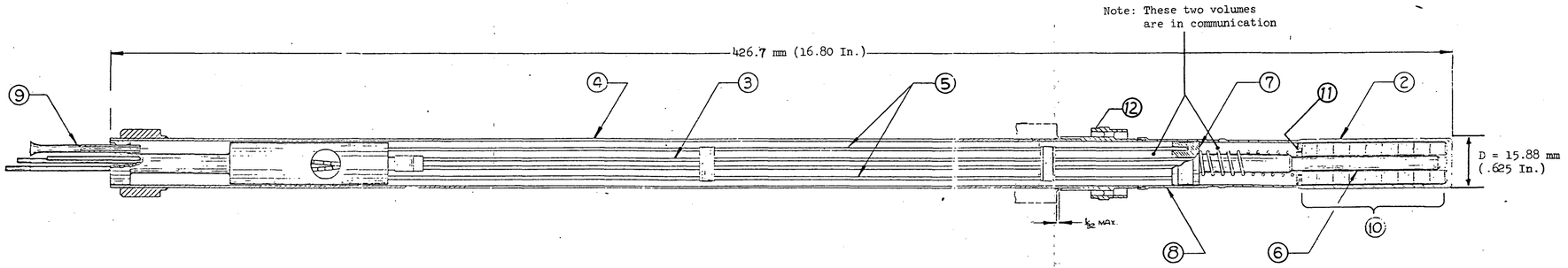

① ASSEMBLY

Item List

1. Fueled Capsule Assembly.
2. Tungsten Clad - 1mm(.040 in.) thick.
3. High Temperature Fuel Thermocouple Assembly.
4. Inconel Fission Product Chamber
5. Remote Chromel-Alumel Thermocouple
6. Fuel Thermocouple Well
7. Tantalum Transition Piece for Fuel Thermocouple Well
8. Tantalum Transition Piece for Fuel Cup
9. Copper Pinch-Off Tube
10. Fuel Samples
11. Thermal Radiation Shield
12. Inconel Spider

Fig. 3(a). Fuel containment assembly of V-2C and V-2D capsules

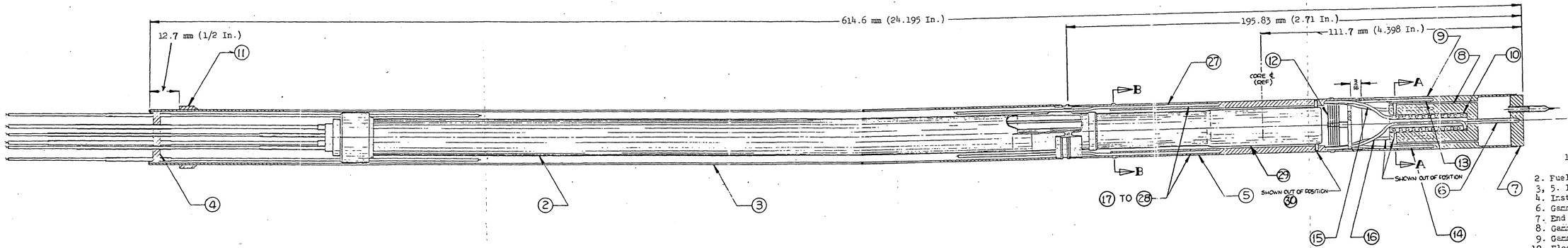

① ASSEMBLY

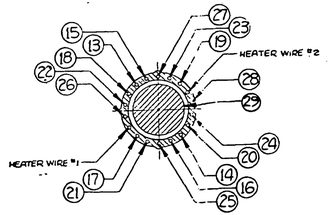

SECTION B-B

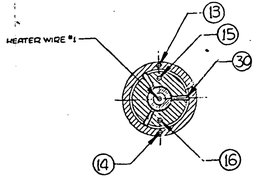

SECTION A-A

Item List

1. Fuel Capsule Primary Containment Assy.
2. Fueled Capsule Assy
3, 5. Inconel Containment Tube.
4. Instrument Lead Seal Flange.
6. Gamma Calorimeter Support.
7. End Plate Seal.
8. Gamma Heat Calorimeter.
9. Gamma Heat Sink.
10. Electrical Heater.
11. Spacer.
12. Radiation Shields.
13, 14. Gamma Meter Heat Sink Thermocouples.
15, 16. Gamma Meter Thermocouples.
17 to 28. Inner Group of Chromel-Alumel thermocouple for radial calorimeter
29. Neon Gas Gap
30. Tungsten Stand-Off Pins

Fig. 3(b). Inconel primary containment assembly of V-2C and V-2D capsules.

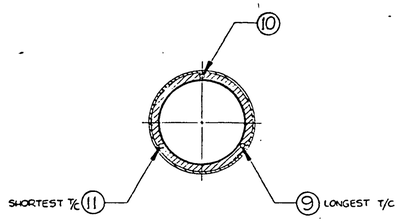

SECTION A-A

Item List

1. Outer Containment Assembly.
2. Capsule Primary Containment Assembly
3. Instrument Lead Seal Flange.
4 - 8. Stainless Steel Containment Tube.
9 -11. Outer group Chromel-Alumel Thermocouples for the radial calorimeter
12 -13. Backfill Valve and Seal Assembly
14. Helium Gas Gap

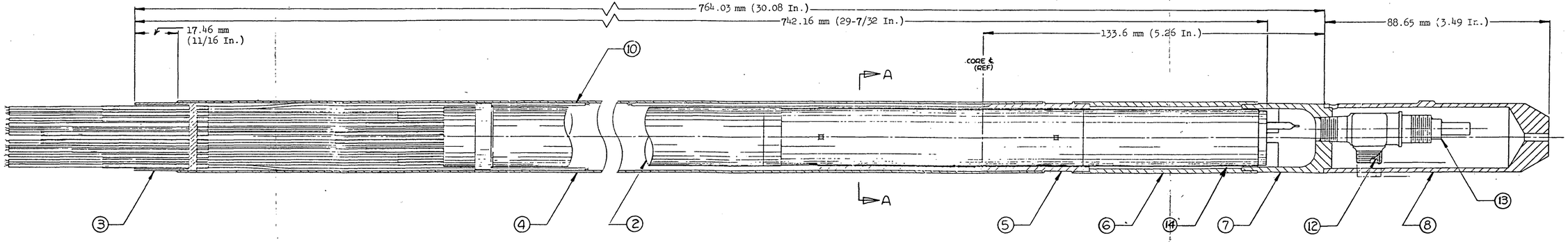

(1) ASSEMBLY

Fig. 3(c). Stainless steel outer containment assembly of V-2C and V-2D capsules

TABLE 1

SUMMARY OF TEST DATA FOR CAPSULES V-2C AND V-2D

Capsule Designation	Total Testing Time (Hours)	Average Fuel Burnup**		Neutrons/cm^2 NVT Sub-Cadmium n/cm^2	Average Cladding Heat Flux (Watts/cm^2)	Average Fission Power Density (Watts/c. c.)	Maximum Designed Cladding Temperature ($^\circ$K)	Maximum Measured Fuel Temperature ($^\circ$K)
		Fission/c. c.	At%Total U					
V-2C	11089	3.0×10^{20}	1.5	0.87×10^{20}	~ 50 first 1732 hours. 70-74 afterwards*	~ 174 first 1732 hours. 258-268 afterwards*	1920	2040
V-2D	12031	2.1×10^{20}	1.7	0.61×10^{20}	~ 40 first 7984 hours. 53 - 56 afterwards*	~145 first 7984 hours. 192 - 205 afterwards*	1920	1990

* Change in heat transfer characteristics due to leakage of helium from outer containment into primary containment of the capsule.

** Determined by calorimetric means using capsule thermocouples. The volume (cm^3) is the annular space occupied by the fuel.

scribe mark was made at Plum Brook on the flex-tube of each capsule to indicate the orientation of each capsule with respect to the reactor core. This mark was transferred to the rigid section of the capsule. For V-2C the mark indicates the side of the capsule facing the reactor core during the irradiation. For V-2D, the mark indicated the side which was 180° away from the reactor core.

2.2. Capsule Puncturing Arrangement

An arrangement was setup in the hot cell for puncturing the capsule and collecting gas sample from each capsule containment for analyzing its fission gas content. Figure 4 illustrates schematically the components in the arrangement and Fig. 5 shows the apparatus with the capsule in position for the puncturing operation. The essential features of the apparatus are as follows.

(1) The ports of the puncturing chamber can accommodate the diameters of the V-2C and V-2D capsules to make a tight seal when the surrounding O-rings are pressed down by the sealing flanges.

(2) The capsule containment is punctured by drilling. Mechanical stops are incorporated into the drilling device to insure that each containment can be punctured successively without the danger of damaging the one underneath.

(3) Four stainless steel expansion chambers of known volume are attached to the puncturing chamber. These chambers can be

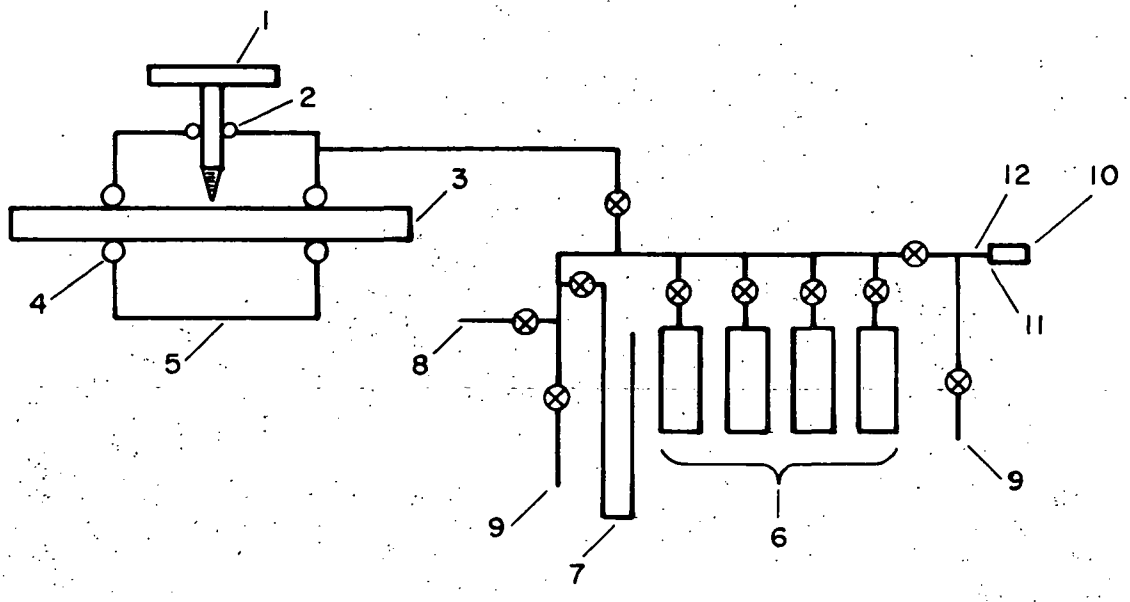

1. Drilling head with mechanical stops
2. O-ring seal for drill
3. Capsule
4. O-ring seal for puncturing chamber
5. Puncturing chamber
6. Stainless steel expansion chambers
7. Mercury mannometer
8. To helium
9. To vacuum
10. Glass ampoule
11. Rubber Seal
12. Hypodermic needle

Fig. 4. Schematic arrangement of capsule puncturing and containment gas collection arrangement

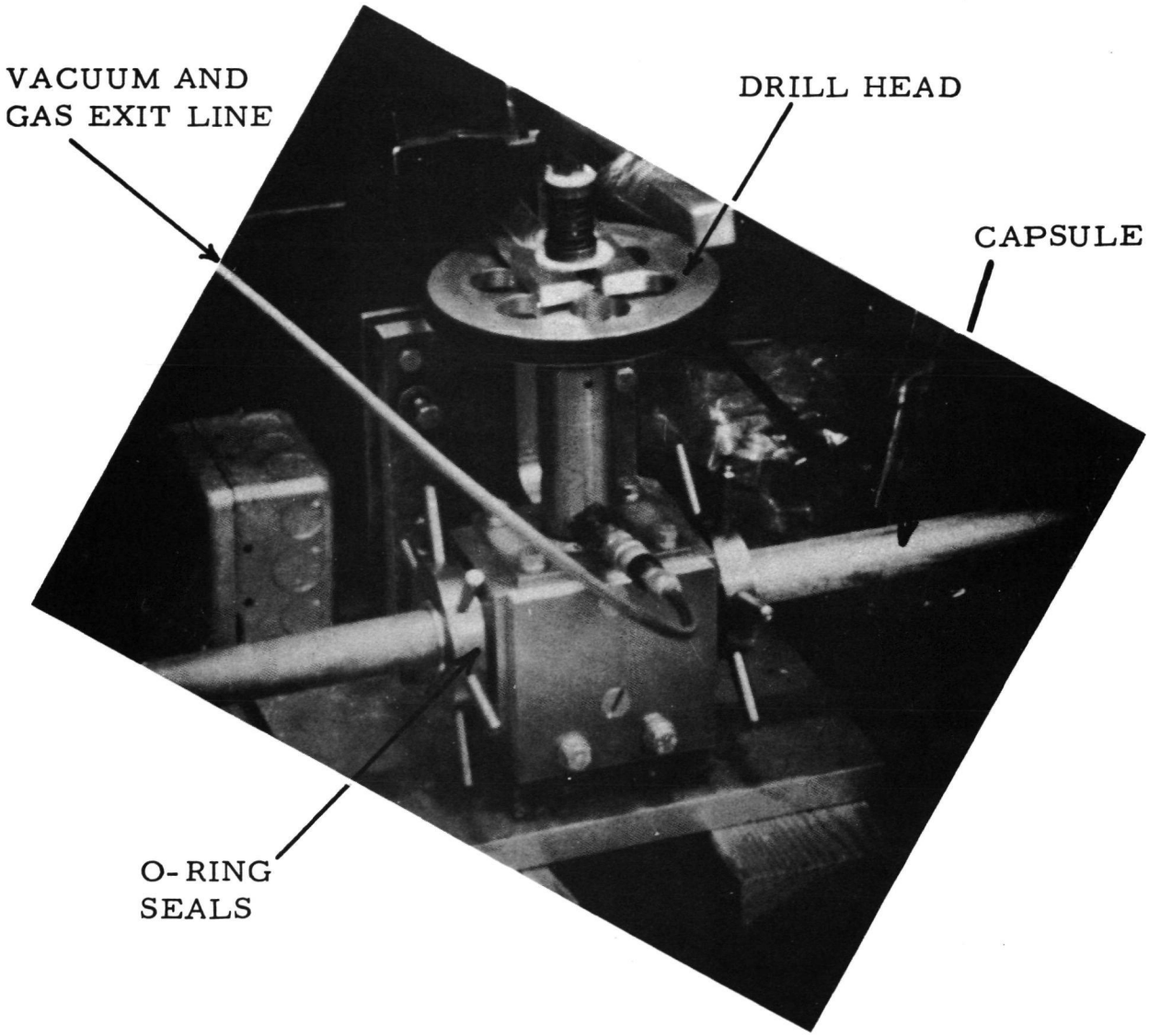

Fig. 5. Capsule containment puncturing apparatus

evacuated for collecting the gases released from the capsule containments and the pressure of the system can be measured before and after the collection of the gases with a mercury mannometer.

(4) The gases collected in the expansion chambers, if radioactive, can be sampled with a hypodermic needle arrangement attached to the rubber seal of a glass ampoule for radioactive counting.

(5) The volume of the capsule containments, puncturing chamber, and connecting lines can be determined by expanding helium gas of known volume and pressure from the expansion chamber into the system to be measured and observing the pressure change.

2.3. Determination of Fission Gas Contents in Capsule Containments

(1) Capsule V-2D

Capsule V-2D was installed into the puncturing chamber and the assembly was evacuated and leak-checked. The stainless steel containment was then punctured at a location which was 451 mm (18 inches) from the end of the capsule. The gas collected was found to be non-radioactive and contained no neon and argon, which were present in the Inconel primary containment and the fuel containment respectively. This indicates that the Inconel primary containment remained leak tight and the observed change in the heat transfer characteristics of the capsule during the irradiation, if attributed

to the presence of helium in the primary containment, may be due to helium diffusion through the Inconel containment wall or the joints between the primary and the secondary containments.

While no fission gas was present in the stainless steel secondary containment, the gas collected after the Inconel containment was punctured was highly radioactive, indicating that the fuel containment was in communication with the Inconel containment. Study by gamma-spectrometry showed that the radioactive component was essentially Kr^{85}. Counting data yielded a total of 3.1×10^{18} atoms of Kr^{85}. Since the estimated burnup from thermal data is 2.1×10^{20} fission/c.c. of fuel cavity volume (excluding the volume occupied by the thermocouple well), the total number of Kr^{85} formed in the fuel body is $2.1 \times 10^{20} \times 6.06 \times 2.93 \times 10^{-3} = 3.73 \times 10^{18}$ atoms where 6.06 = volume of fuel cavity in c.c., and 2.93×10^{-3} is the fission yield of Kr^{85}. If any radioactive decay is neglected because of the long half life of Kr^{85} (10.3 years), the release of Kr^{85} from the fuel body is $\frac{3.16 \times 10^{18}}{3.73 \times 10^{18}} = 0.85$, or 85%.

(2) Capsule V-2C

Puncturing of the containments of V-2C capsule and collection of the gases in the containments followed the same procedures as that used for Capsule V-2D. Radioactivity was detected in the gas collected from the stainless steel containment, indicating that the stainless steel containment, the Inconel containment, and the fuel containment were in communication.

Radioactive counting results showed that the fission gas present was essentially Kr^{85} and a total of 1.34×10^{17} atoms was collected. The gas collected after the puncturing of the Inconel containment showed a much higher radioactivity. Here again, only Kr^{85} was detected and a total of 3.42×10^{18} atoms was collected. There was no increase in the Kr^{85} atoms collected when the fuel containment was punctured. These results indicate that the leak between the fuel containment and the Inconel containment was large, while the leak between the Inconel containment and the stainless steel containment was very small so that no equalization of the fission gas concentration could be achieved at the end of 11,089 hour irradiation and eight months of cooling period.

The total number of Kr^{85} formed in the fuel body, calculated from the fission density (3.03×10^{20} fission/c. c.) deduced from thermal data, was 5.39×10^{18}. Since the total number of Kr^{85} atoms collected from all three containments was $(3.42 + 0.13) \times 10^{18}$ or 3.55×10^{18}, the fractional release is therefore about 66%.

2.4. Removal of Stainless Steel Outer Containment and Inconel Primary Containment and Recovery of Thermocouples

(1) Capsule V-2D

After the removal of the punctured capsule from the puncturing chamber, dry kerosene was introduced into the capsule through the puncturing holes to protect the fuel samples from oxidation and hydrolysis. The lead

tube was cut off at a location 965 mm (38 inches) from the capsule bottom. The capsule was then circumferentially cut at a location 762 mm (30 inches) from the capsule bottom. Attempt to slide off the stainless steel containment from the Inconel containment was unsuccessful. The bottom 95.25 mm (3-3/4 inches) of the capsule was then cut off and the stainless steel containment was cut lengthwise at two locations 90° from the scribe mark. These cuts extended into the Inconel containment (Fig. 6), but the Inconel containment wall was not cut through in the fuel sample region. The three Chromel-Alumel thermocouples in the stainless steel containment wall were recovered and tagged.

The Inconel containment was plunge cut at the location of the puncturing hole and then circumferentially cut at the top of the weld to the Inconel spider. The assembly was stored under dry kerosene overnight. Efforts were then made to recover the Chromel-Alumel thermocouples in the Inconel containment wall. Six thermocouples were recovered; the rest were either broken off or stuck in the cavities.

After the recovery of these thermocouples, the gamma heat meter portion was cut off at a location just below the radiation shields between the bottom of the fuel pin and the top of the gamma heat meter. To remove the fuel pin from the Inconel sleeve, a circumferential cut was made at about 3.2 mm (1/8 inch) below the weld of the Inconel spider to the as-fabricated blackened Inconel sleeve around the fuel pin. All the thermocouples stuck inside the Inconel containment wall were also cut at this location. When the Inconel sleeve

Fig. 6. Inconel primary containment of Capsule V-2D

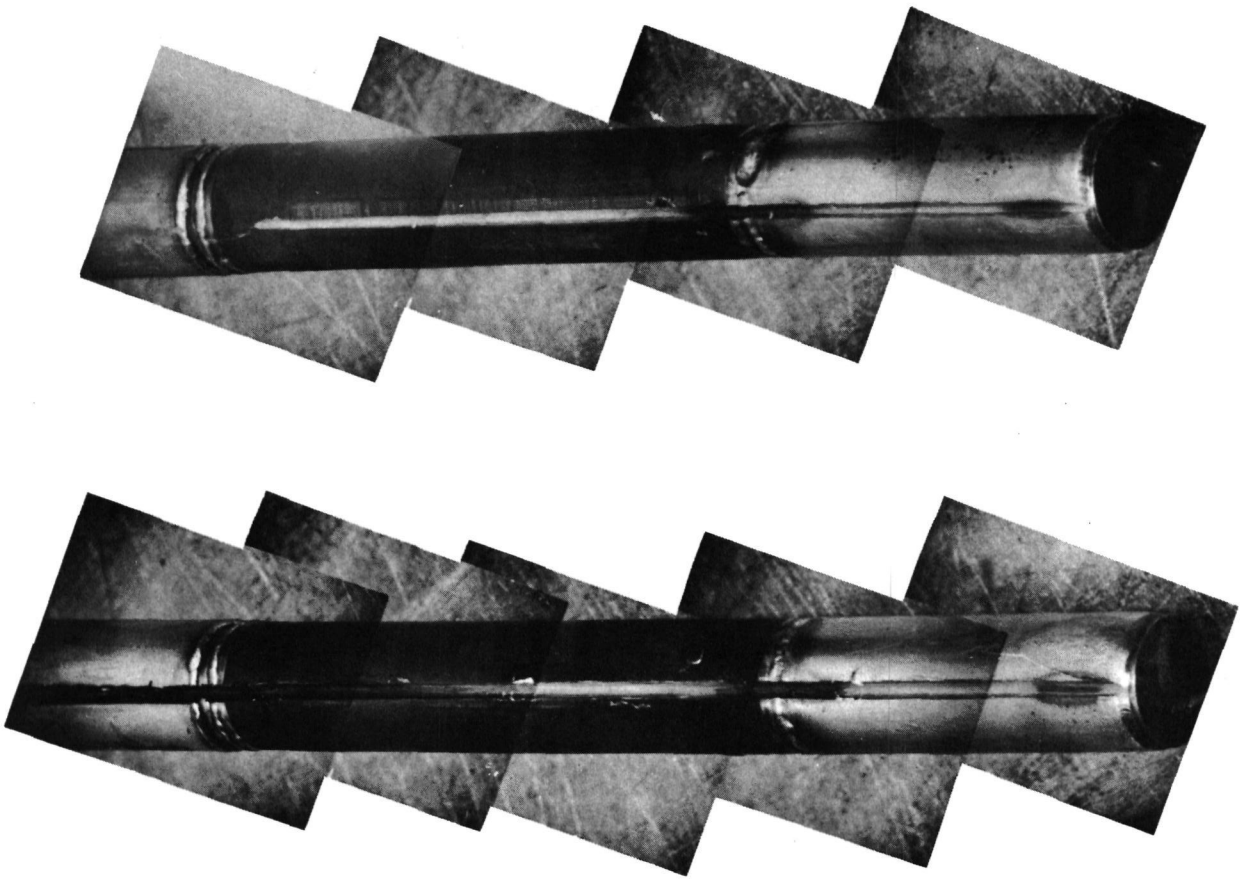

THE MARKS WERE MADE DURING LONGITUDINAL SLITTING OF THE OUTTER STAINLESS STEEL CONTAINMENT. ONE VIEW IS 180° FROM THE OTHER VIEW.

was pulled away slowly from the Inconel spider holding the fuel pin, the latter broke into two pieces, with the upper piece (about 27.9 mm long) attached to the Inconel spider and the bottom piece remained inside the Inconel sleeve (Fig. 7). The interface was jagged and a small piece of tungsten cladding broke off from the assembly. The fuel pellet at the broken interface appeared to be in excellent shape. There seemed to be very little changes in the appearances of the fission gas venting holes and grooves from their pre-irradiation conditions. A .51 mm (20 mil) drill rod could be pushed into these holes, indicating no significant change from the pre-irradiation value (.55 mm).

Since the fuel pin could not be removed from the Inconel sleeve in one piece, it was decided, with the approval of the NASA Project Manager, to reassemble the fuel pin from the two broken pieces for epoxy potting and subsequent gamma-scanning and metallographic examinations of the cross sections. The thermocouple assembly containing the two Chromel-Alumel thermocouples attached to the tantalum transition of the tungsten thermocouple well and the three high temperature (W-3Re)-(W-26Re) fuel thermocouples inside the tungsten thermocouple well were removed from the upper portion of the fuel pin. All thermocouples were removed intact except the bottom high temperature fuel thermocouple which was broken at one inch from the tip. All thermocouples and the tip of the bottom high temperature fuel thermocouple were tagged and stored. To assemble the two broken portions of the fuel pin, the remnant of the fission gas chamber attached to

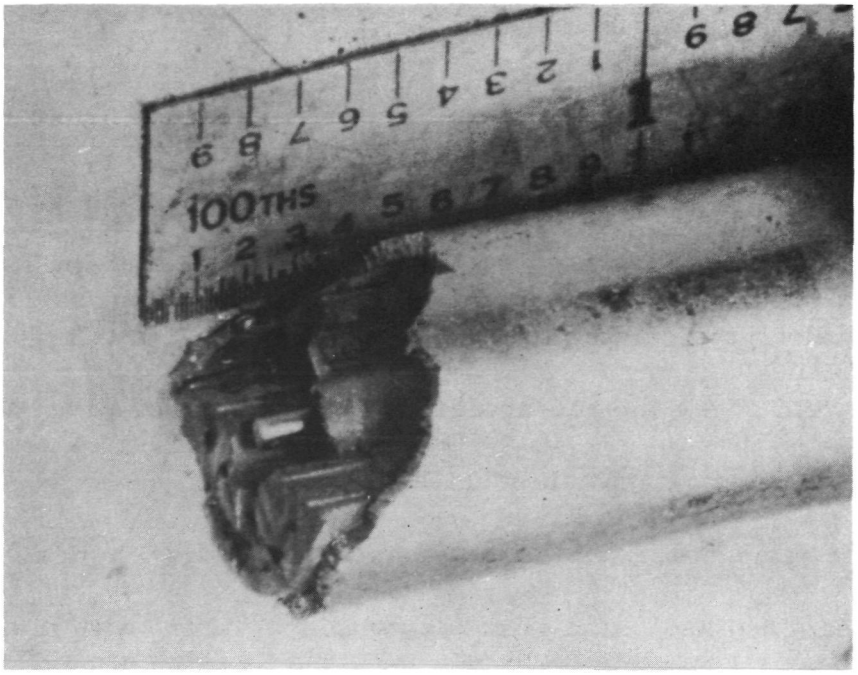

(a) SIDE VIEW

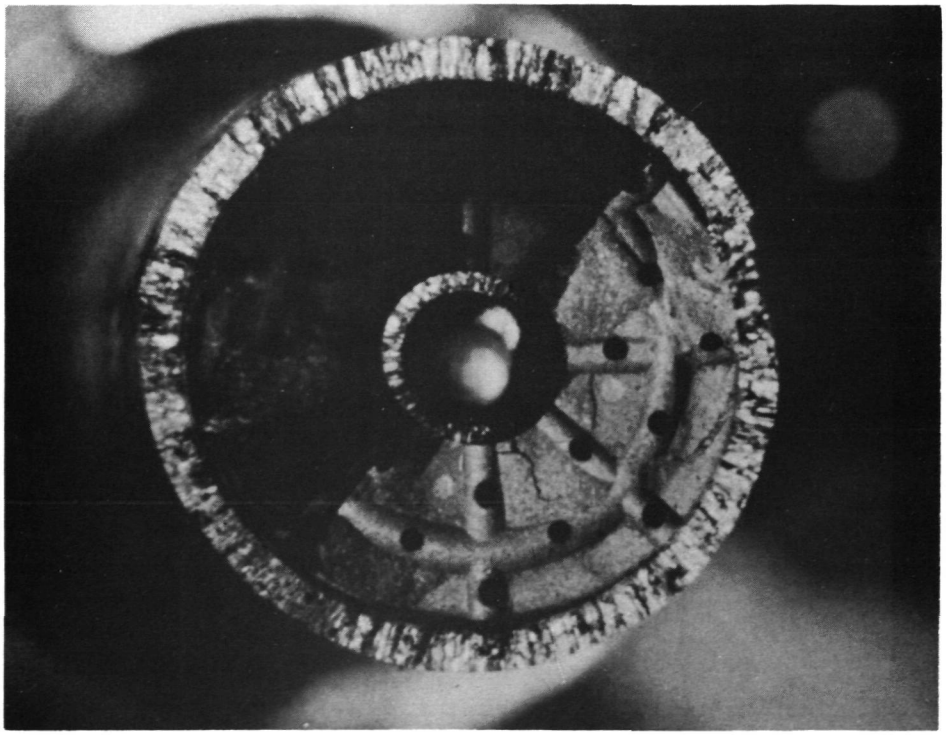

(b) TOP VIEW

Fig. 7. Top part of V-2D fuel pin which separated during removal from Inconel containment

the upper portion was cut off from the Inconel spider. A brass rod of 3.38 mm (0.133 inch) diameter was inserted into the tungsten thermocouple well of the lower portion as a guide. The upper portion of the fuel pin was then lowered along the guide into the Inconel sleeve. By using the scribe mark on the weld of the Inconel spider as a reference, the two parts were rotated with respect to each other until a good fit was achieved. To confirm that a good fit between the two parts was achieved, the length of the assembled piece was measured and found to agree (within .79 mm) with the expected value.

The assembled fuel pin, together with the Inconel sleeve, was rinsed in xylene to remove the kerosene. It was then seated on Apiezone wax in a vacuum dessicator and pumped to remove the xylene. Epoxy was then poured into the thermocouple well through the top of the Inconel spider. The assembly was pumped to remove trapped gases before air was admitted into the system to press the liquid epoxy into the voids of the fuel pin and the fuel body. The potted fuel pin was aged for three days to insure that the epoxy has hardened prior to the gamma scan of the potted fuel pin.

(2) Capsule V-2C

The punctured capsule was evacuated and dry kerosene was sucked into the capsule for the protection of the fuel material during the subsequent operations. The lead tube was cut at a location 965 mm (38 inches) from the capsule bottom and then the stainless steel containment was circumferentially

cut at 686 mm (27 inches) from the capsule bottom. The stainless steel containment slid off easily from the Inconel containment and the three Chromel-Alumel thermocouples located in its wall. These thermocouples were recovered and tagged.

After the removal of the stainless steel containment, the Inconel containment was plunge cut at a location 6.35 mm (1/4 inch) above the hole punctured for the collection of the containment gases. The two Chromel-Alumel thermocouples attached to the tantalum transition of the tungsten thermocouple well fell out easily when the fuel pin was turned upside down. They were tagged and stored. The fuel thermocouple assembly, however, did not fall out.

To remove the thermocouples in the Inconel containment wall, the Inconel containment was circumferentially cut off the top weld to the Inconel spider. The piece cut off was removed to expose the thermocouples. Fourteen thermocouples were recovered; they were all tagged and stored.

To remove the high temperature fuel thermocouples, the portion of the fission gas chamber left on the top of the fuel pin assembly was cut off circumferentially at the weld to the top of the Inconel spider. Efforts made to pull the fuel thermocouples out of the tungsten thermocouple well, however, were unsuccessful.

To avoid the possibility of cracking when the fuel pin was pulled out of the Inconel containment (such as that observed for V-2D fuel pin), it was

decided, with the approval of NASA Project Manager, that the fuel pin and the Inconel containment of V-2C would be potted together as one assembly and that dimensional measurements and metallography will be carried out on transversal cross sections cut at various axial locations. This should provide information on swelling, fuel-cladding reaction, and microstructures over all the radial directions and along the axial direction. Epoxy potting of the fuel pin assembly was carried out by the same procedures as that used for V-2D fuel pin prior to gamma-scan of the potted assembly.

3. GAMMA-SCAN OF FUEL PIN ASSEMBLY

The potted V-2C and V-2D fuel pins were gamma-scanned axially at four circumferential positions. These are:

(1) the position facing the reactor core during irradiation,

(2) the position 180° from the reactor core during irradiation,

(3) the position 90° from the reactor core along a clockwise direction, and

(4) the position 270° from the reactor core along a clockwise direction.

The fuel pin was situated 228 mm (9 inches) away from a slit .51 mm (20 mil) high and 6.35 mm (1/4 inch) side, with a collimation system 1067 mm (42 inches) in length. A 50.8 mm (2 inch) NaI crystal was used as the sensor. The detection system was set for the energy range 0.718 to 0.818 MeV, within

which the emission peak from the fission product Zr^{95} is located. Zr^{95} is a good index for measuring burnup distribution, since Zr forms a stable carbide and therefore any loss by vaporization is minimized.

Figures 8(a), (b), (c), and (d) show the results obtained on the fuel pin of V-2C capsule. Figures 9(a), (b), (c), and (d) show the results obtained on the fuel pin V-2D capsule. The burnup is general appears to be slightly higher at the top and the bottom of the fuel pin, presumably due to neutron streaming through the ends. The data also indicate higher gamma intensity when the fuel pin was at position (1), probably because of the higher burnup in the fuel material facing the reactor core during the irradiation.

4. MACROSCOPIC EXAMINATIONS OF FUEL PIN SECTIONS AT VARIOUS AXIAL LOCATIONS

4.1. V-2C Fuel Pin

V-2C fuel pin was sectioned transversally into six samples. The positions of these samples relative to that of the fuel pellets in the fuel pin are illustrated in Fig. 10. Figures 11(a) through (k) show the macroscopic appearances of the top and bottom surfaces of these samples in the as-sectioned conditions. Figures 12(a) through (d) show the mounted and polished bottom surfaces of Samples No. 2, 3, 4, and 5. Expansion and cracking of the tungsten claddings of Samples No. 2, 3, and 4 are clearly visible at locations close to the reactor core side. Because of the swelling of the fuel pellets

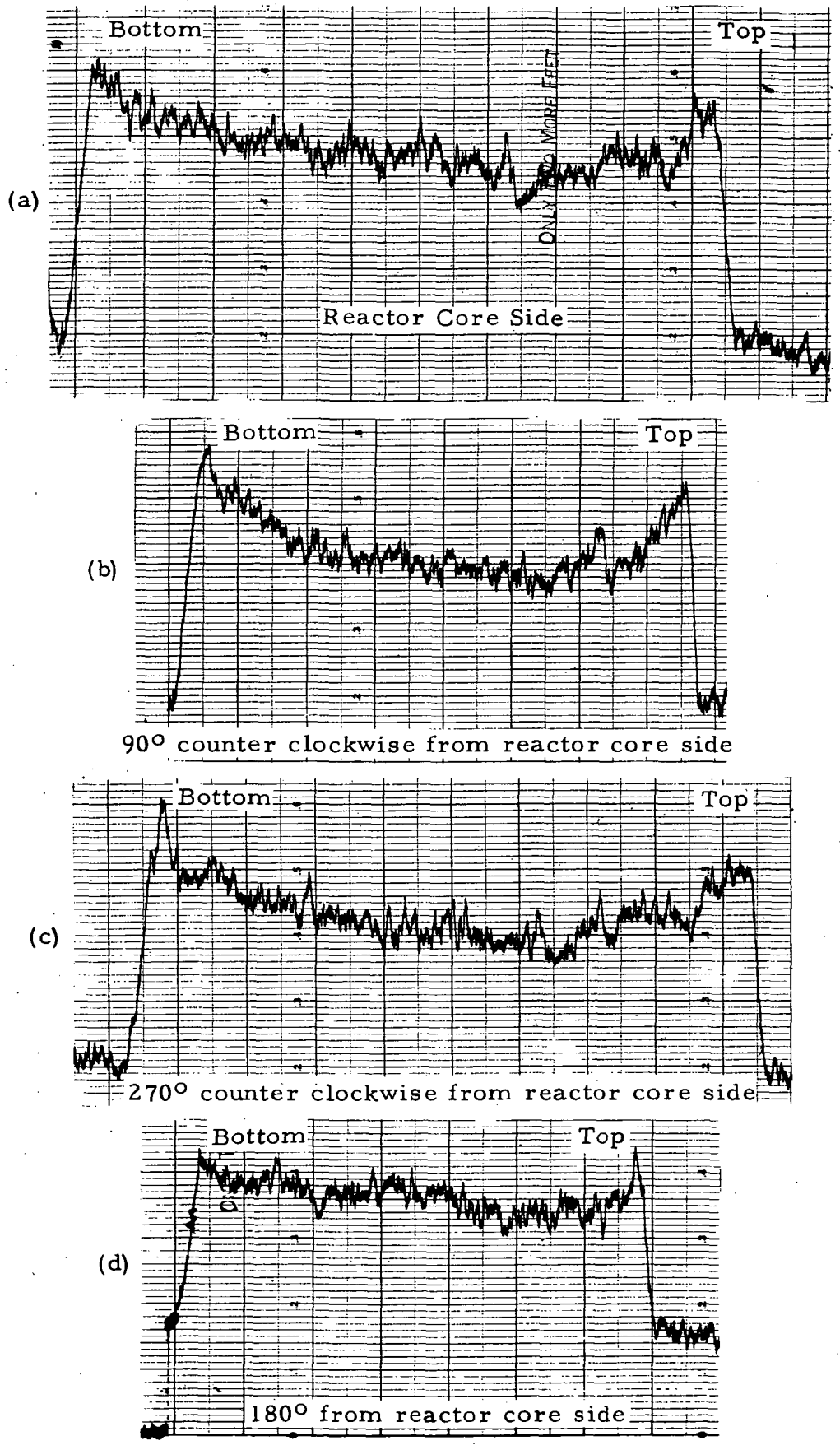

Fig. 8. Gamma-Scans of V-2C fuel pin

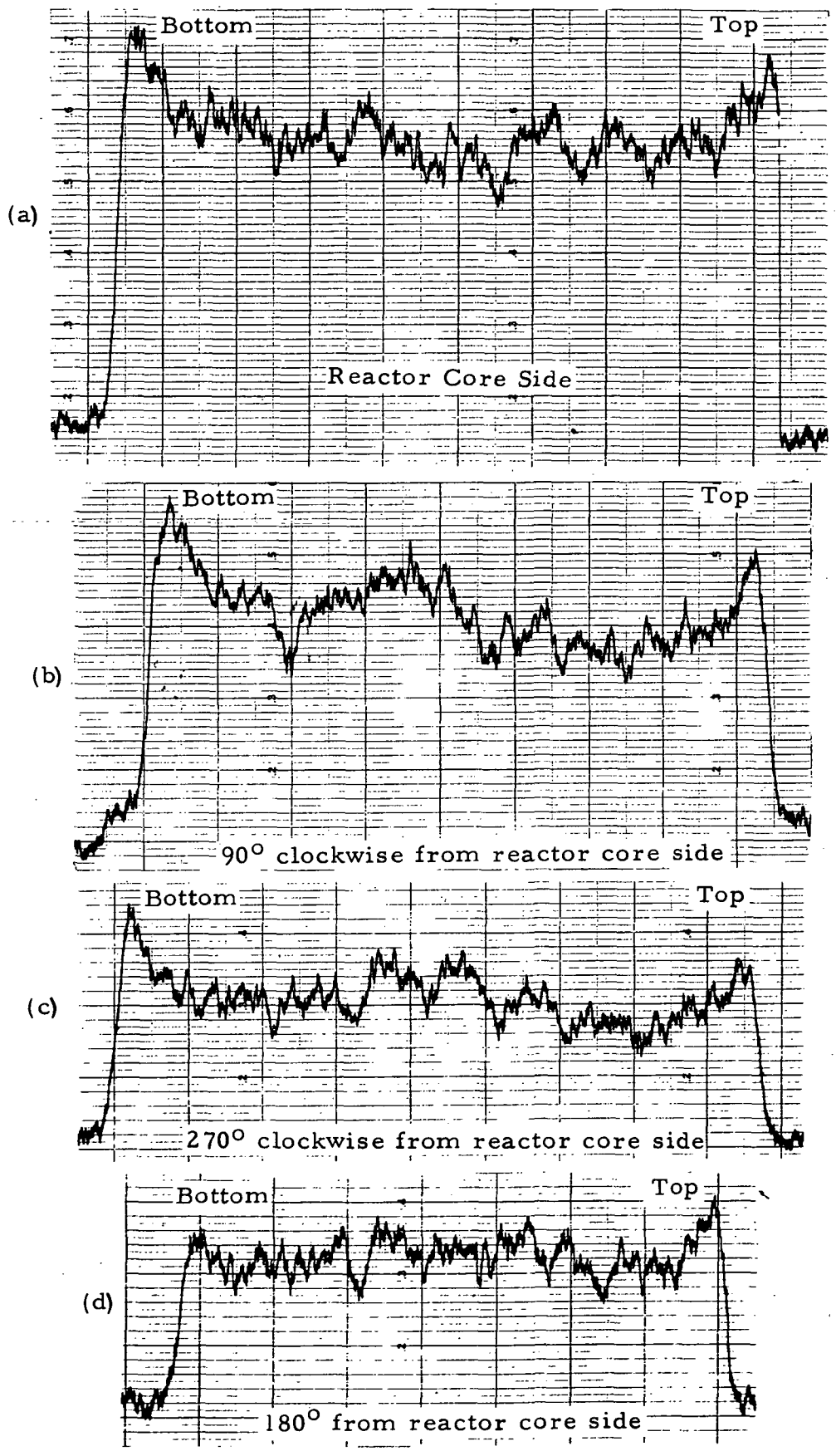

Fig. 9. Gamma-Scans of V-2D fuel pin

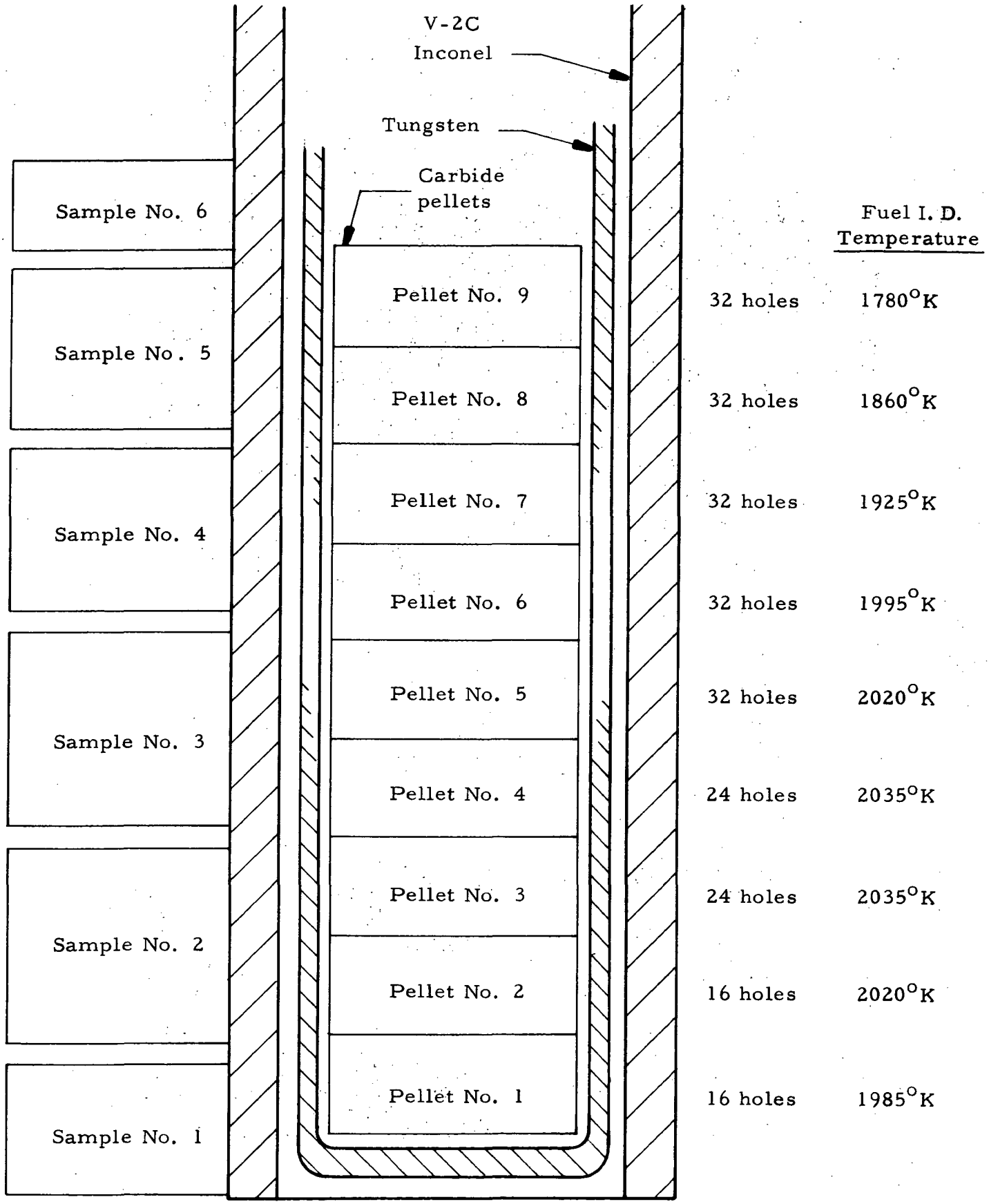

Fig. 10. Positions of samples taken from V-2C fuel pin relative to that of the fuel pellets in the fuel pin

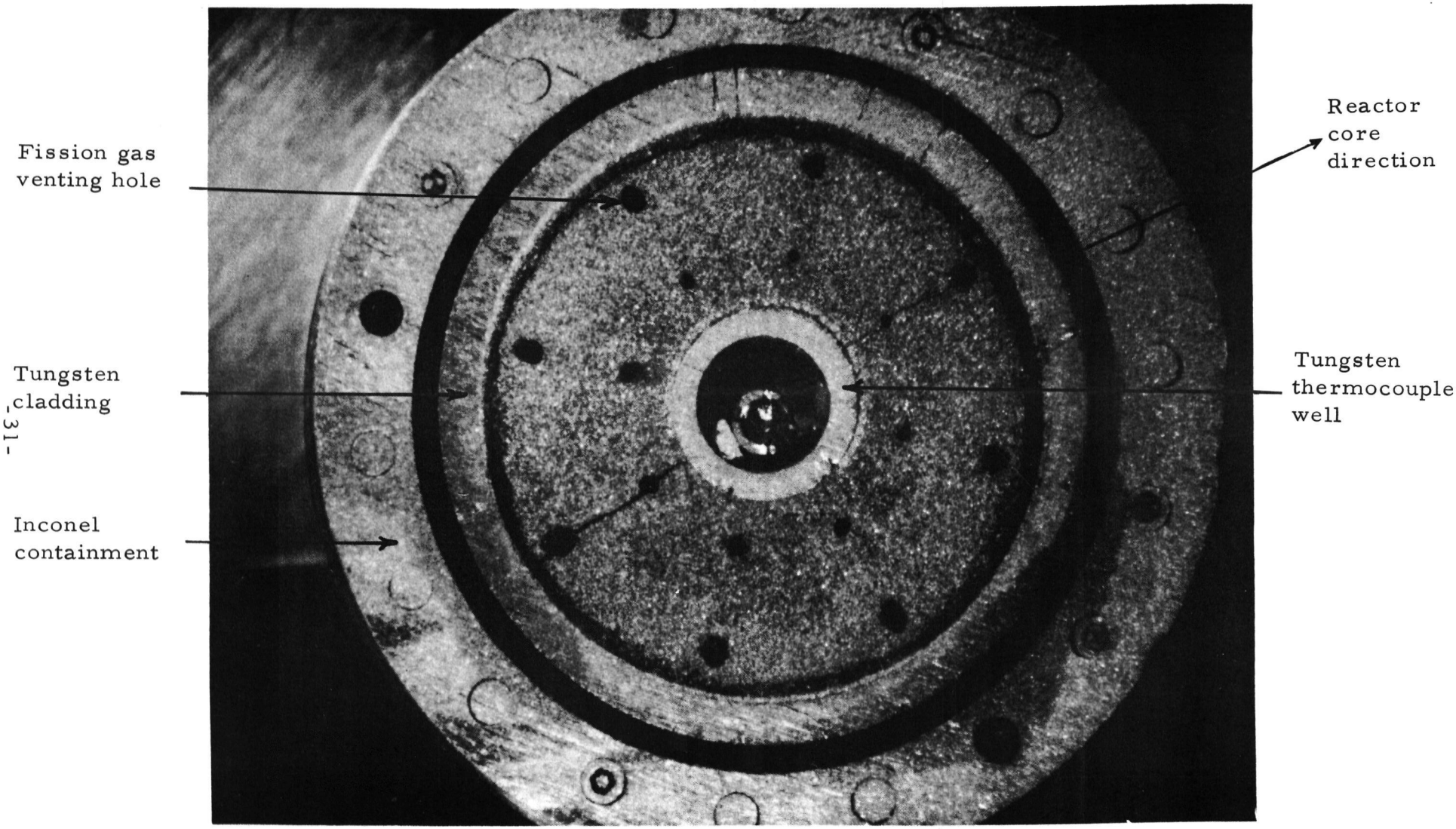

(a) Sample No. 1 top surface

Fig. 11. Macroscopic appearances of the surfaces of sample sections of V-2C fuel pin in the as-sectioned conditions (7.5X) (Sheet 1 of 6)

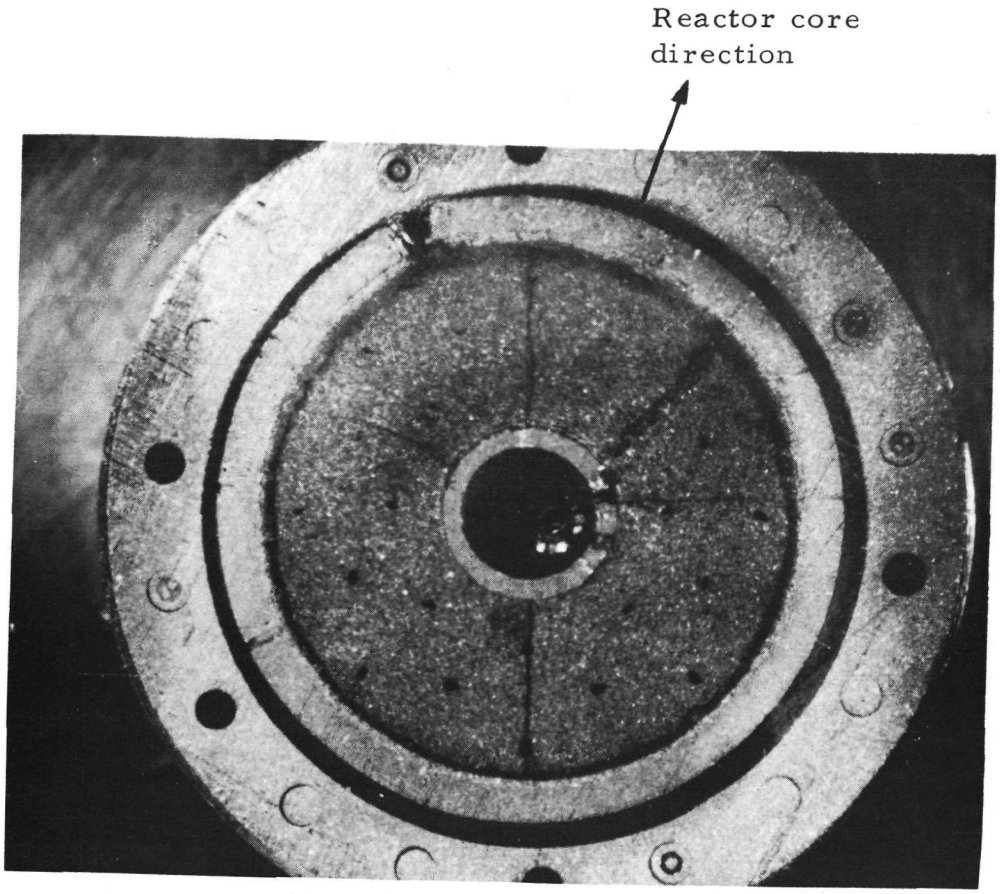

(c) Sample No. 2 top surface

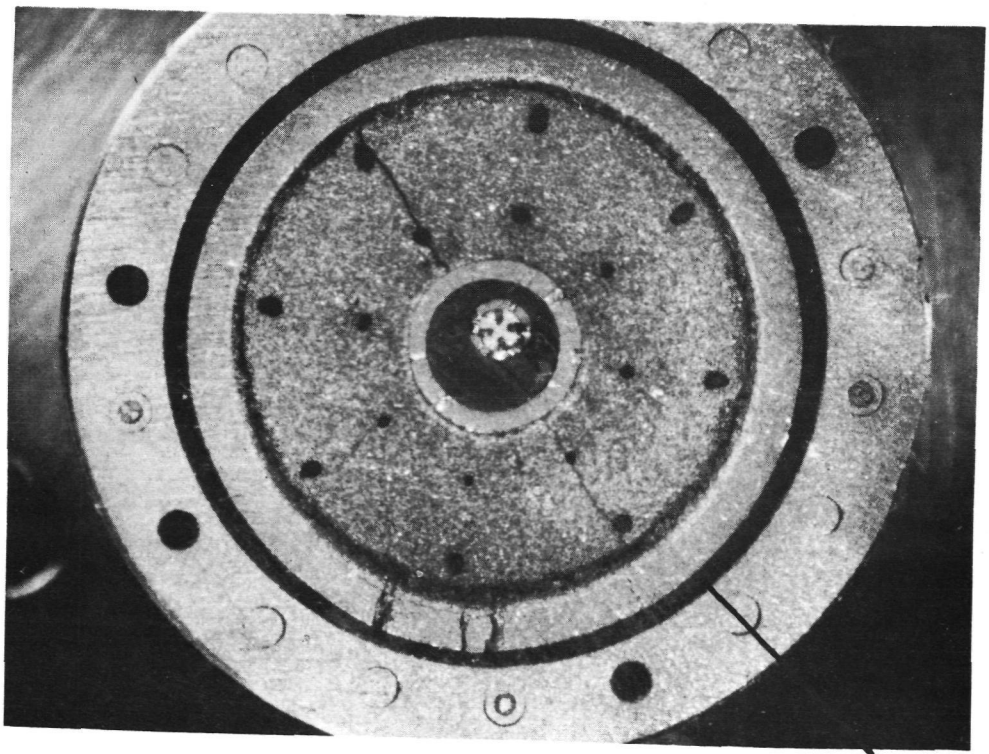

(b) Sample No. 2 bottom surface

Fig. 11. Macroscopic appearances of the surfaces of sample sections of V-2C fuel pin in the as-sectioned conditions (5X) (Sheet 2 of 6)

Reactor core direction

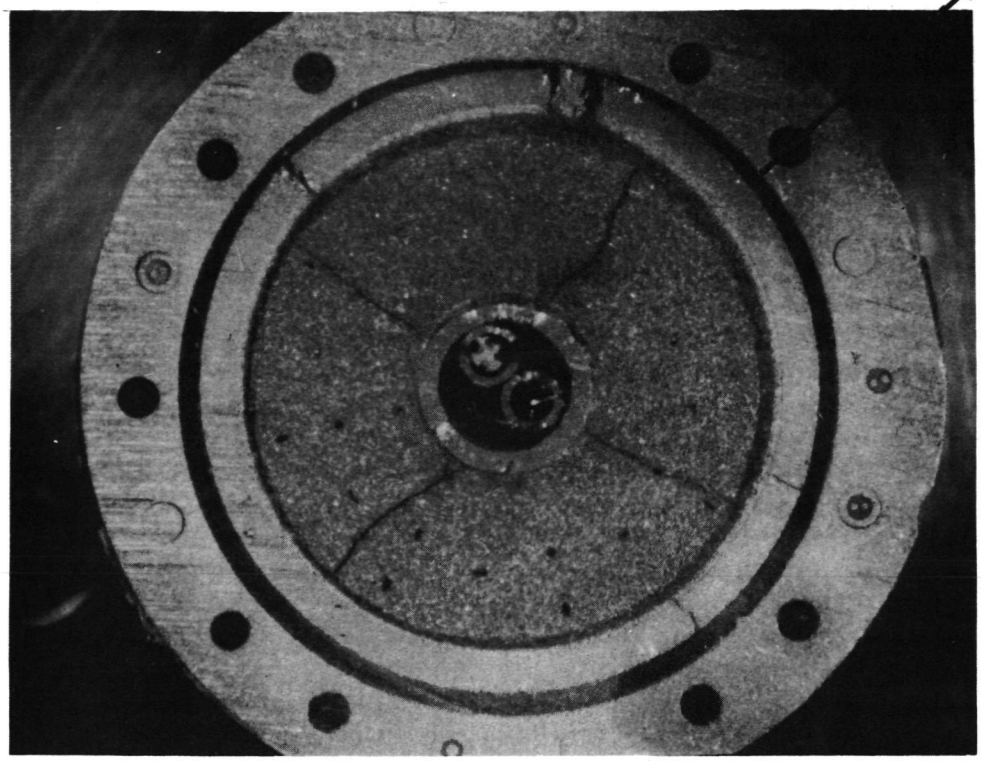

(e) Sample No. 3 top surface

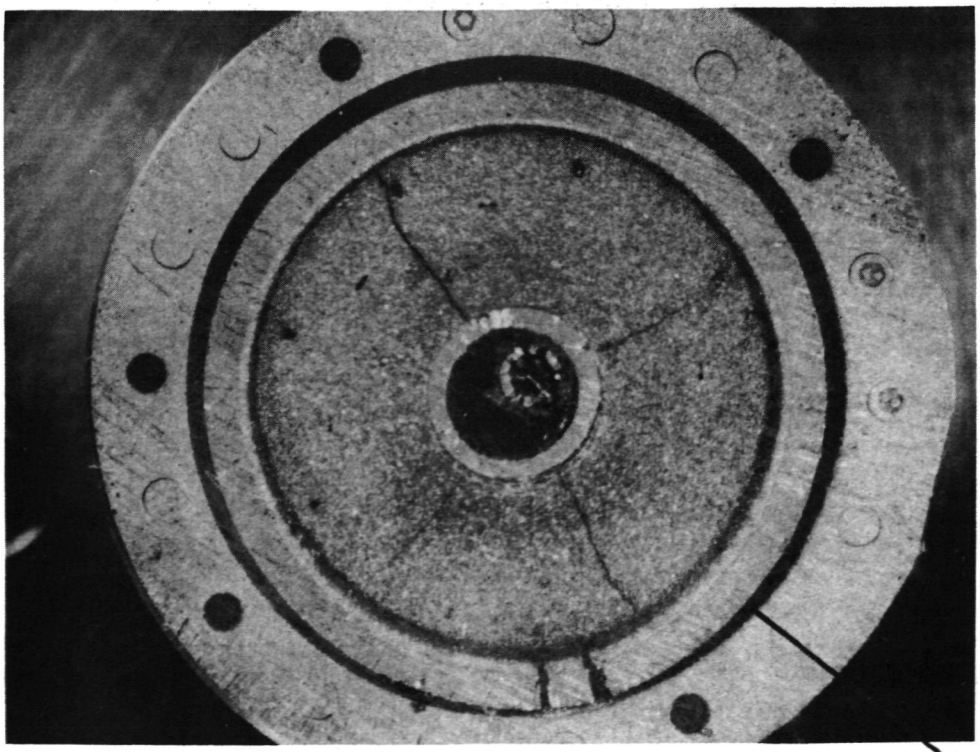

(d) Sample No. 3 bottom surface

Reactor core direction

Fig. 11. Macroscopic appearances of the surfaces of sample sections of V-2C fuel pin in the as-sectioned conditions (5X) (Sheet 3 of 6)

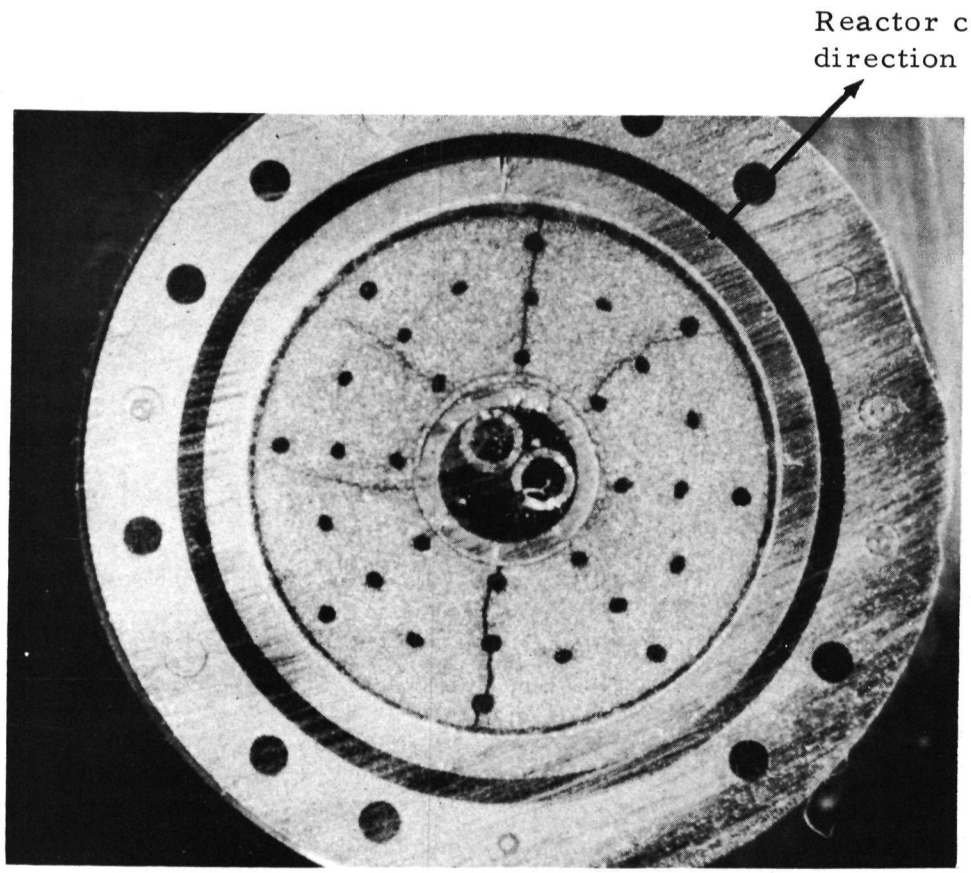

(g) Sample No. 4 top surface

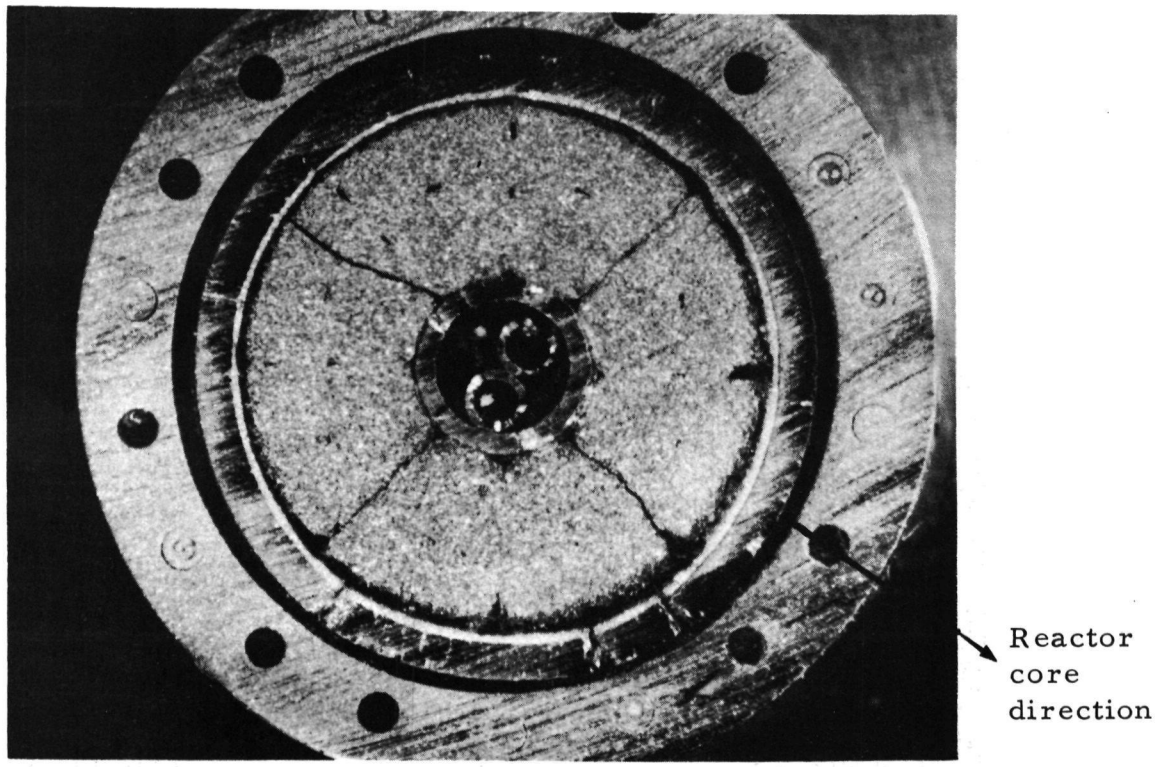

(f) Sample No. 4 bottom surface

Fig. 11. Macroscopic appearances of the surfaces of sample sections of V-2C fuel pin in the as-sectioned conditions (5X) Sheet 4 of 6)

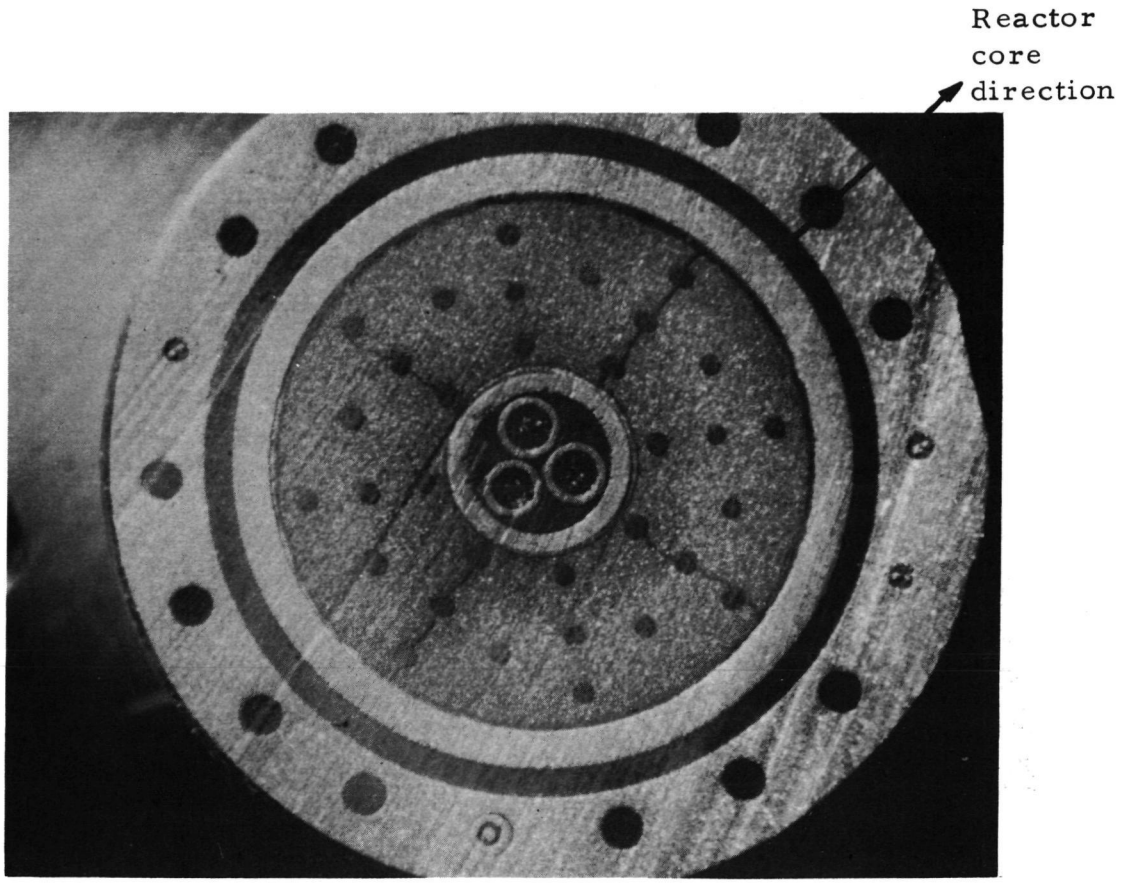

(i) Sample No. 5 top surface

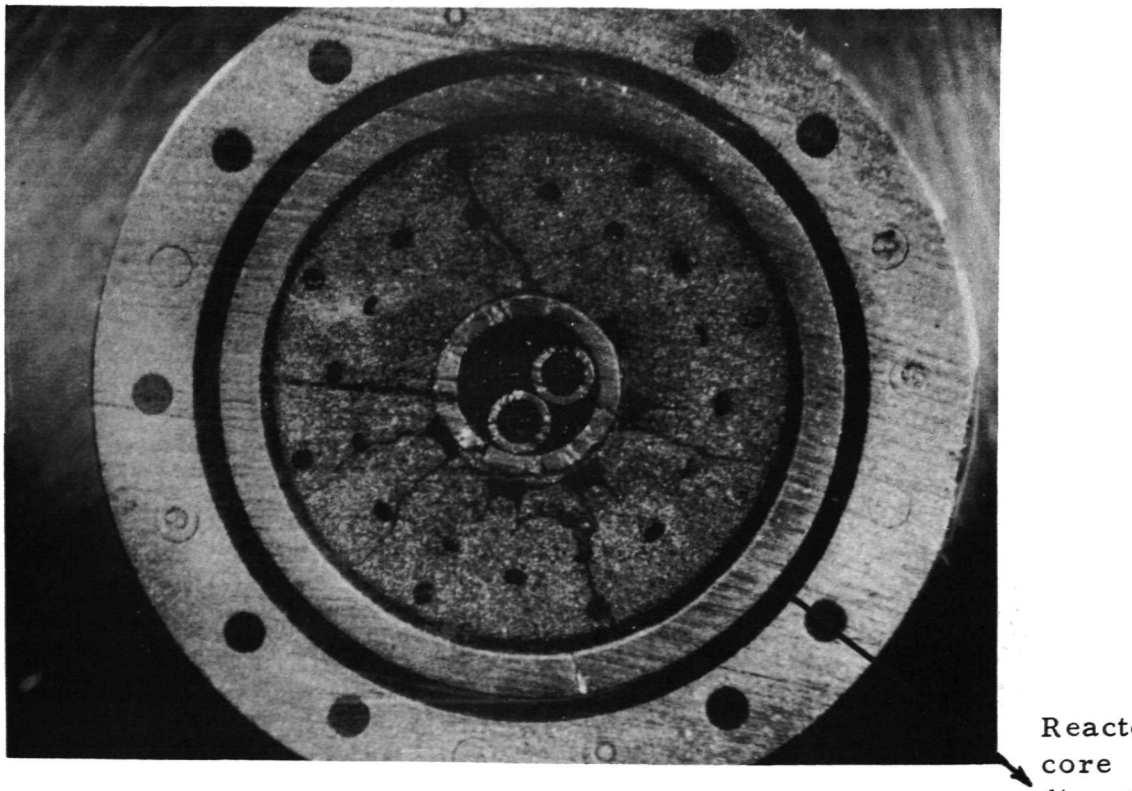

(h) Sample No. 5 bottom surface

Fig. 11. Macroscopic appearances of the surfaces of sample sections of V-2C fuel pin in the as-sectioned conditions (5X) (Sheet 5 of 6)

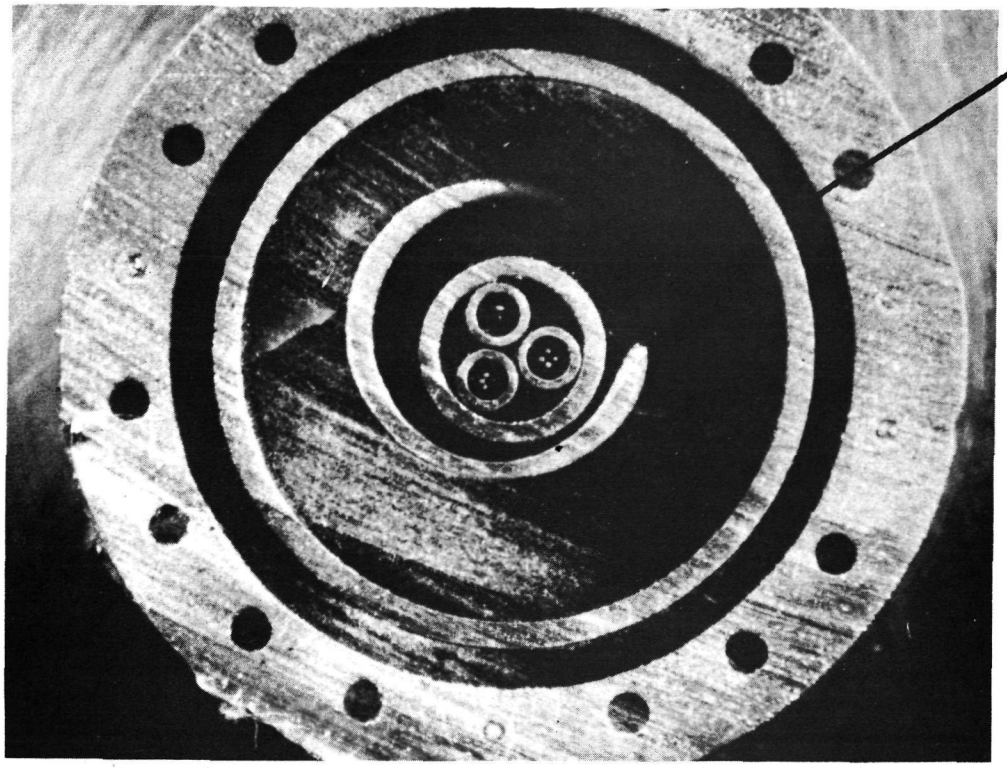

(k) Sample No. 6 top surface

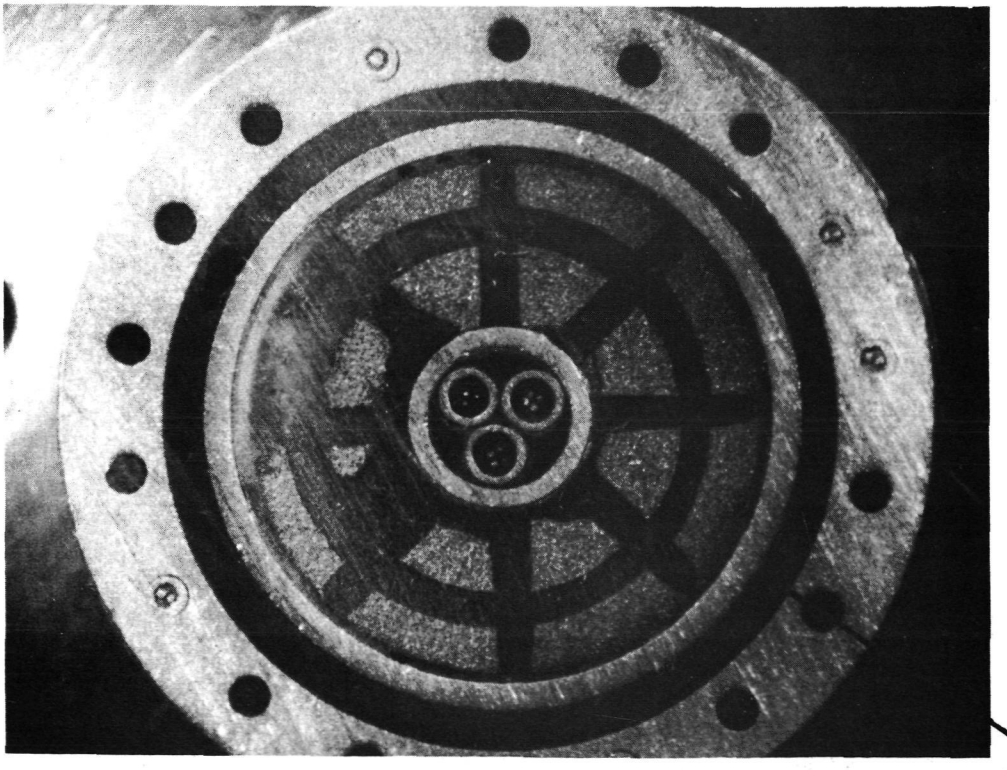

(j) Sample No. 6 bottom surface. Note fission gas venting grooves

Fig. 11. Macroscopic appearances of the surfaces of sample sections of V-2C fuel pin in the as-sectioned conditions (5X) (Sheet 6 of 6)

Reactor core direction

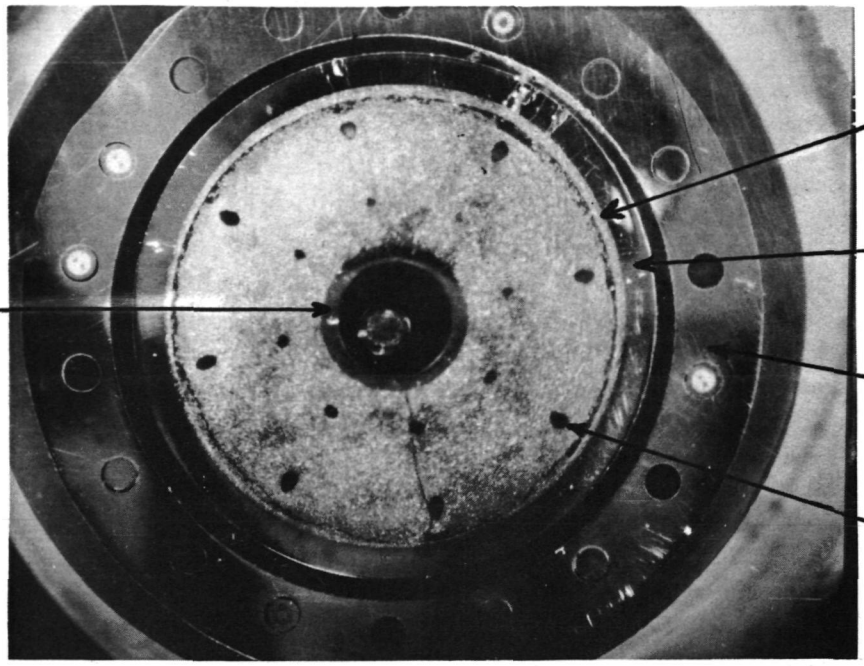

(a) Sample V-2C-2B*

Reactor core direction

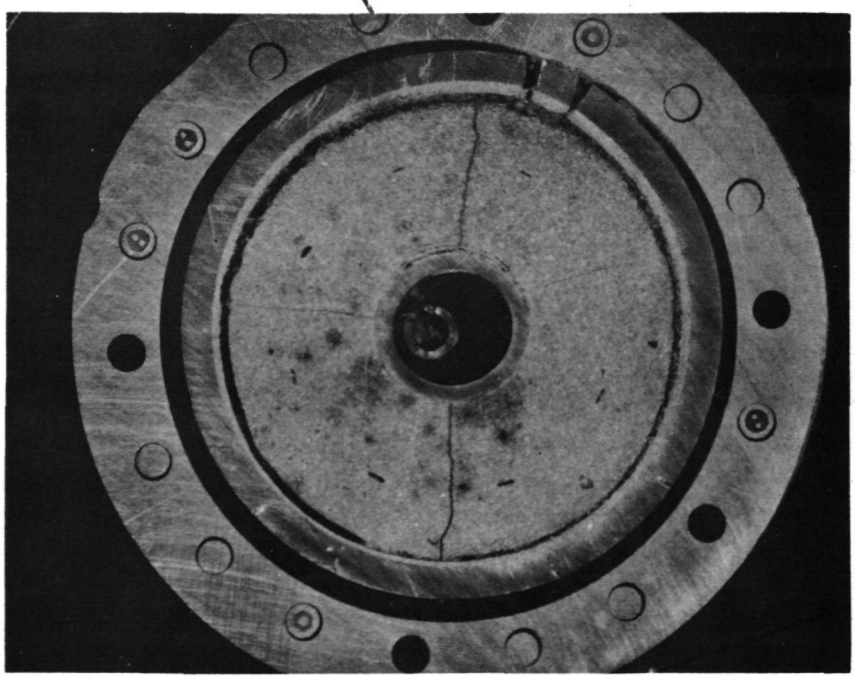

(b) Sample V-2C-3B*

Fig. 12. Macroscopic appearances of polished bottom surfaces of Samples No. 2, 3, 4, and 5 of V-2C fuel pin. (4.5X)
*B refers to bottom surface of sample (Sheet 1 of 2)

Reactor core direction

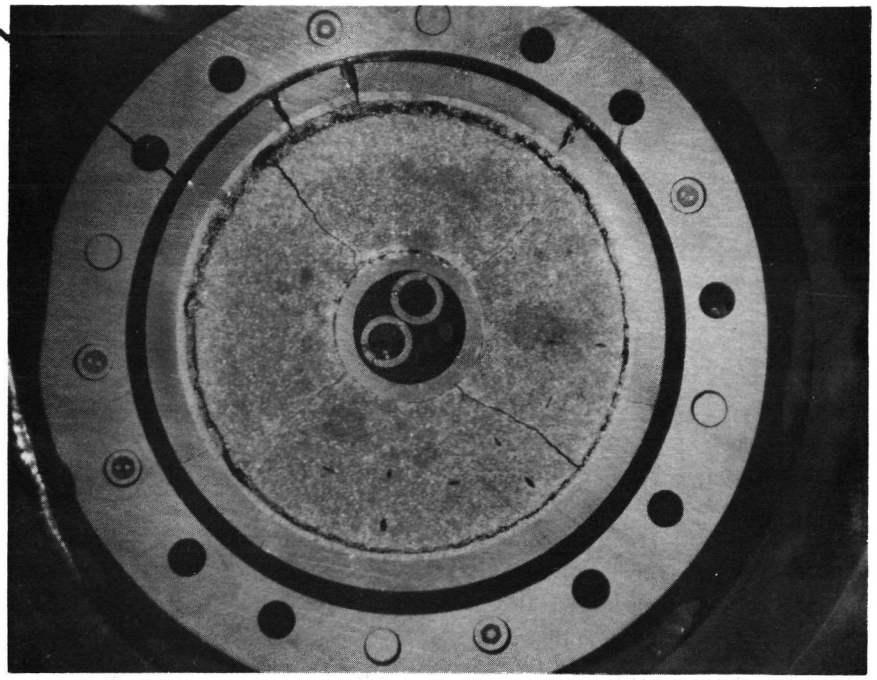

(c) Sample V-2C-4B*

Reactor core direction

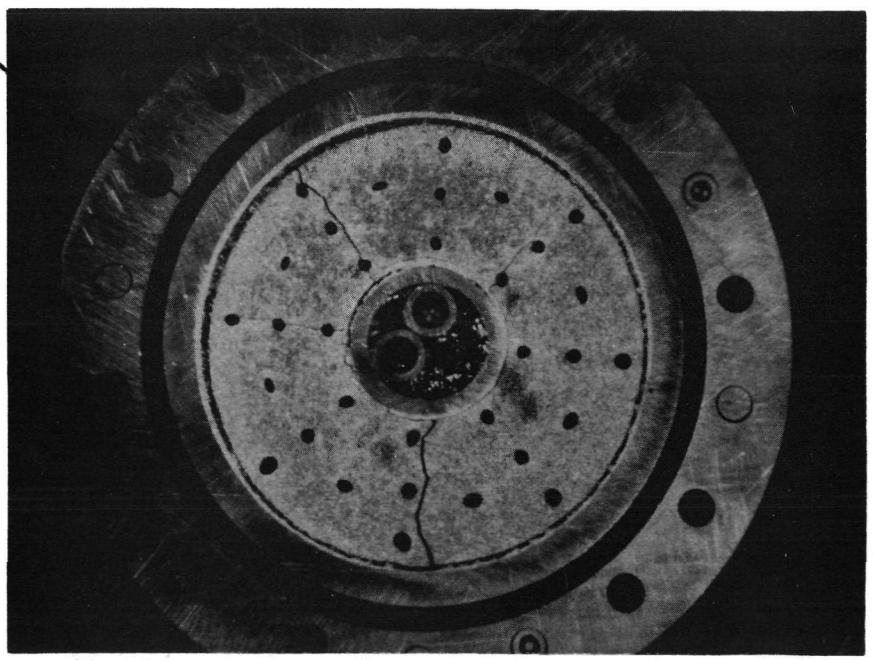

(d) Sample V-2C-5B*

Fig. 12. Macroscopic appearances of polished bottom surfaces of Samples No. 2, 3, 4, and 5 of V-2C fuel pin. (4.5X)
*B refers to bottom surface of sample (Sheet 2 of 2)

the fission gas venting holes have shrunk to various degrees in these samples, depending upon the temperature of the fuel pellet and the relative position of these holes with respect to the reactor core. For instance, the fission gas venting holes in Samples V-2C-3T and V-2C-4B (2000°K) have been reduced to slits, but no significant change in the size of the fission gas venting holes occurred in Sample V-2C-5B which is cooler (1885°K), (see Fig. 10). Within the same carbide body of Sample No. 3, the fission gas venting holes disappeared on the side close to the reactor core, while on the opposite side, remnants of some of the holes can still be found. The fuel-cladding interaction layer appears as a thin white ring at the fuel-cladding interface in the polished samples. For each sample, the reaction layer is the thickest at the location where high temperature and high burnup rate are expected and where cladding expansion and cracking occurred.

4.2. V-2D Fuel Pin

V-2D fuel pin was sectioned into five samples. The positions of these samples relative to that of the fuel pellets in the fuel pin are illustrated in Fig. 13. Figure 14(a) through (i) show the macroscopic appearances of the top and bottom surfaces of these samples in the as-sectioned conditions. Figure 15(a) through (d) show the mounted and polished bottom surfaces of Samples No. 2, 3, 4, and 5. Cracks occurred in the claddings of all four samples, and Sample No. 3 lost part of its cladding during attempts to remove the V-2D fuel pin from the Inconel containment (see Section 2 of this report). Although the deformation of the cladding is apparent for Samples No. 2, 3,

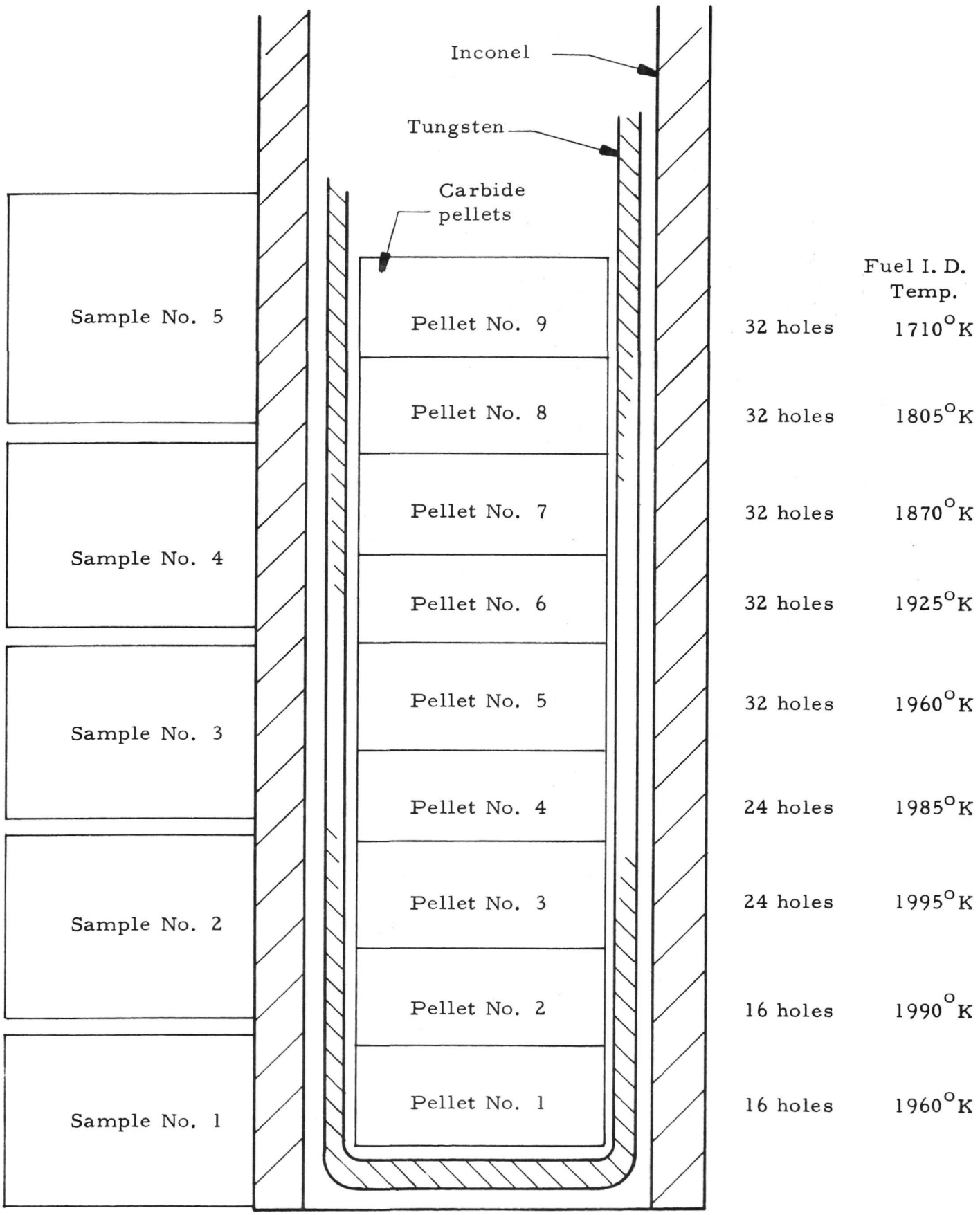

Fig. 13. Positions of samples taken from V-2D fuel pin relative to that of the fuel pellets in the fuel pin

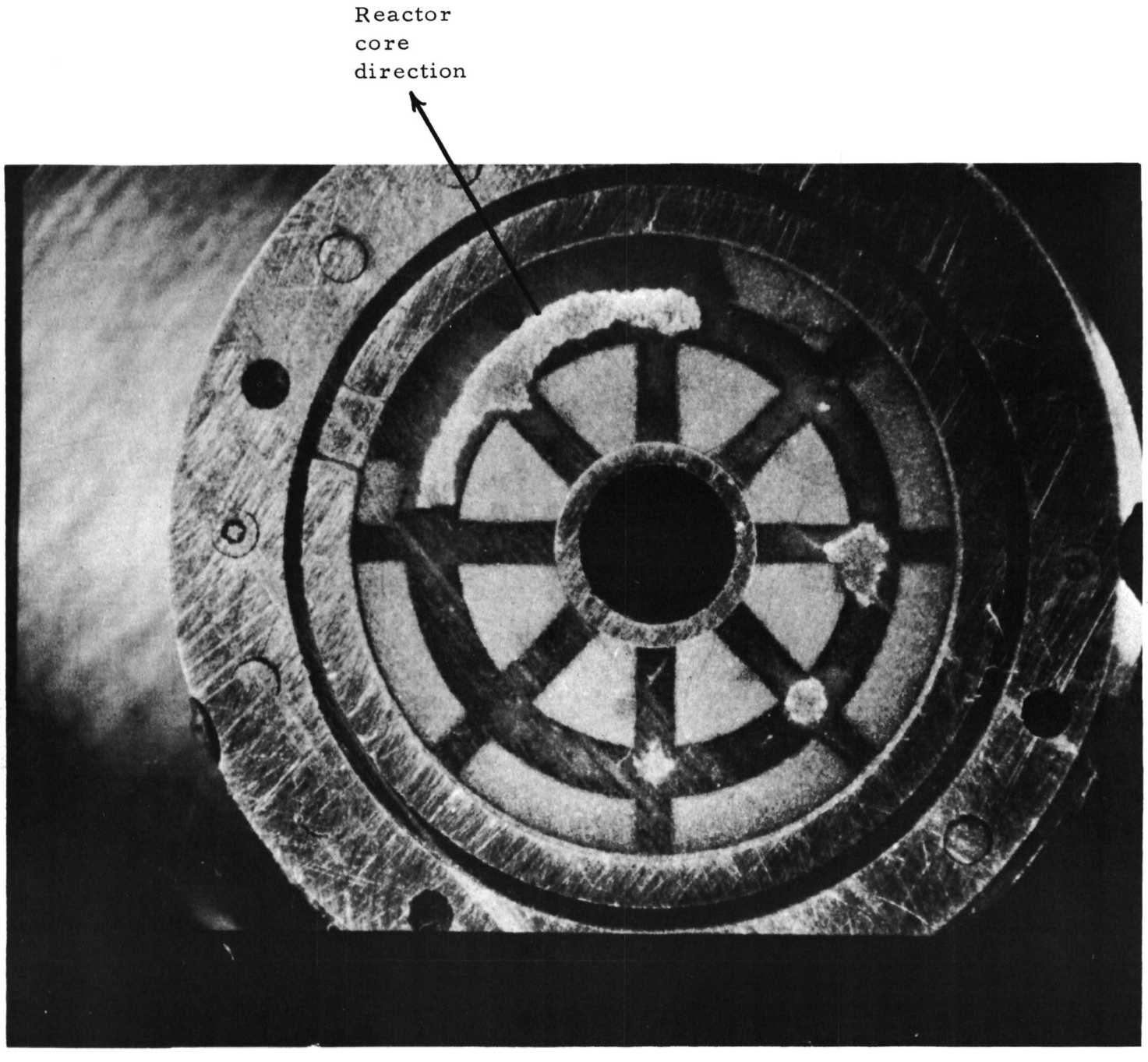

(a) Sample No. 1 top surface. Note fission gas venting grooves

Fig. 14. Macroscopic appearances of the surfaces of sample sections of V-2D fuel pin in the as-sectioned conditions (7.5X) (Sheet 1 of 5)

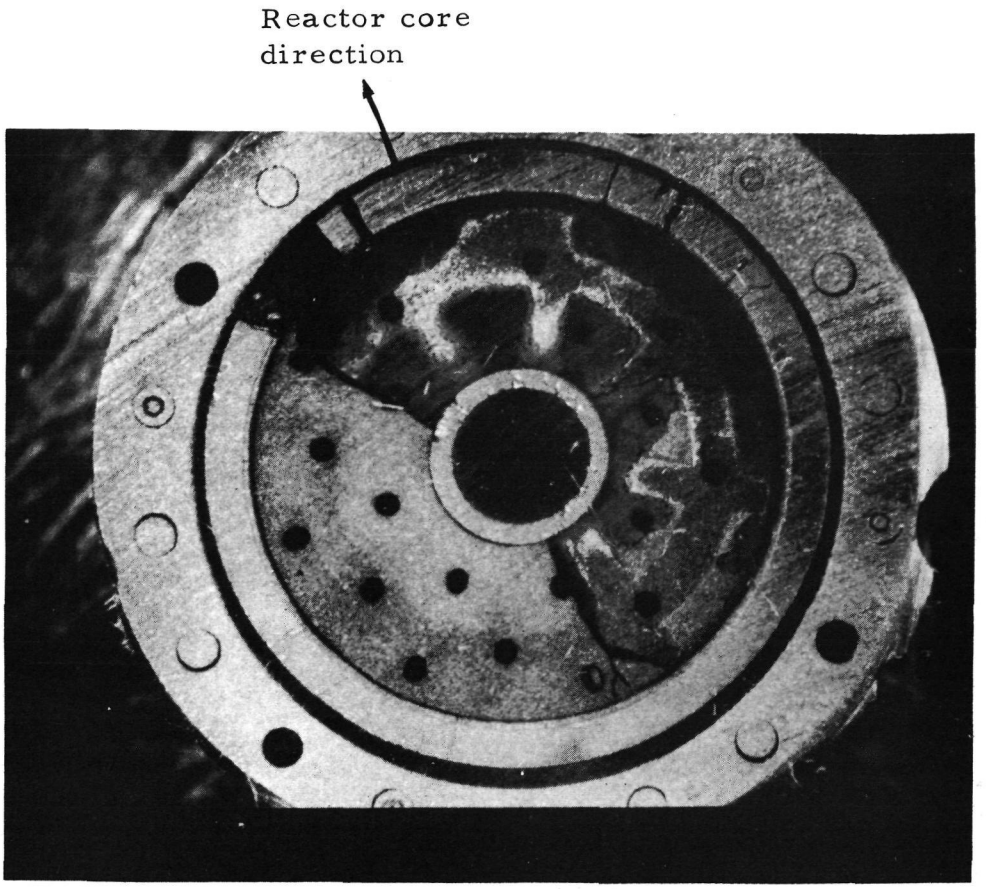

(c) Sample No. 2 top surface

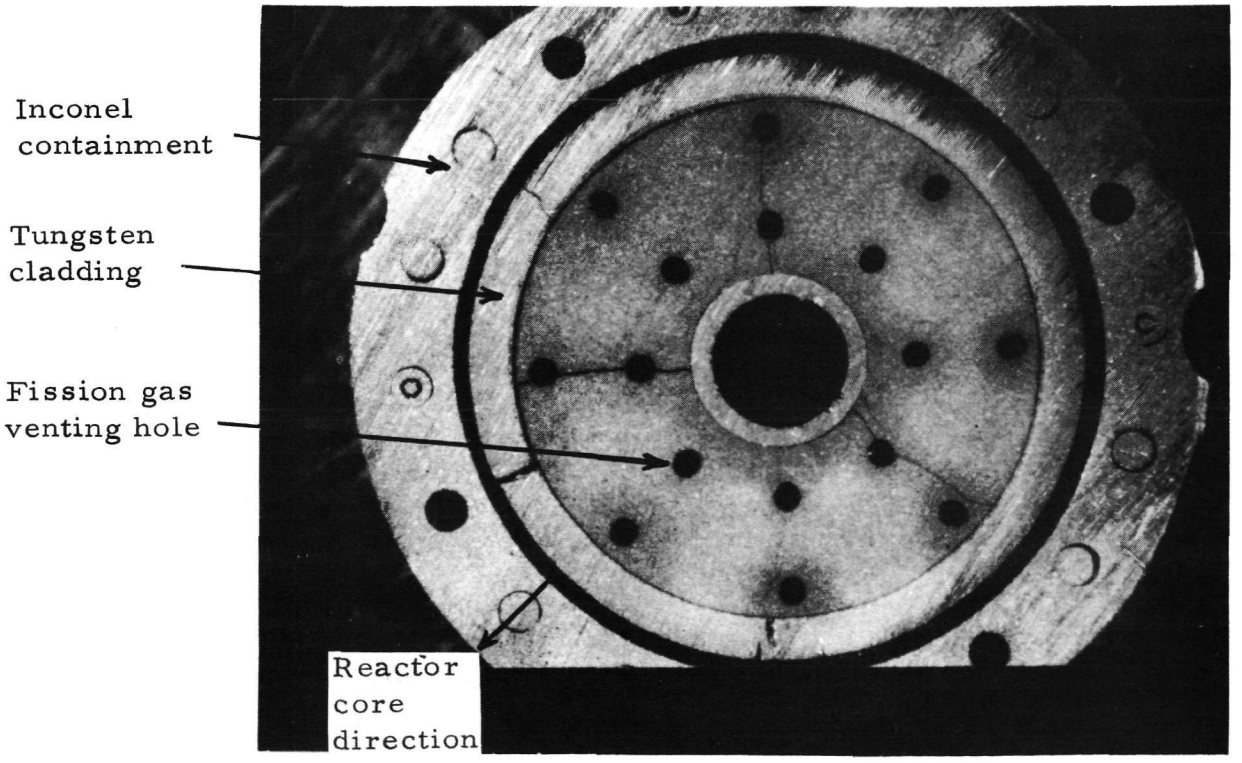

(b) Sample No. 2 bottom surface

Fig. 14. Macroscopic appearances of the surfaces of sample sections of V-2D fuel pin in the as-sectioned conditions (5X) (Sheet 2 of 5)

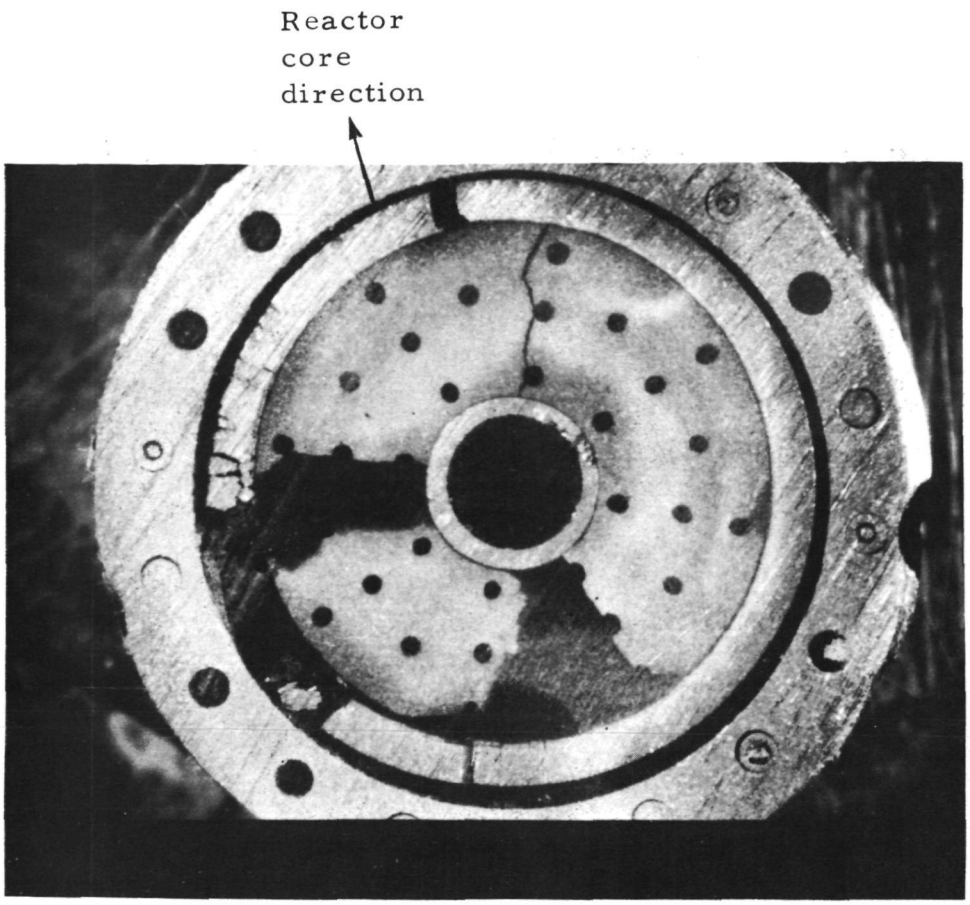

(e) Sample No. 3 top surface

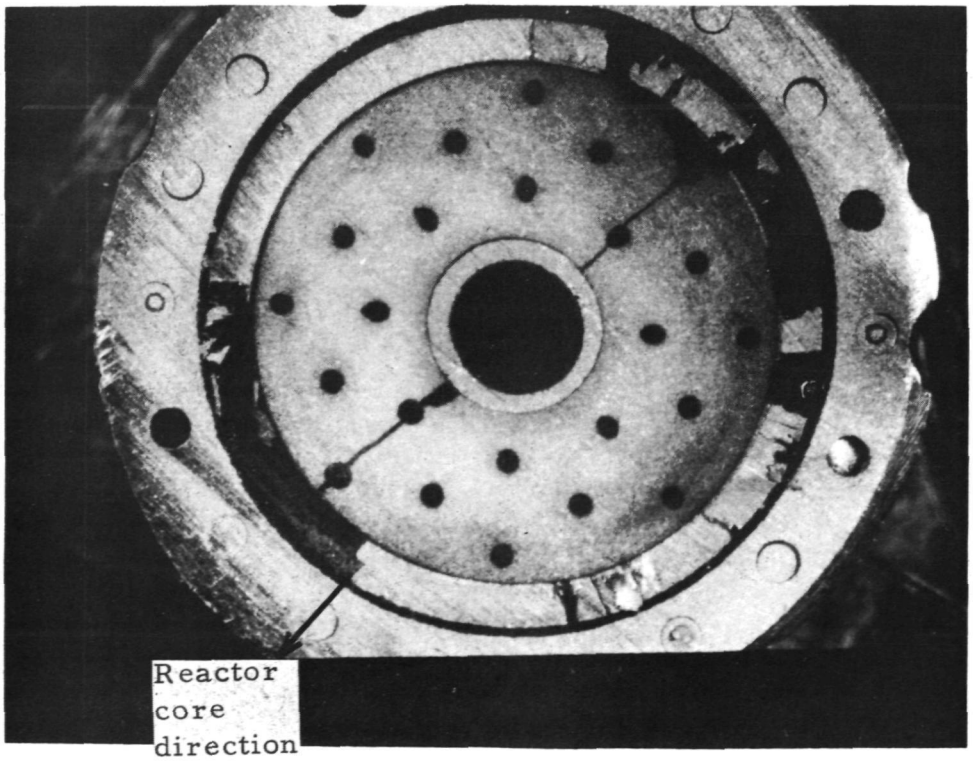

(d) Sample No. 3 bottom surface

Fig. 14. Macroscopic appearances of the surfaces of sample sections of V-2D fuel pin in the as-sectioned conditions (5X) (Sheet 3 of 5)

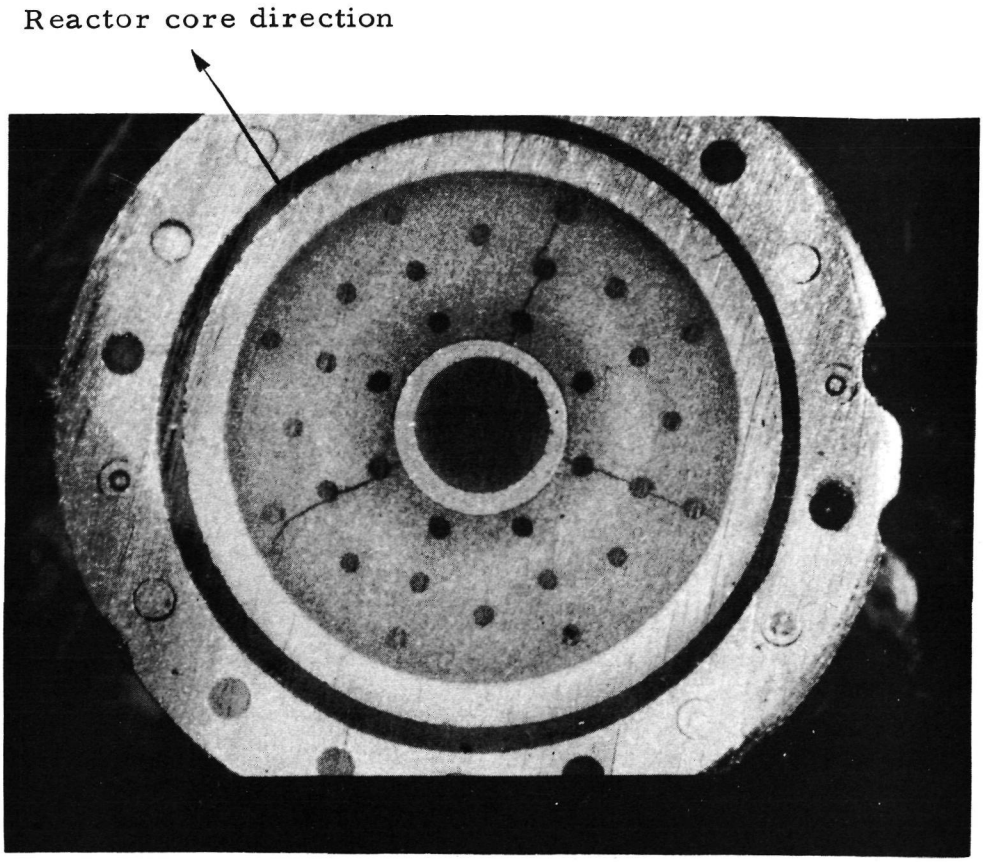

(g) Sample No. 4 top surface

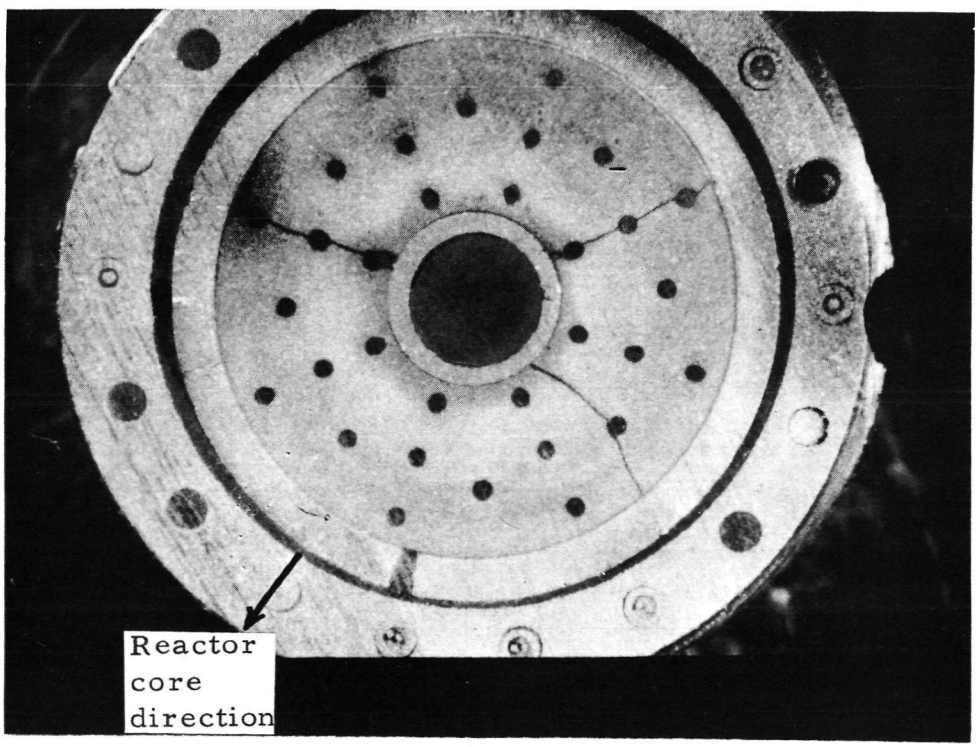

(f) Sample No. 4 bottom surface

Fig. 14. Macroscopic appearances of the surfaces of sample sections of V-2D fuel pin in the as-sectioned conditions (5X) (Sheet 4 of 5)

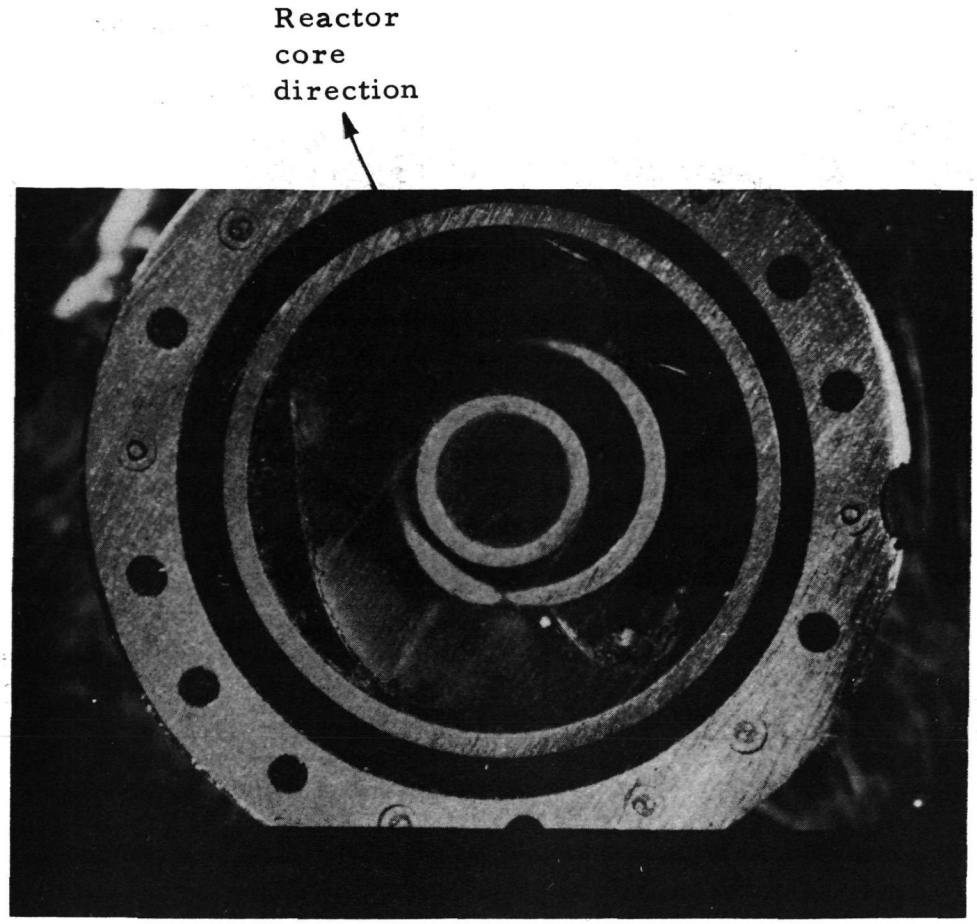

(i) Sample No. 5 top surface

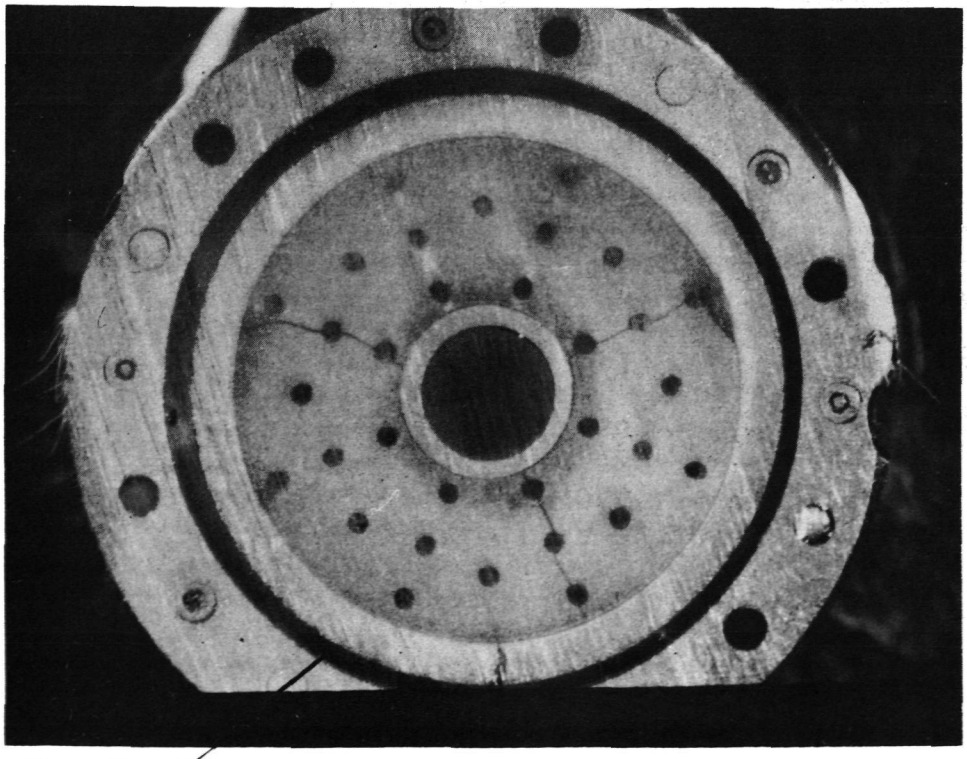

(h) Sample No. 5 bottom surface

Fig. 14. Macroscopic appearances of the surfaces of sample sections of V-2D fuel pin in the as-sectioned conditions (5X) (Sheet 5 of 5)

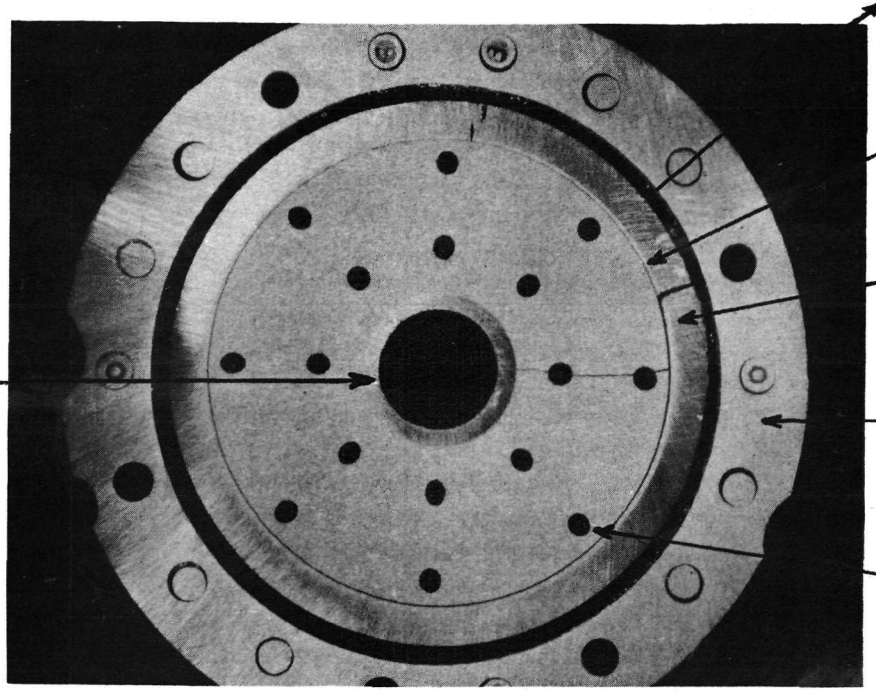

(a) Sample V-2D-2B*

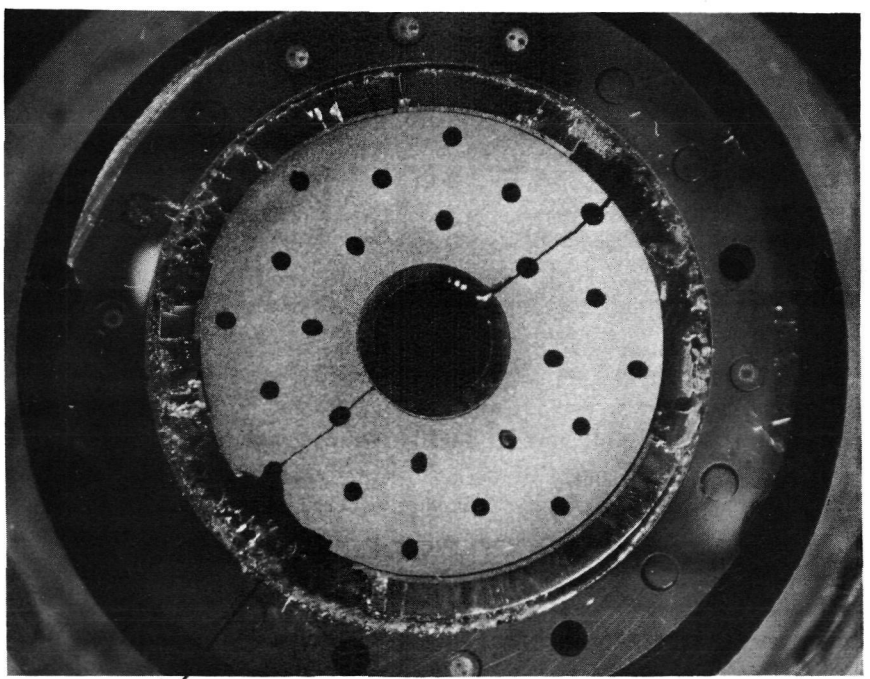

(b) Sample V-2D-3B*

Fig. 15. Macroscopic appearances of polished bottom surfaces of Samples No. 2, 3, 4, and 5 of V-2D fuel pin. (4.5X)
*B refers to bottom surface of sample (Sheet 1 of 2)

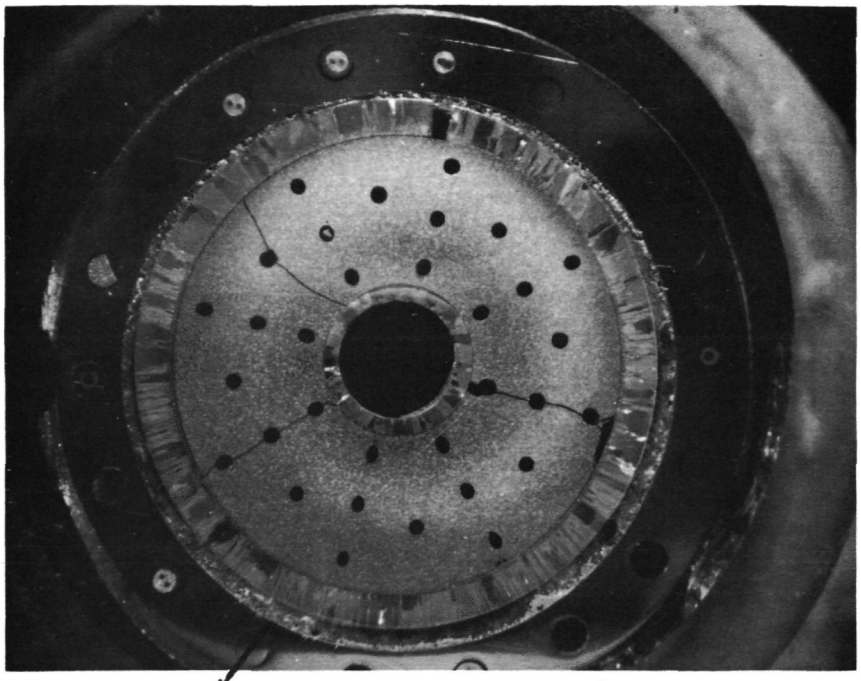

Reactor core direction

(c) Sample V-2D-4B*

Reactor core direction

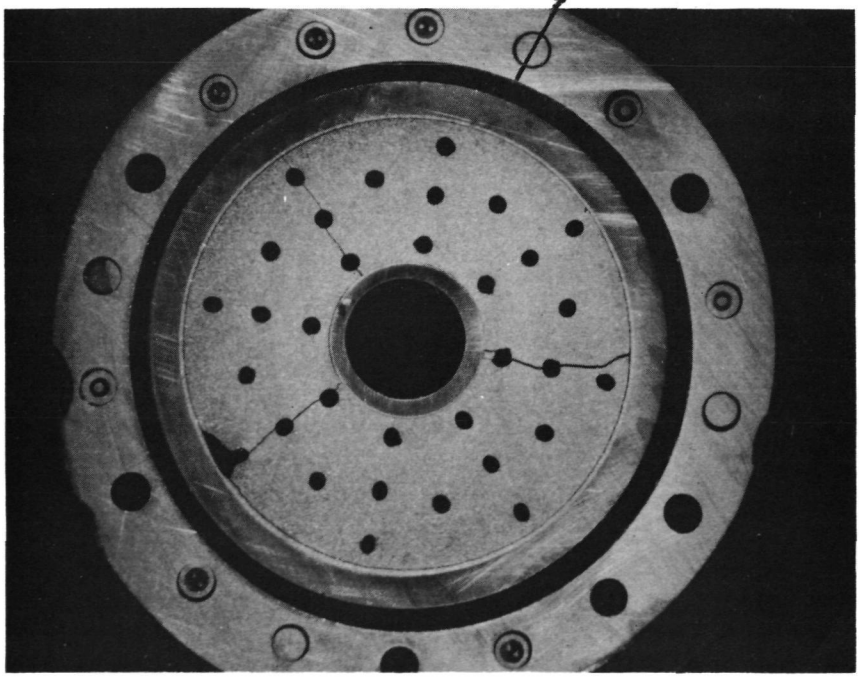

(d) Sample V-2D-5B*

Fig. 15. Macroscopic appearances of polished bottom surfaces of Samples No. 2, 3, 4, and 5 of V-2D fuel pin. (4.5X)
*B refers to bottom surface of sample (Sheet 2 of 2)

and 4, the fission gas venting holes remain in excellent shape in all cases. It is believed that the 50UC-50ZrC fuel material is stronger than 90UC-10ZrC; therefore the swelling of the fuel material did not deform the fission gas venting holes but caused the expansion and cracking of the tungsten cladding. The thicknesses of the fuel-cladding interaction layers are much less than that observed for the V-2C fuel pin, and do not vary significantly in the temperature range for V-2D fuel pin irradiation.

5. DIMENSION MEASUREMENTS

Measurements were made at various circumferential positions on the outside diameters of the tungsten claddings and the thermocouple wells of Samples V-2C-2B, V-2C-3B, V-2C-4B, V-2C-5B for the V-2C fuel pin, and Samples V-2D-2B, V-2D-3B, V-2D 4B, V-2D-5B, for the V-2D fuel pin. (B refers to bottom surface of the sample.) Composite photographs at 5X magnification were taken of each sample, with a calibrated scale lying across the positions where the measurements were to be made. The scale, graduated in 0.25 mm (10 mil) divisions, was used to obtain the magnification factor of the photographs taken. The dimensions of the sample on the photograph, measured with the same scale, were converted to the true dimensions by using the magnification factor determined. It is estimated that the uncertainty of the measurements is about ±.025 mm (± 1 mil).

The results obtained on the expansion of the tungsten claddings of these samples are shown in Fig. 16 for V-2C fuel pin and in Fig. 17 for V-2D fuel

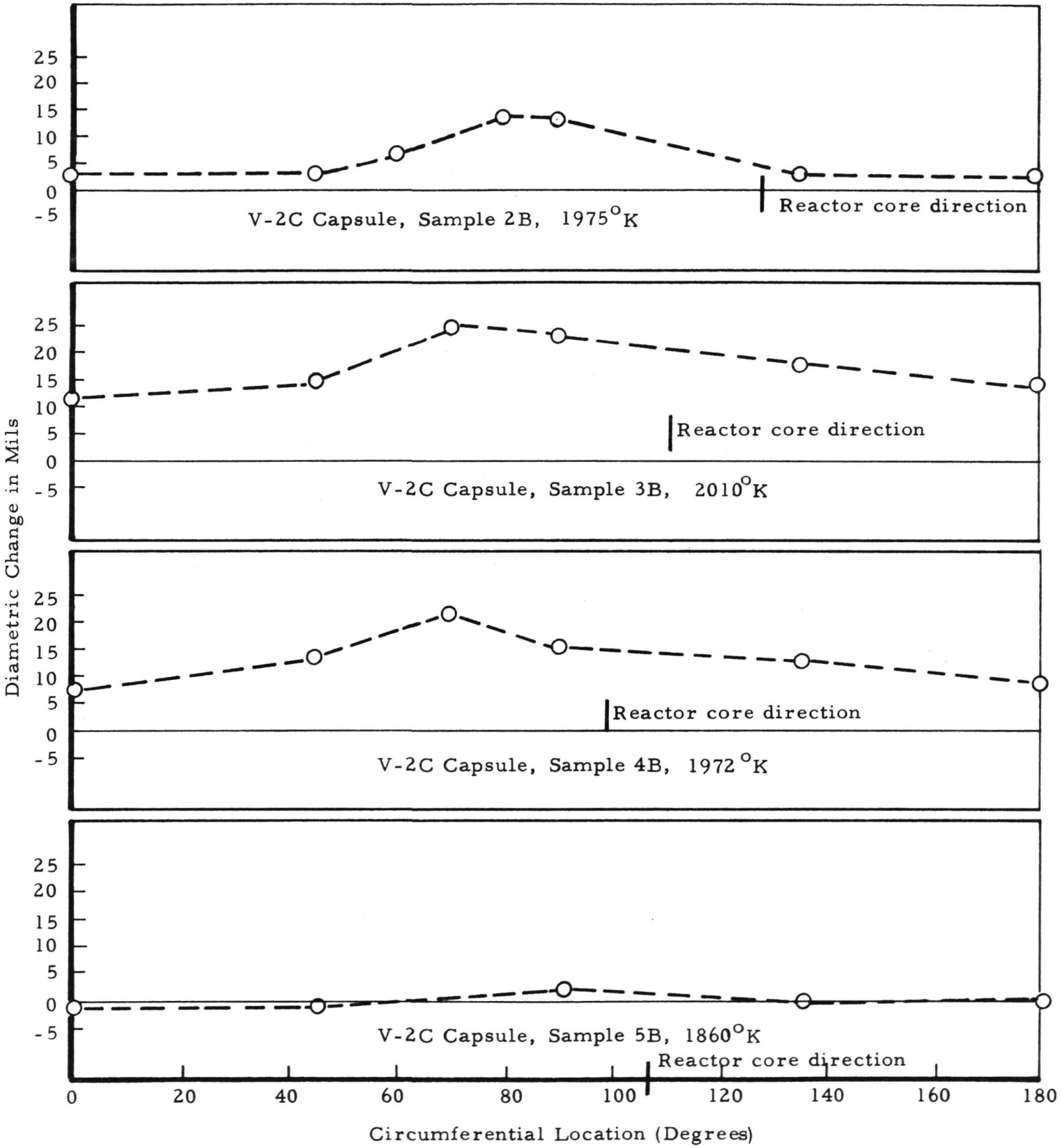

Fig. 16. Swelling behaviors of V-2C fuel pin at various axial locations and average fuel temperature

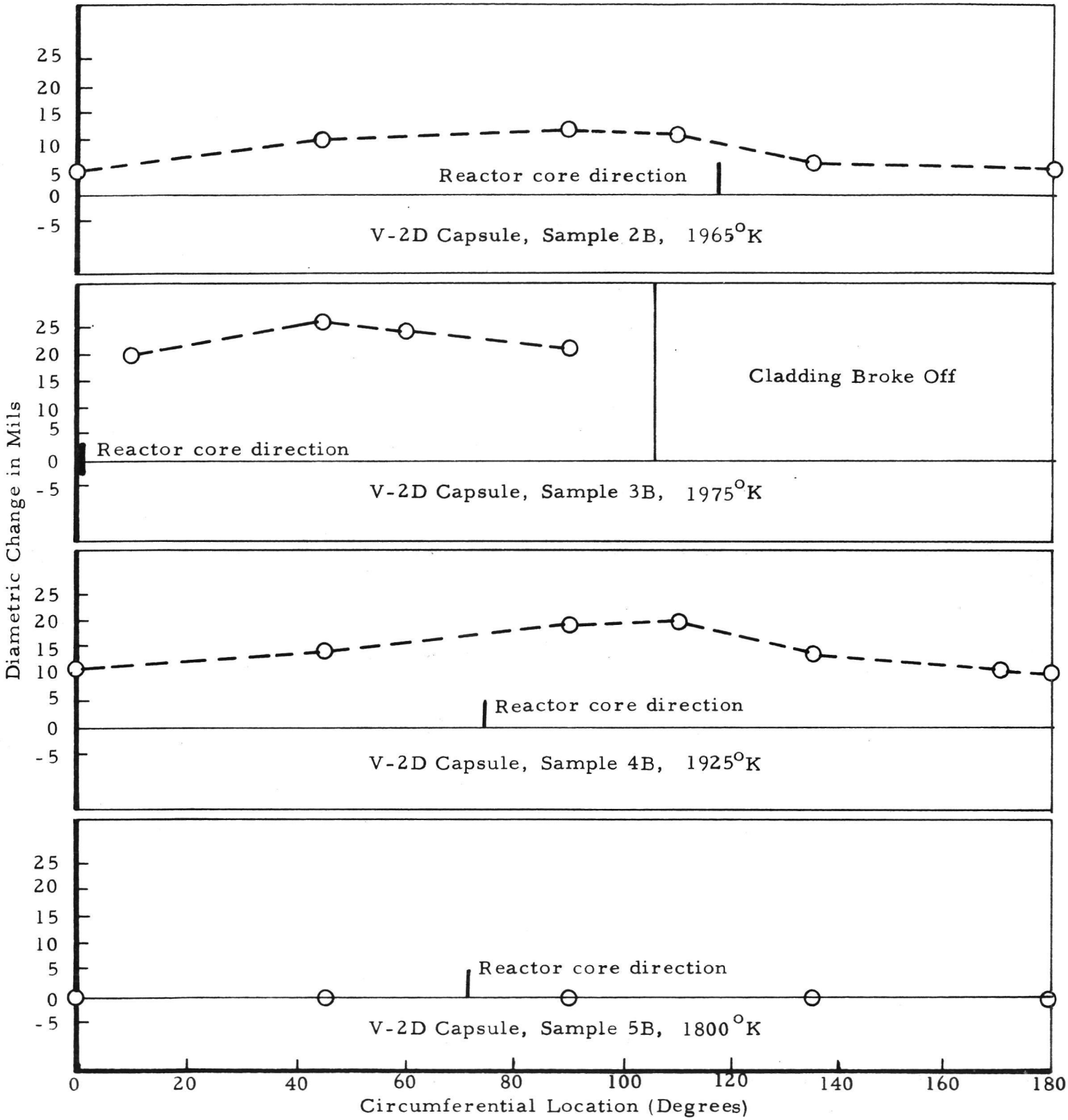

Fig. 17. Swelling behaviors of V-2D fuel pin at various axial locations and average fuel temperature

pin. The swelling is non-uniform with respect to circumferential positions for both fuel pins. Using the scribe mark made at Plum Brook it is estimated that the maximum swelling for V-2C fuel pin occurs at a position about 40° from the reactor core side and the maximum swelling for V-2D fuel pin occurs at a position about 50° from the reactor core side, see Fig. 18. It is interesting to note that the swelling is very temperature sensitive. Sample V-2C-5B and Sample V-2D-5B, which were irradiated at 1860° and 1800°K respectively, show no significant cladding expansion. On the other hand, Sample V-2C-3B and Sample V-2D-3B, which were irradiated at 2010°K and 1975°K respectively, show maximum diametric expansions of .64 mm (25 mils).

The measured diameters of the tungsten thermocouple wells in the fuel pins at various circumferential positions are listed in Table 2. It can be seen that the thermocouple well at Samples V-2C-2B, V-2C-4B, V-2C-5B, V-2D-2B, and V-2D-5B are essentially round and the measured diameters do not differ significantly from the design value (4.57 mm). The thermocouple well at Samples V-2C-3B, V-2D-3B, and V-2D-4B, however, have been deformed into elliptical shape by fuel swelling. In each case, the major axis of the ellipse is about 45° from the position of the maximum bulge of the cladding in a clockwise direction. The differences between the major and the minor axes amount to .33mm (13 mils), .23 mm (9 mils), and .10 mm (4 mils) for Sample V-2C-3B, V-2D-3B, and V-2D-4B respectively.

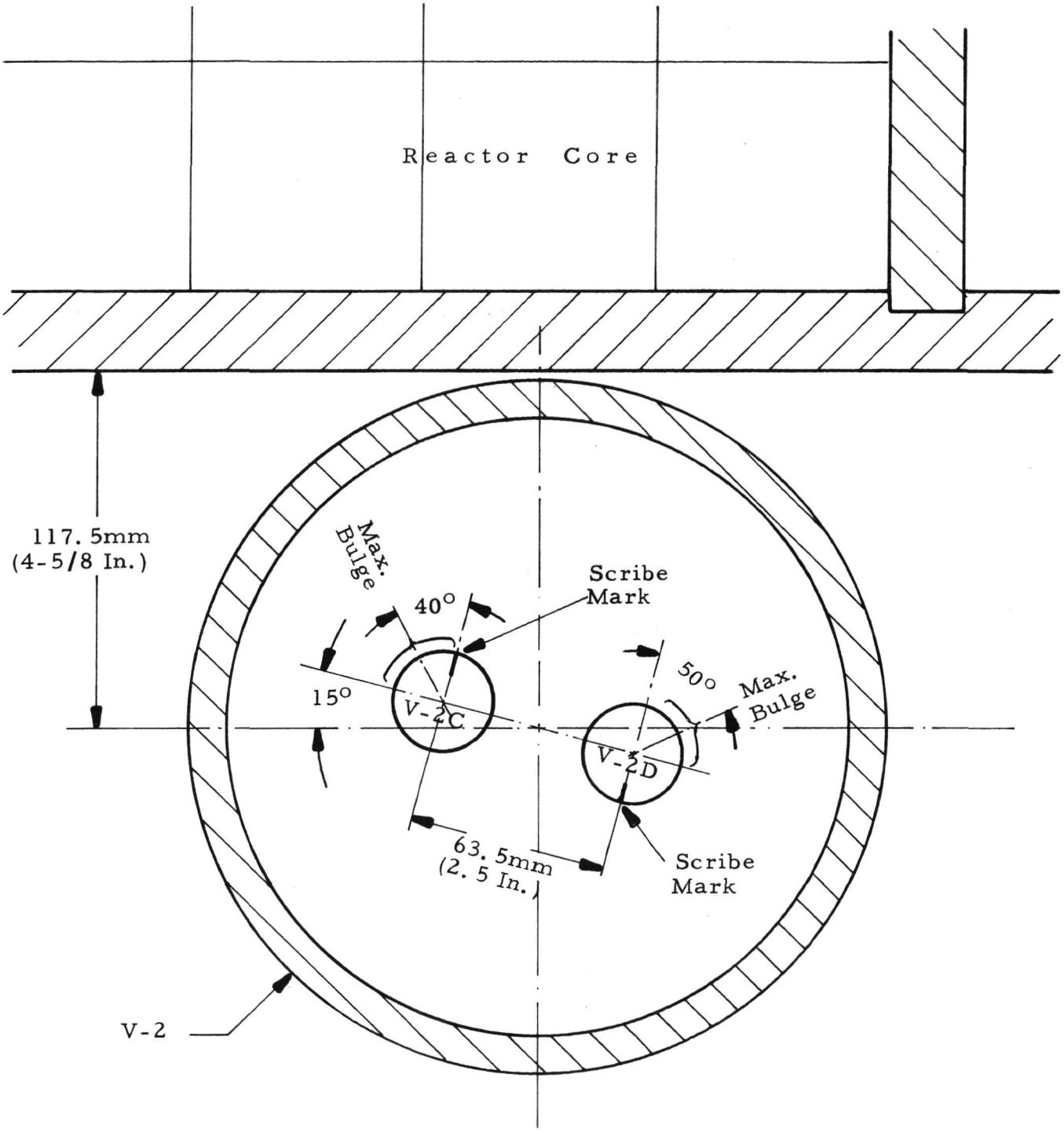

Fig. 18. Plan view of V-2C and V-2D during irradiation

TABLE 2

MEASURED DIAMETERS OF TUNGSTEN THERMOCOUPLE WELLS IN V-2C AND V-2D FUEL PINS AT VARIOUS CIRCUMFERENCIAL POSITIONS

Fuel Pin Designation	Sample Designation	Diameter mm (Inch)				Difference* Between Maximum Diameter and Minimum Diameter (mils)
		Maximum Cladding Bulge Position	45° Clockwise From Maximum Bulge	90° Clockwise From Maximum Bulge	135° Clockwise From Maximum Bulge	
V-2C	V-2C-2B	4.62 (0.182)	4.57 (0.180)	4.62 (0.182)	4.57 (0.180)	-
	V-2C-3B	4.52 (0.178)	4.78 (0.188)	4.45 (0.175)	4.52 (0.178)	.33 (13)
	V-2C-4B	4.57 (0.180)	4.62 (0.182)	4.57 (0.180)	4.57 (0.180)	-
	V-2C-5B	4.57 (0.180)	4.57 (0.180)	4.62 (0.182)	4.57 (0.180)	-
V-2D	V-2D-2B	4.57 (0.180)	4.62 (0.182)	4.62 (0.182)	4.57 (0.180)	-
	V-2D-3B	4.70 (0.185)	4.80 (0.189)	4.57 (0.180)	4.57 (0.180)	.23 (9)
	V-2D-4B	4.57 (0.180)	4.65 (0.183)	4.57 (0.180)	4.55 (0.179)	.10 (4)
	V-2D-5B	4.57 (0.180)	4.62 (0.182)	4.62 (0.182)	4.60 (0.181)	-

* Any difference less than .051mm (2 mils) is neglected.

6. METALLOGRAPHIC EXAMINATIONS OF FUEL PIN COMPONENTS

Metallographical examinations were carried out on the microstructures of the fuel materials, the tungsten claddings, the tungsten thermocouple wells and the fuel-cladding interfaces of Samples V-2C-2B, V-2C-3B, V-2C-4B, and V-2C-5B of the V-2C fuel pin, and Samples V-2D-2B, V-2D-3B, V-2D-4B, and V-2D-5B of the V-2D fuel pin. In addition, similar studies were made on the longitudinal cross sections of Sample No. 1 of V-2C fuel pin and Sample No. 1 of V-2D fuel pin, which contain the bottoms of these fuel pins. The results are described as follows.

6.1. V-2C Fuel Pin

(1) Carbide fuel material

The microstructures of the irradiated 90UC-10ZrC fuel material differ from that of the unirradiated 90UC-10ZrC fuel material. The difference is illustrated by Figures 19(a) and (b). Figure 19(a) shows the microstructures of the irradiated 90UC-10ZrC fuel material in Sample V-2C-2B near the bulge side of the cladding, while Fig. 19(b) represents the microstructures of the unirradiated V-2C-2B fuel material at the same magnification. It can be seen that the fine porosities in the fuel material become agglomerated into much larger voids. This change in microstructures was not observed in out-of-pile isothermal sintering studies; therefore it must be caused by factors closely associated with in-pile irradiation. It is possible that the sintering process is accelerated by the presence of lattice defects produced

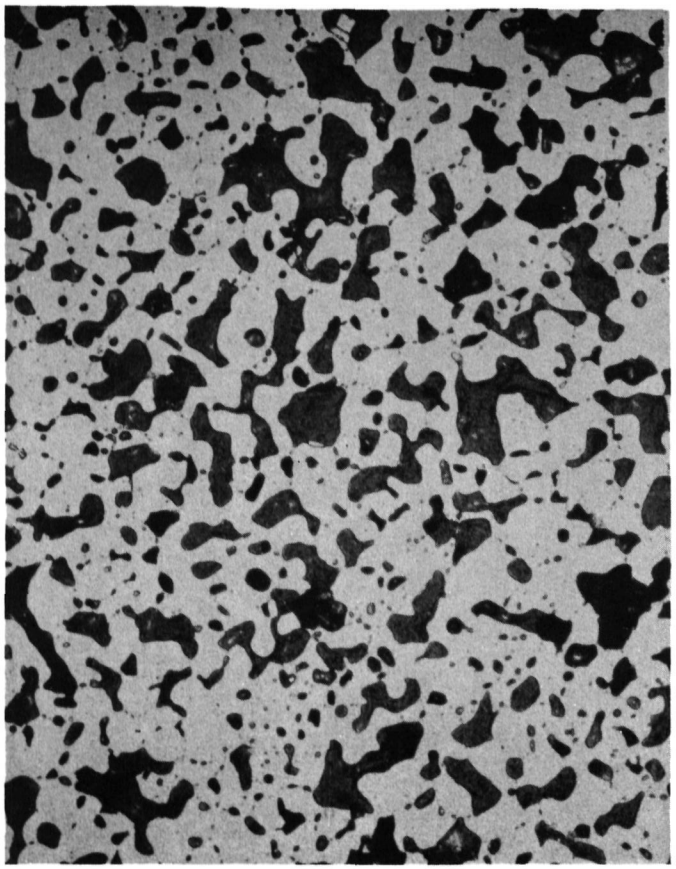

(a) Irradiated, near bulge side of cladding

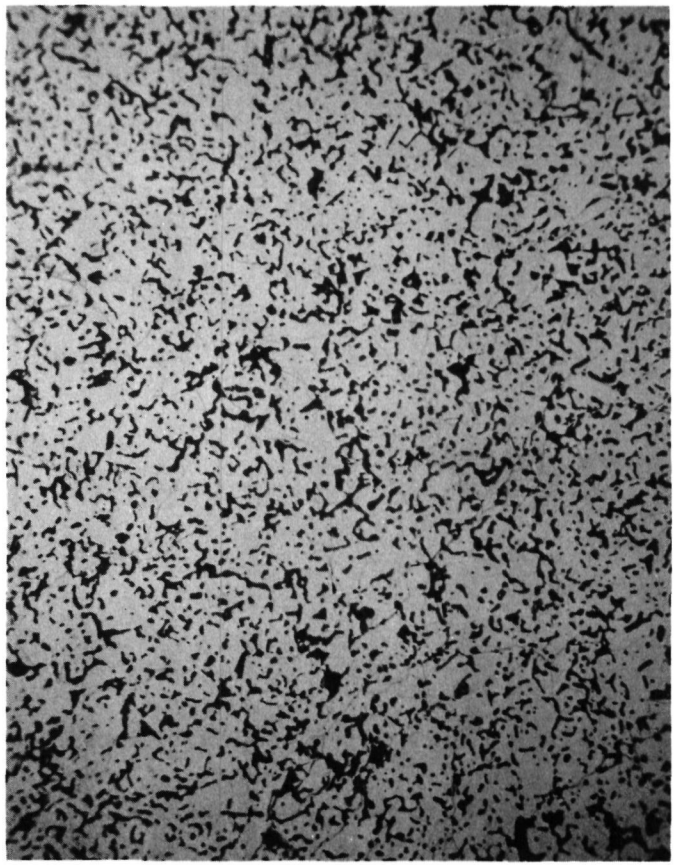

(b) Unirradiated

Fig. 19. Comparison of the microstructures of irradiated and unirradiated 90UC-10ZrC fuel materials of Sample V-2C-2B (200X)

by fission fragments and the enrgy deposited in the lattice when the fission fragments pass through. It is also possible that the pressure generated by fission gas trapped in closed pores may eliminate neighboring open pores by mechanical effects similar to hot pressing. A third possibility is the sweep of fine pores up the radial temperature gradient of the fuel body by vapor transport. This, however, is not believed to be an influential factor because of the high thermal conductivity and low vaporization rate of the carbide fuels. The disappearance of fine porosities does not imply that the irradiated fuel material has become denser. In fact quantitative metallographical analysis of Figs. 19(a) and (b) showed that while the unirradiated fuel is 76% dense, the irradiated fuel is only 60% dense. Thus at least some of the large pores are closed pores filled with fission gas. It is not known, however, what fraction of these pores consists of closed pores.

Figures 20(a), (b) and (c) show respectively the irradiated fuel structures of Samples V-2C-3B, V-2C-4B , and V-2C-5B near the bulge side of the cladding. The irradiated fuel structures for Samples V-2C-3B, V-2C-4B do not differ significantly from each other and from that of Sample V-2C-2B (Fig. 19(a)). The irradiated fuel structures for Sample V-2C-5B which showed much less fuel swelling than Samples V-2C-2B, V-2C-3B, and V-2C-4B, appear to be slightly denser. Quantitative metallographical analysis yielded densities of about 55% of theoretical value for the fuel materials of Samples V-2C-3B and V-2C-4B, and about 65% for the fuel material of Sample V-2C-5B.

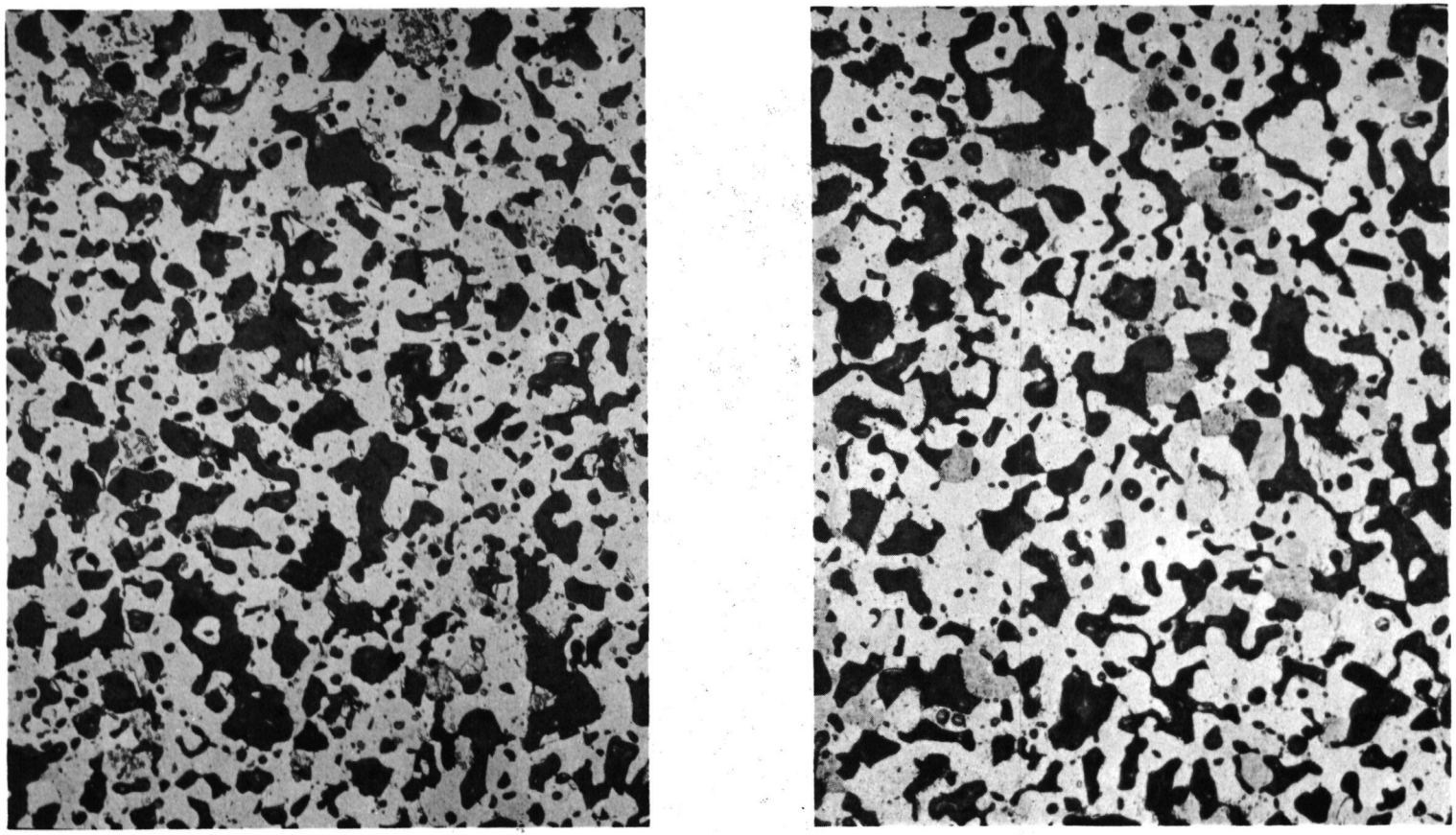

(a) Sample V-2C-3B

(b) Sample V-2C-4B

Fig. 20. Microstructures of irradiated 90UC 10ZrC fuel materials in Samples V-2C-3B, V-2C-4B, and V 2C-5B near the bulge side of the cladding (200X) (Sheet 1 of 2)

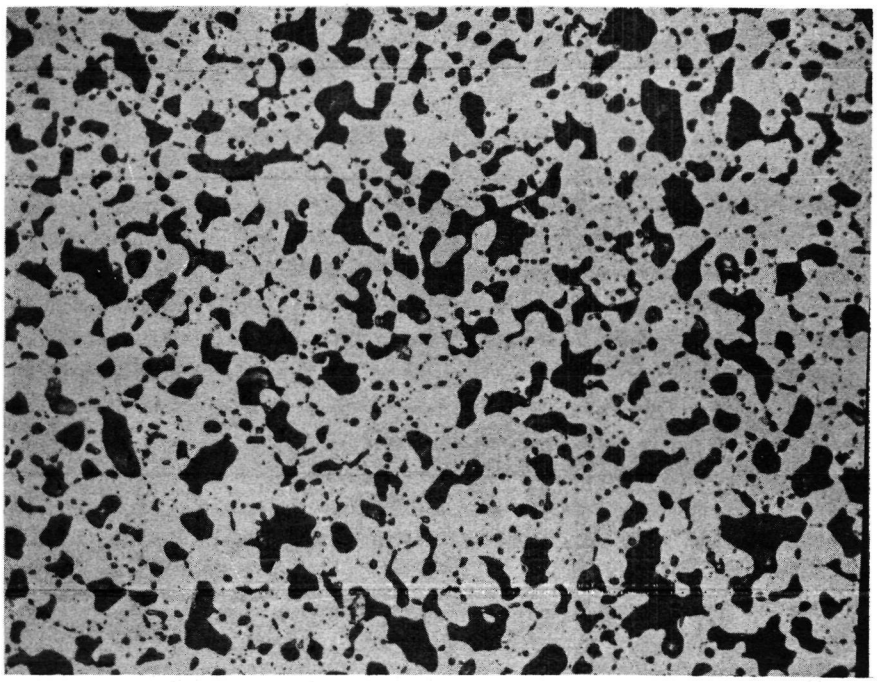

(c) Sample V-2C-5B

Fig. 20. Microstructures of irradiated 90UC-10ZrC fuel materials in Samples V-2C-3B, V-2C-4B, and V 2C-5B near the bulge side of the cladding (200X) (Sheet 2 of 2)

Figure 21 compares the irradiated 90UC-10ZrC fuel structures of Sample V-2C-3B near the cladding and near the tungsten thermocouple well at four different circumferential positions. The difference, if any, is slight. The fuel near the thermocouple well is usually about several percent less dense than that near the cladding, presumably due to the high temperature and the higher fission gas pressure in the closed pores. These observations also apply to the fuel materials in Samples V-2C-2B, V-2C-4B , and V-2C-5B.

Figures 22(a) and (b) show typical microstructures of irradiated fuel materials which were etched to bring out the dispersed phases. It can be seen that the fuel near the central thermocouple well is more porous than that near the cladding. There does not seem to be any difference in the distribution of the white-colored dispersion phases at these two locations. The composition of these dispersion phases will be discussed in a latter section of this report.

(2) Tungsten cladding

In all the samples examined, the irradiated cladding showed no excessive grain growth and the irradiated cladding essentially retained its columnar grain structures. On the side of the cladding that exhibited maximum deformation, i. e. the bulge side, the cladding failed by grain boundary void formation and cracking. Typical examples are shown in Figs. 23(a) through (c) for Samples V-2C-2B, V-2C-3B and V-2C-4B, respectively. It is believed that the defects generated by the high stress existing at these locations migrated toward the fluorine bubbles present in the fluoride tungsten cladding.

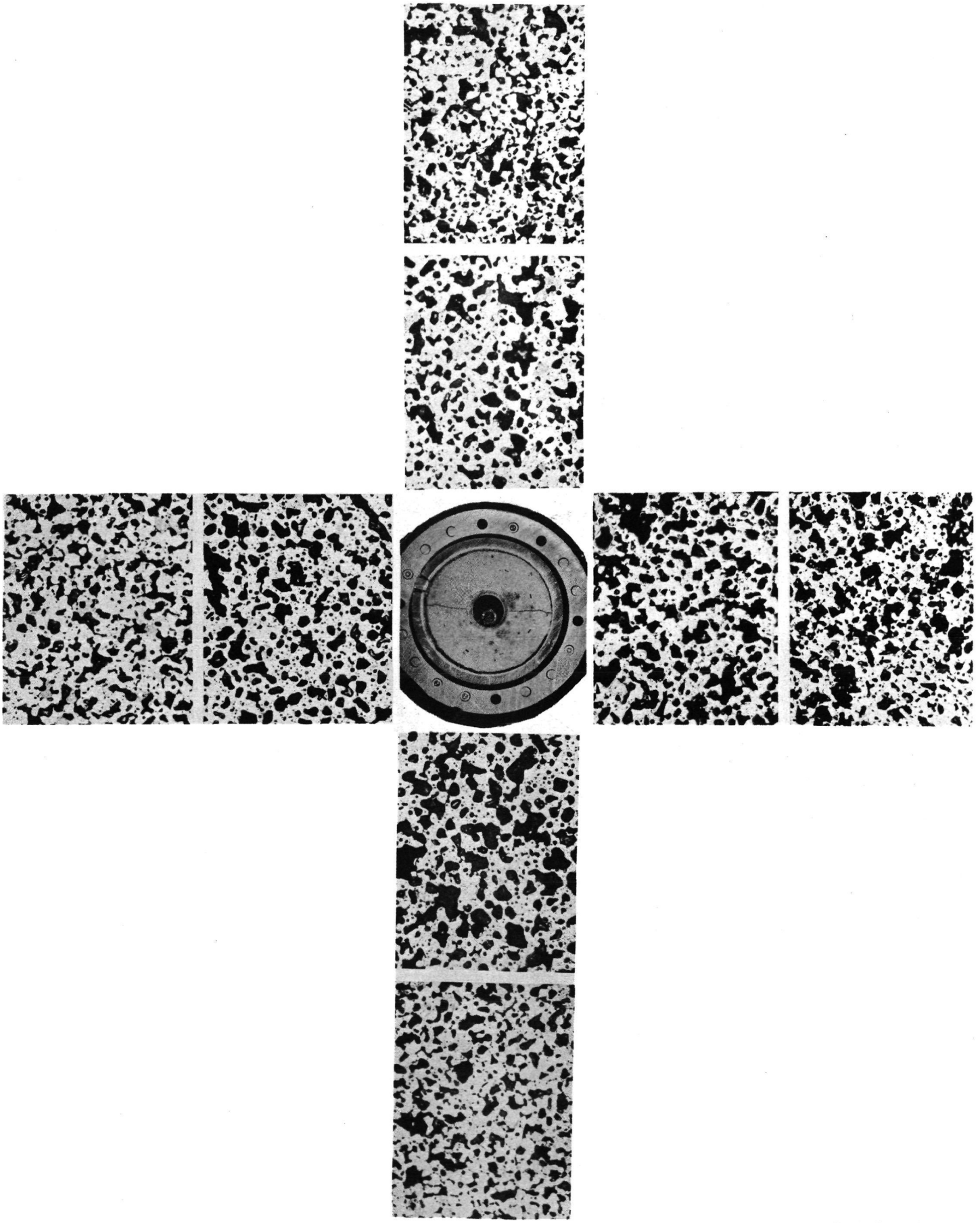

Fig. 21. Microstructures of 90UC-10ZrC fuel material in Sample V-2C-3B at various radial and circumferential positions (90X)

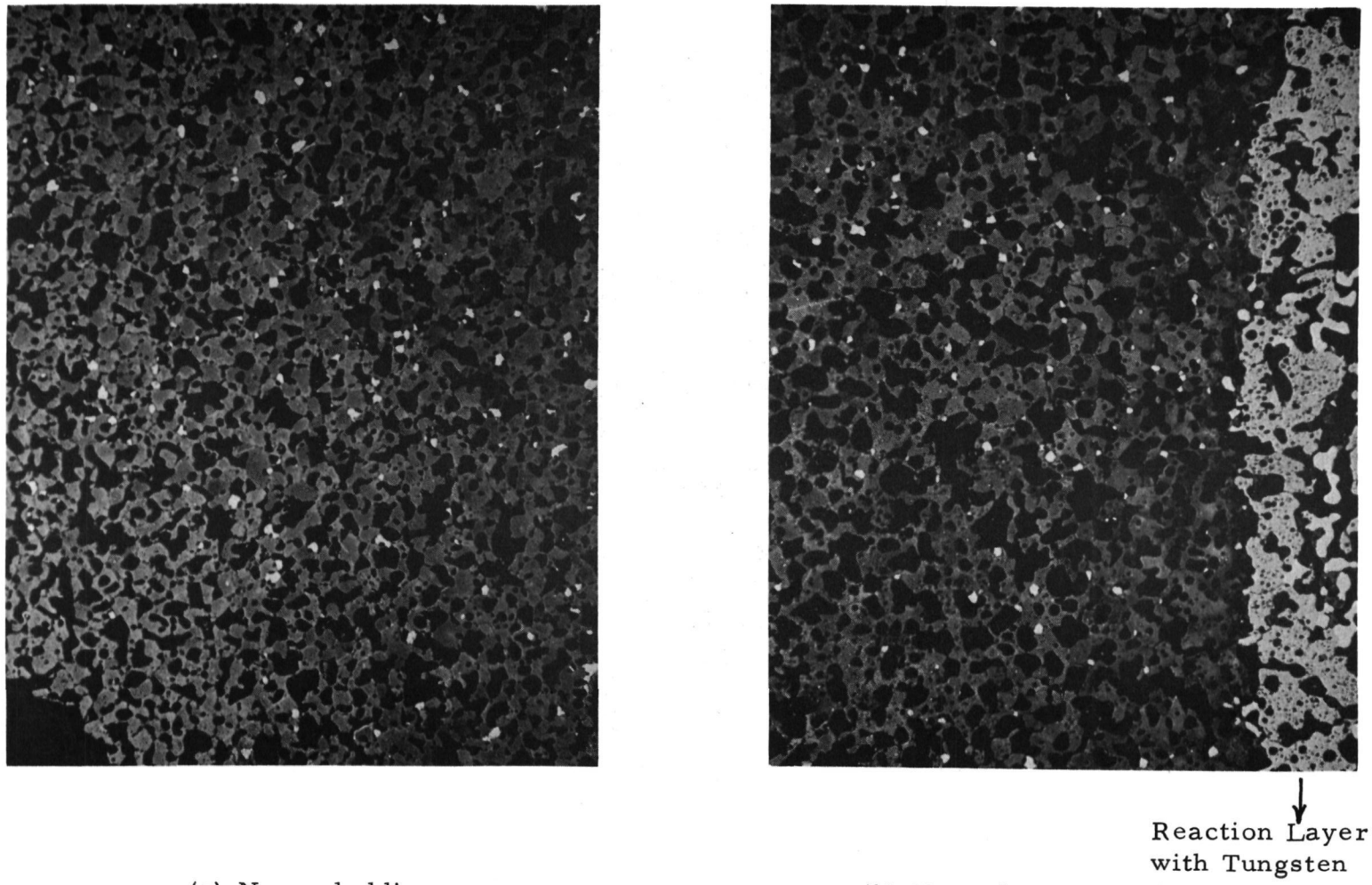

(a) Near cladding

(b) Near thermocouple well

Fig. 22. Microstructures of etched 90UC-10ZrC fuel material of Sample V-2C-2B at the bulge side (100X)

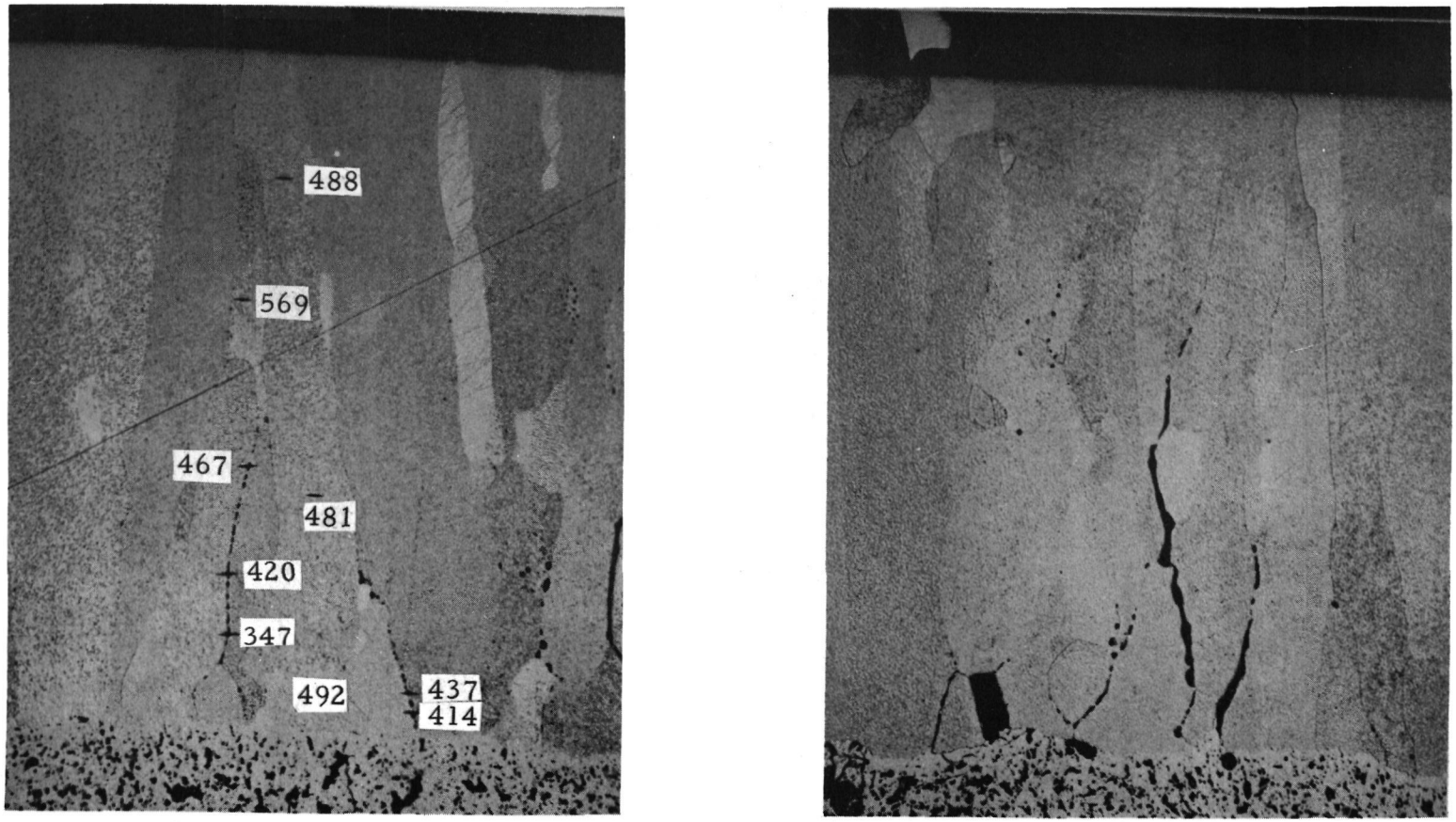

(a) Sample V-2 C-2B

(b) Sample V-2C-3B

Fig. 23. Microstructures of fluoride tungsten cladding near the bulge sides of Samples V-2C-2B, V-2C-3B, and V-2C-4B (100X) (Sheet 1 of 2) Numbers indicated in (a) are Knoop hardness numbers

(c) Sample V-2C-4B

Fig. 23. Microstructures of fluoride tungsten cladding near the bulge sides of Samples V-2C-2B, V-2C-3B, and V-2C-4B (100X) (Sheet 2 of 2)

If the bubbles are greater than a certain critical size which is determined by the prevailing stress level, the bubbles will grow continuously into voids. This will eventually lead to grain boundary separation and cracking. Microhardness measurements (see Fig. 23(a)) indicated no embrittlement of the grain boundaries of the cladding by carbide fuel components. In fact, the microhardness numbers of the grain boundaries, as shown in Fig. 23(a), are lower than that inside the grains, and the microhardness numbers inside the grains are slightly lower than that for unirradiated fluoride tungsten of similar fluoride content (Knoop hardness number = 500-600). Although Sample V-2C-5B showed no significant cladding expansion, the cladding also exhibits grain boundary cracking on the side in line with the bulge side of Samples V-2C-3B and V-2C-4B. It is believed that the cracks observed are merely the extension of the cracks in the cladding of V-2C-3B and V-2C-4B.

For Samples V-2C-3B and V-2C-4B, which showed excessive fuel swelling and cladding expansion, grain boundary voids and cracks were also observed in regions away from the bulge area of the cladding. For Samples V-2C-2B which showed less fuel swelling and cladding expansion, and V-2C-5B which showed no significant fuel swelling and cladding expansion, the claddings were essentially free from grain boundary voids and cracks except in the vicinity of the bulged area or the area in line with the bulge of the neighboring samples. This is illustrated by Figs. 24(a) through (d) which show respectively the microstructures of the tungsten cladding 180° away from the cracked areas of Samples V-2C-2B, V-2C-3B, V-2C-4B, and V-2C-5B. The microhardness

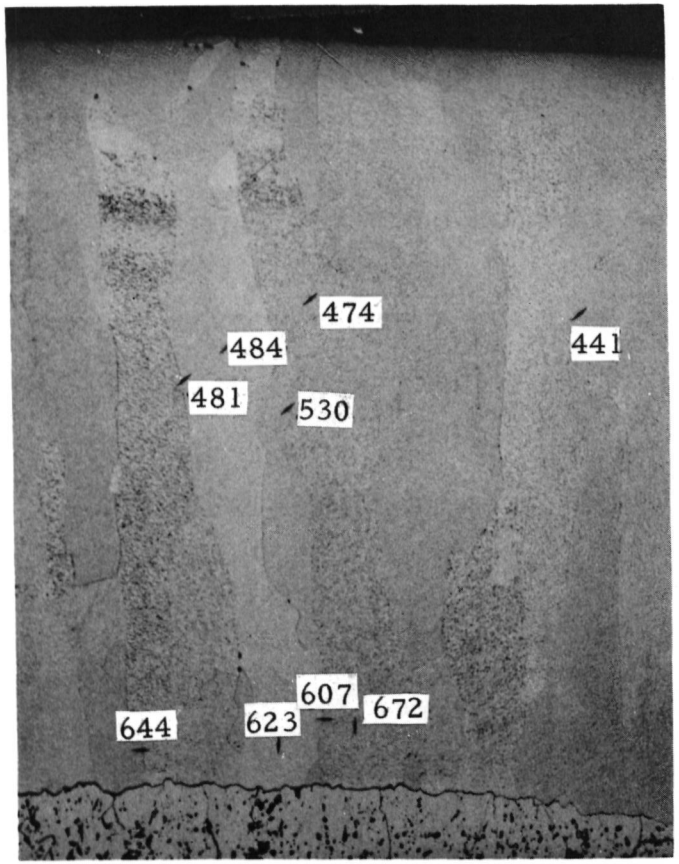

(a) Sample V 2C-2B. Note absence of grain boundary voids

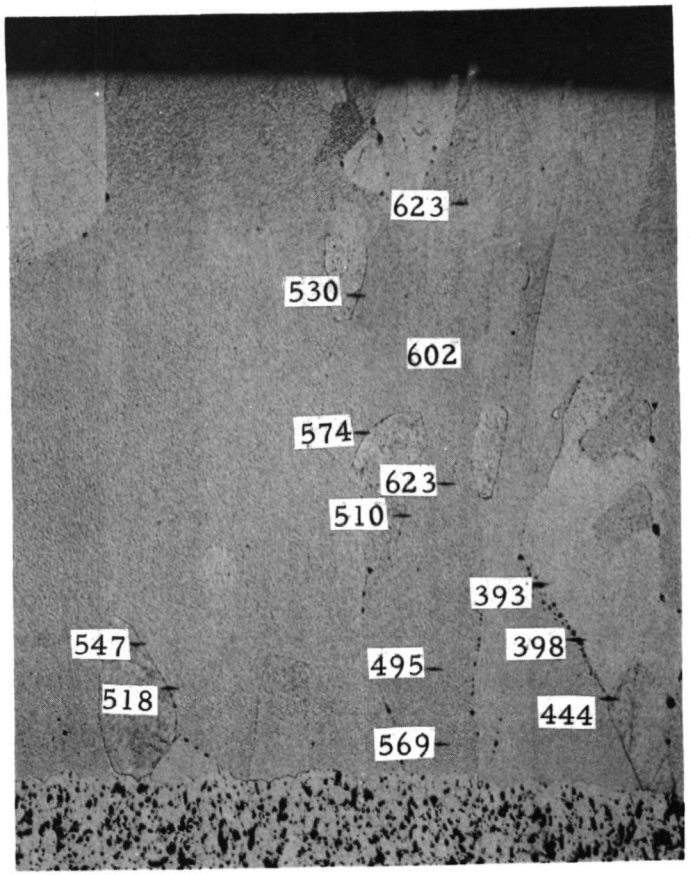

(b) Sample V-2C 3B. Note grain boundary voids

Fig. 24. Microstructures of fluoride tungsten cladding 180° from the bulge side of V-2C fuel pin (100X) (Sheet 1 of 2)
Numbers indicated are Knoop hardness numbers

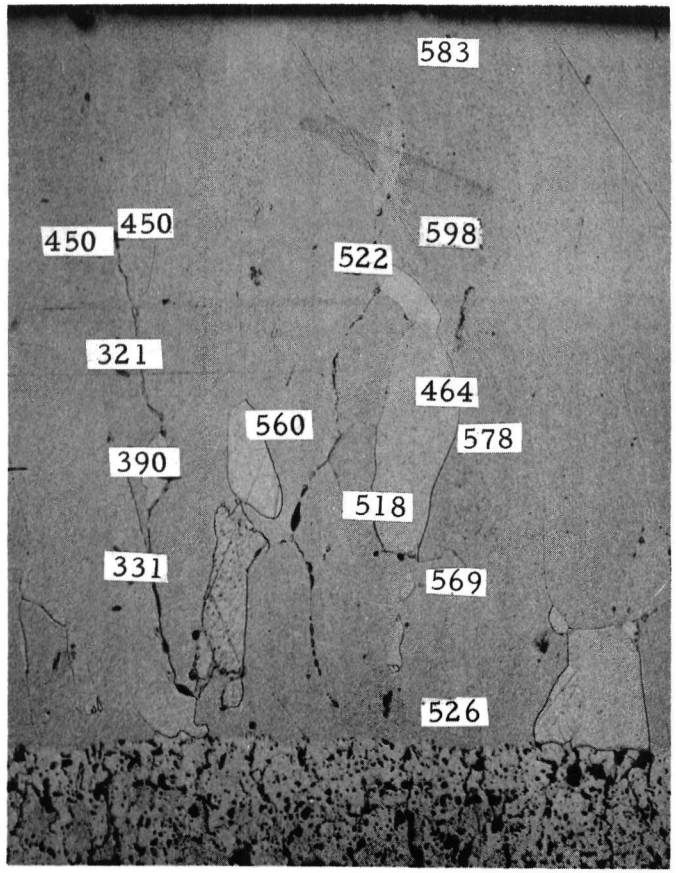

(c) Sample V-2C 4B. Note grain boundary voids

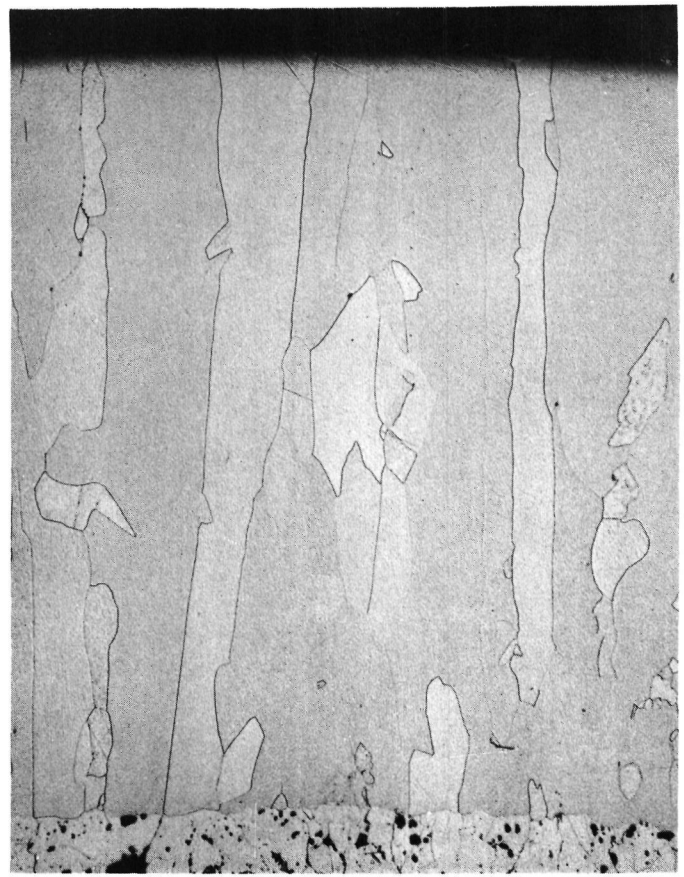

(d) Sample V-2C-5B, Note absence of grain boundary voids

Fig. 24. Microstructures of fluoride tungsten cladding 180° from the bulge side of V-2C fuel pin (100X) (Sheet 2 of 2)
Numbers indicated are Knoop hardness numbers

data again indicate that the grain boundary regions in Sample V-2C-3B and V-2C-4B are softer because of the presence of voids and that no significant embrittlement of the cladding by carbide fuel components has occurred.

(3) Tungsten thermocouple well

Excessive grain growth was observed in all the CVD fluoride tungsten thermocouple wells examined. Such rapid grain growth is attributed to the sharp curvature of small diameter tubing, which precludes low angle grain boundaries in the cross section of the tubing. Figure 25 shows the microstructures of the tungsten thermocouple well in Sample V-2C-3B at four circumferential positions. In some cases, voids were found to exist at grain boundaries. Figures 26(a) and (b) show the microstructures of the tungsten thermocouple well of Sample V-2C-2B at the bulge side and at the side 180° from the bulge. The microhardness results indicate that the grain boundary was softer because of the presence of voids and that the tungsten was not embrittled by carbide fuel even though fuel-tungsten interaction layers can be seen in Figs. 25 and 26. The interaction layer does not seem to adhere to the tungsten thermocouple well. It is possible that the interaction layer has a lower thermal expansion coefficient than that of tungsten so that upon cooling the layer becomes detached from the thermocouple well. The composition of such interaction layer will be discussed in a latter section of this report.

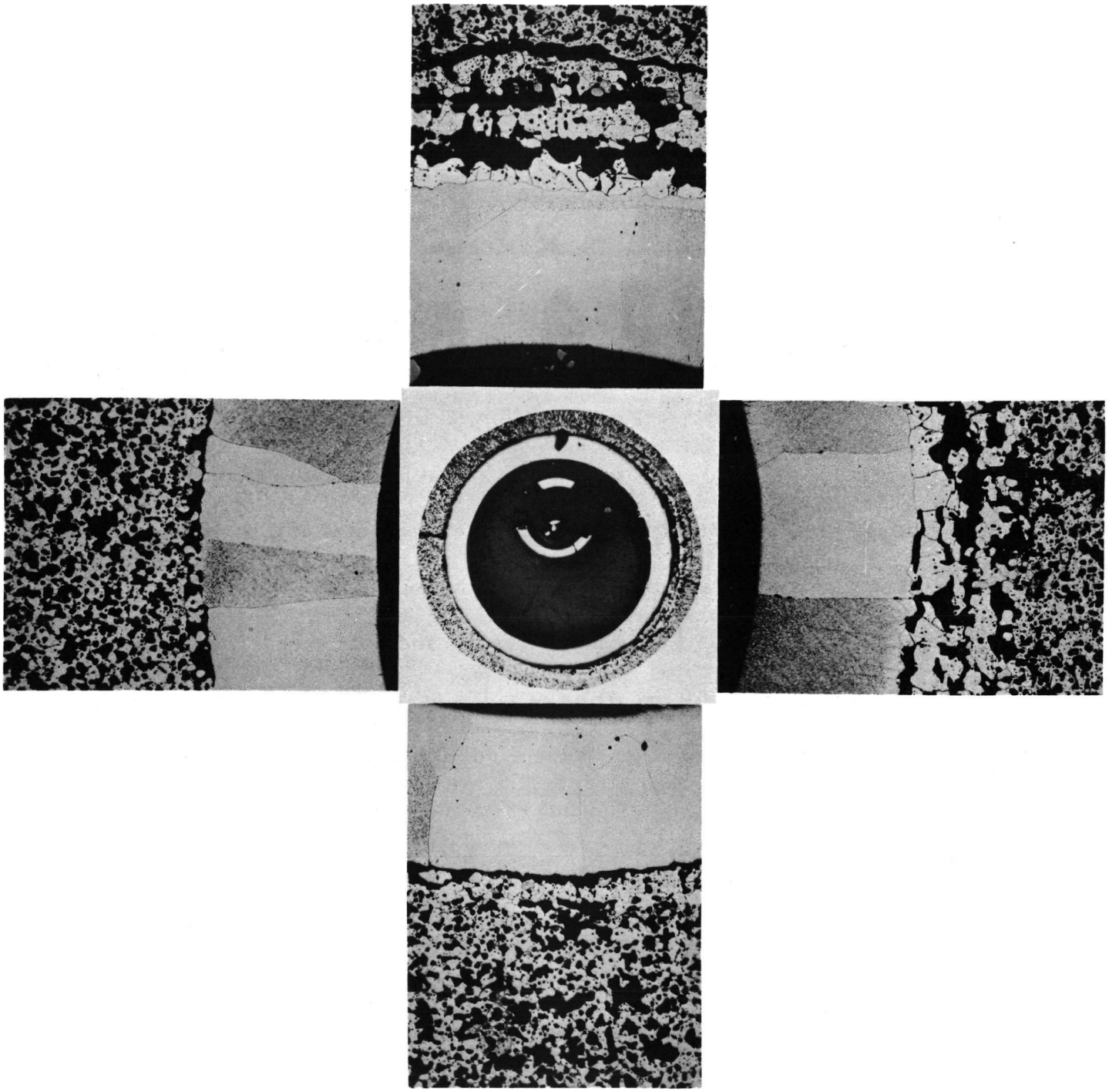

Fig. 25. Microstructures of tungsten thermocouple well of Sample V-2C-3B at four circumferential positions (8X)

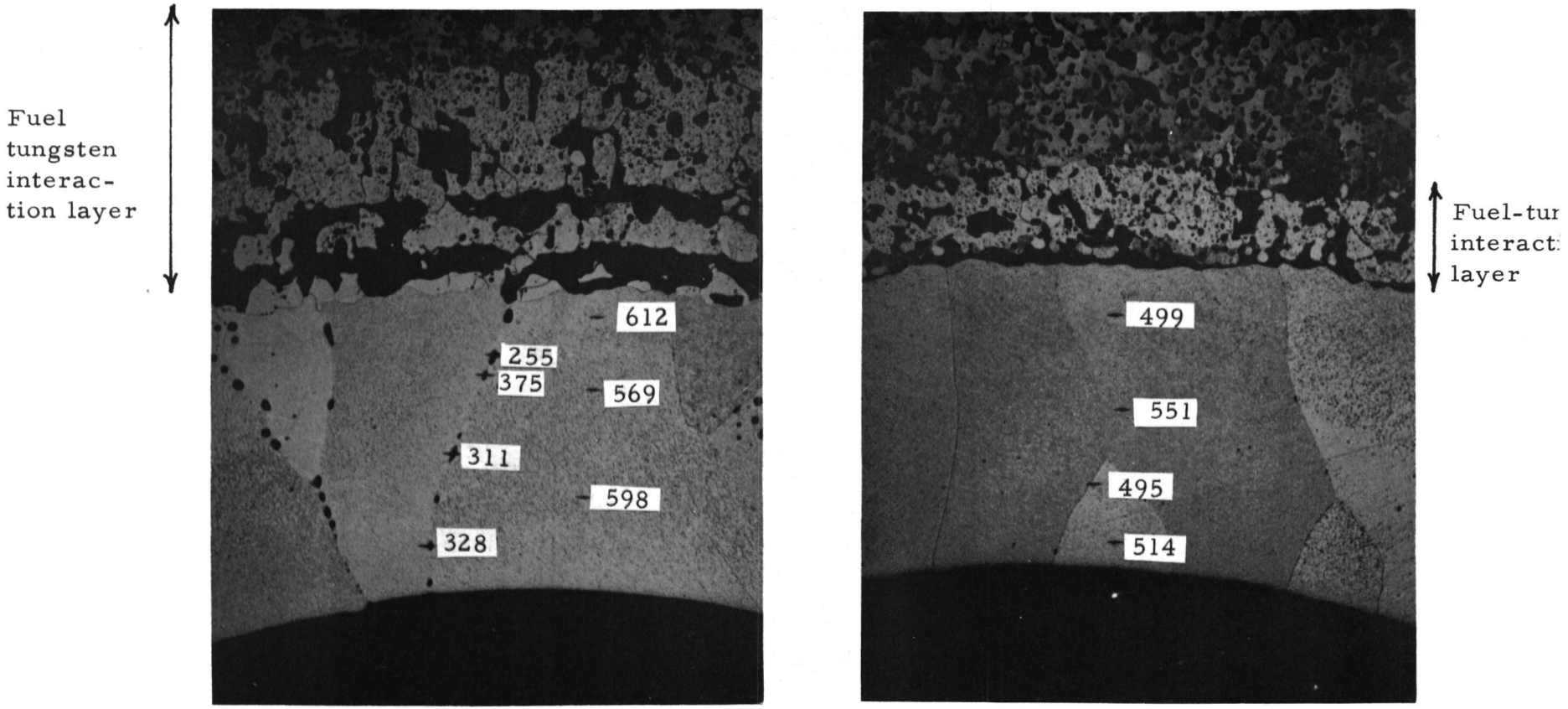

(a) Bulge side

(b) 180° from bulge side

Fig. 26. Microstructures and microhardness of tungsten thermocouple well in Sample V-2C-2B(100X)

(4) Fuel-tungsten interaction layer

Fuel-tungsten interaction layer was observed at both the fuel-cladding interface and at the fuel-thermocouple well interface. The microstructures of the interaction layer at the fuel-thermocouple well interface was shown in Figs. 25 and 26. Figure 27 illustrates the typical microstructures of the fuel-cladding interaction layer. While the fuel-thermocouple well interaction layer tends to detach from the thermocouple well, the fuel-cladding interaction layer adheres to the cladding. It is difficult to measure the thickness of the fuel-thermocouple well interaction layer quantitatively since it does not form a compact layer. The thickness of the fuel-cladding interaction layer can be determined from photomicrographs taken of the fuel-cladding interface. Generally speaking, both the fuel-thermocouple well interaction layer and the fuel-cladding interaction layer have the maximum thickness on the bulge side of the fuel pin and the minimum thickness on the side 180° from the bulge side. This is probably due to the higher fuel temperature and higher burnup rate (thus more fission fragment damage to the tungsten) on the bulge side.

Table 3 lists the maximum thicknesses of the fuel-cladding interaction layers in the various samples examined as a function of the average fuel temperature. The maximum thickness of the fuel-cladding interaction in Sample V-2C-5T was also estimated from the macrophotographs taken of the as-sectioned sample (see Fig. 11(i)). The maximum losses of the thickness of the tungsten cladding due to the formation of the fuel-cladding interaction layer, as measured from the photomicrographs taken of the samples examined, are also included in Table 3.

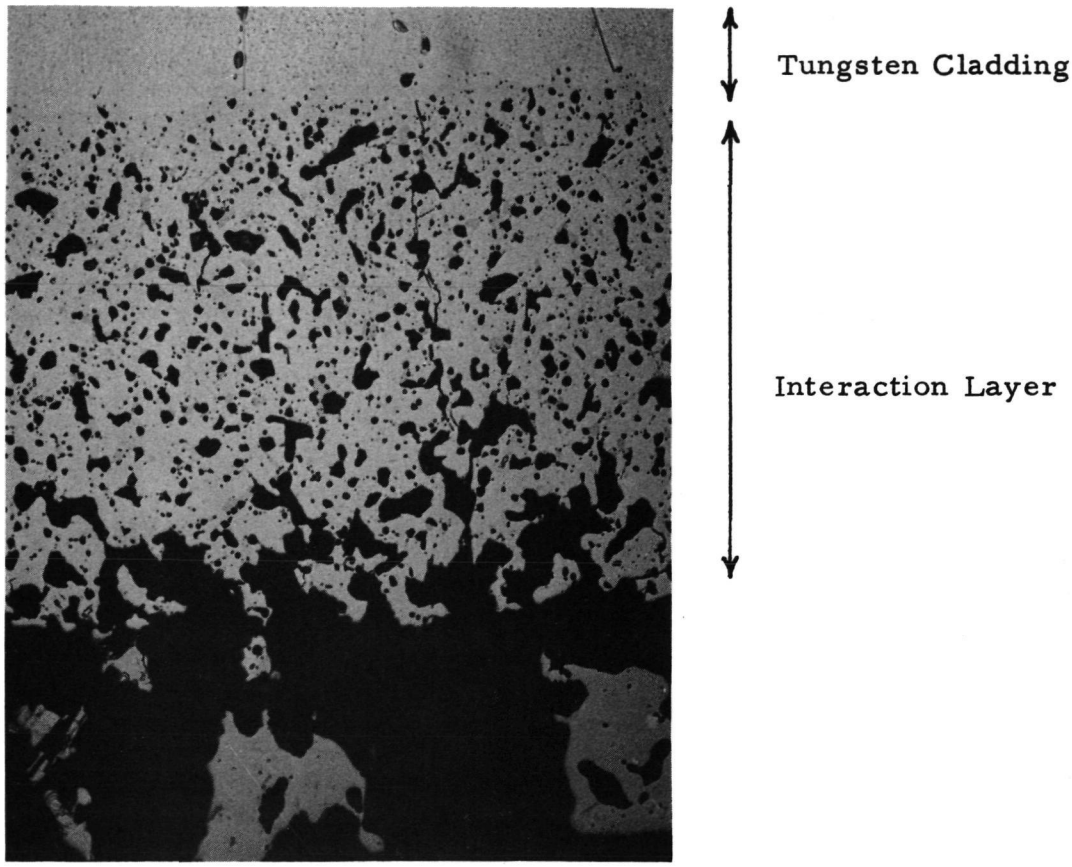

Fig. 27. Fuel-cladding interaction layer in Sample V-2C-2B at the bulge side of the cladding (200X)

TABLE 3

MAXIMUM FUEL-CLADDING INTERACTION LAYER THICKNESS AND TUNGSTEN CLADDING CONUMPTION IN V-2C FUEL PIN AS A FUNCTION OF AVERAGE FUEL TEMPERATURE AFTER 11089 HOUR OPERATION IN NASA PLUMB BROOK REACTOR

Sample	Average Fuel Temperature (°K)	Maximum Fuel-Cladding Interaction Layer Thickness mm	(Mils)	Thickness of Tungsten Cladding Consumed mm	(Mils)
V-2C-2B	1975	0.33	(13)	0.15	(6)
V-2C-3B	2010	0.38	(15)	0.15	(6)
V-2C-4B	1972	0.31	(12)	0.15	(6)
V-2C-5B	1860	0.31	(12)	0.10	(4)
V-2C-5T	1730	0.08	(3)	0.05	(<2)

It can be seen that the maximum thickness of the fuel-cladding interaction layer is strongly temperature dependent, and that the thickness of the tungsten cladding consumed is about half of the thickness of the interaction layer. The composition of the fuel-cladding interaction layer will be discussed in a latter section of this report.

(5) Fuel pin bottom

Sample No. 1 (see Fig. 11(a)), which is located at the bottom of V-2C fuel pin, was sectioned longitudinally along the cylindrical axis of the fuel pin into two halves. Figure 28 shows the appearance of the sectioned surface. One of the three tungsten alignment pins for centering the fuel pin in the Inconel containment, can also be seen in this figure.

No deformation of the bottom of the tungsten fuel pin and the bottom of the tungsten thermocouple well can be detected. The tungsten pedestal for the fuel pellets was pushed downward at its central region by fuel swelling. Some extrusion of fuel material around the corner of the thermocouple well into the central fuel cavity has occurred. The annular fission gas venting groove located at the bottom of the fuel pellet, however, remained open and showed no significant change in dimensions.

Figures 29(a), (b), and (c) show the microstructures of the 90UC-10ZrC fuel materials near the cladding, near the thermocouple well, and near the fuel pedestal respectively. The estimated densities by using quantitative metallography techniques are 62%, 50%, and 57%. Figure 30 shows the etched

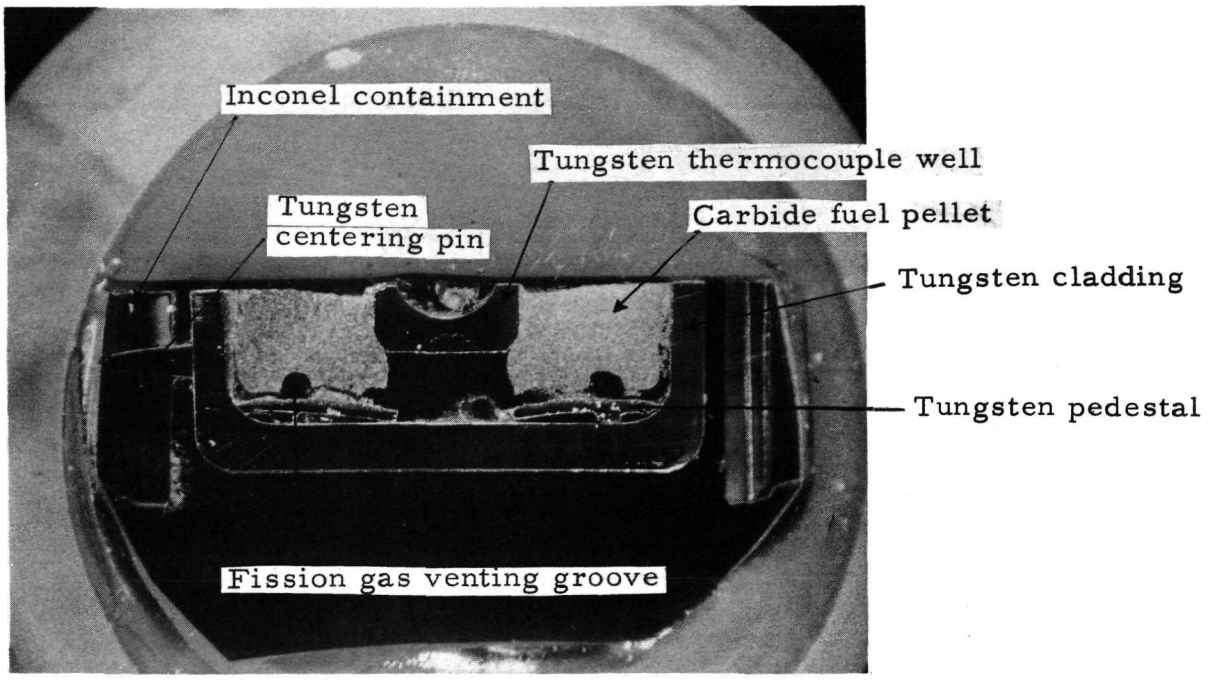

Fig. 28. Macroscopic appearance of the longitudinal cross section of Sample No. 1 of V-2C fuel pin. Designated as Sample V-2C-1T (4.3X)

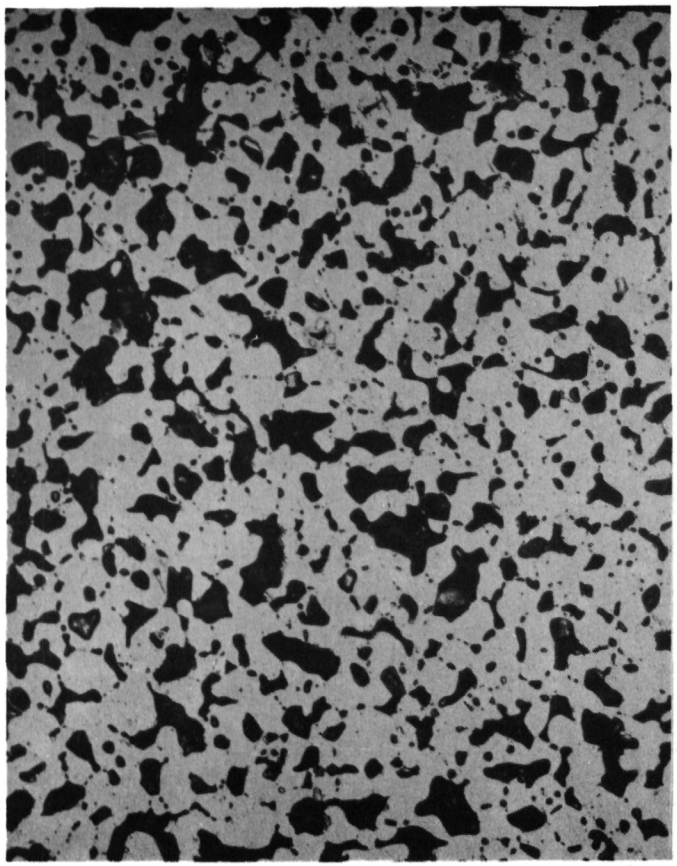

(a) Near cladding

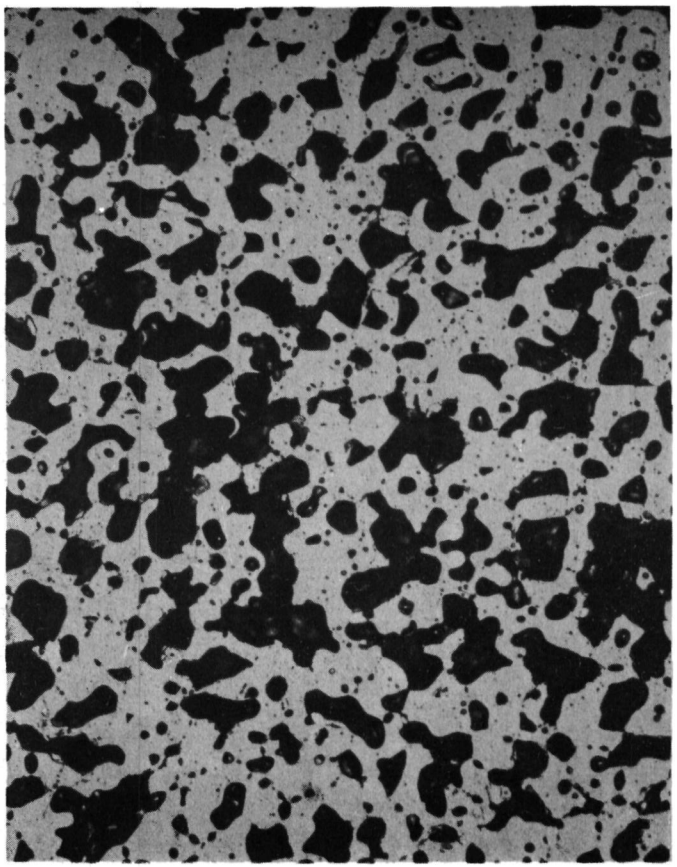

(b) Near thermocouple well

Fig. 29. Microstructures of 90UC-10ZrC fuel material in Sample V 2C-1T (200X) (Sheet 1 of 2)

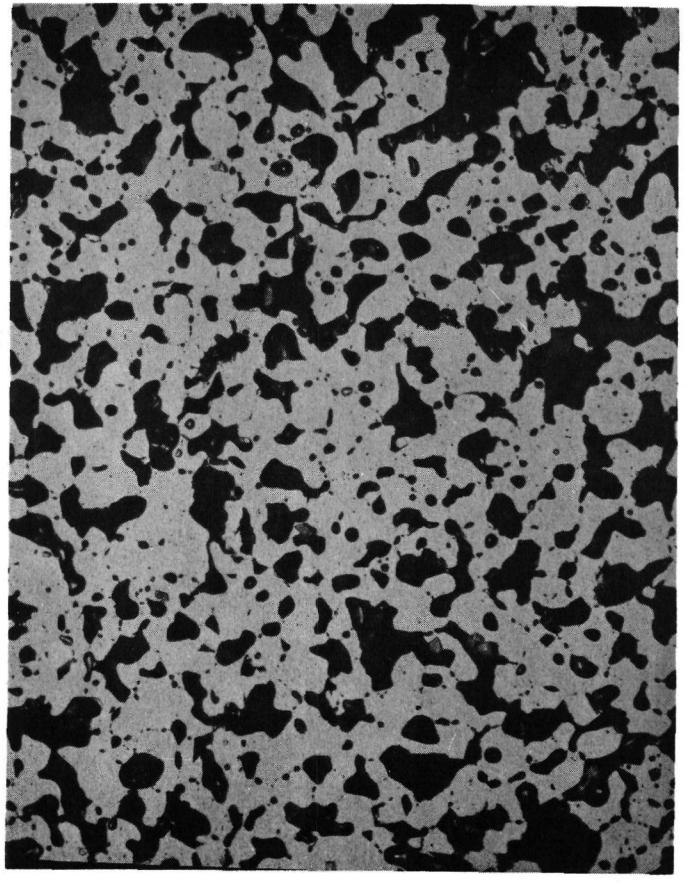

(c) Near fuel pedestal

Fig. 29. Microstructure of 90UC-10ZrC fuel material in Sample V-2C-1T (200X) (Sheet 2 of 2)

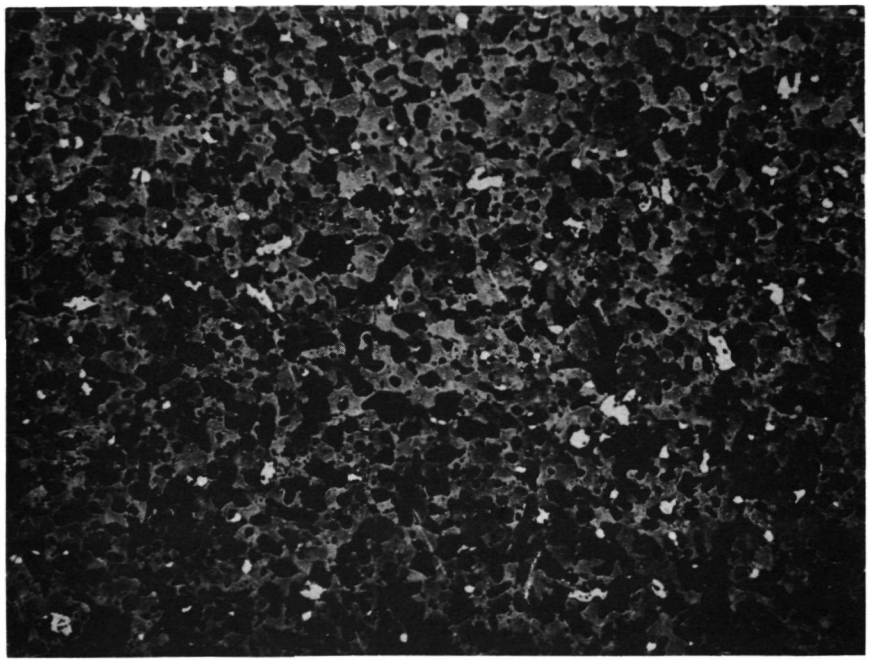

Fig. 30. Etched 90UC-10ZrC fuel structures in Sample V-2C-1T near the fuel pedestal (100X)

fuel structures and the dispersion phases. These fuel structures are similar to that in other V-2C fuel samples.

Figures 31(a), (b), and (c) represent the microstructures of the cladding of Sample V-2C-1T. The bottom of the cladding exhibited normal grain structures of fluoride tungsten (Fig. 31(a)). The region in the vicinity of the tungsten centering pin, however, developed grain boundary voids and cracks (Figs. 31(b) and (c)), presumably because of the stress imposed by the tungsten centering pin on the cladding when the fuel pin was brought to its operating temperature. It can be seen in Fig. 31(c) that the surface of the cladding, which was in contact with the tungsten centering pin at the operating temperature, has suffered from mechanical deformation and fragmentation. Thus, the presence of the tungsten centering pin tends to jeopardize the structural integrity of the cladding.

Figure 32 shows the appearance of the end of the tungsten thermocouple well of V-2C fuel pin. A crack has developed along the grain boundaries in the center region of the bottom. The excessive grain growth is similar to that observed on other parts of this thermocouple well.

Figures 33(a), (b), and (c) illustrate the microstructures of the fuel-tungsten interaction layers at the fuel-cladding, the fuel-pedestal, and the fuel-thermocouple well interfaces respectively. The interaction layer adheres well to the cladding and the pedestal but was detached from the thermocouple well. This is in agreement with that observed in other fuel samples.

(a) Center of bottom

Fig. 31. Microstructures of cladding near the bottom region of V-2C fuel pin (75X) (Sheet 1 of 2)

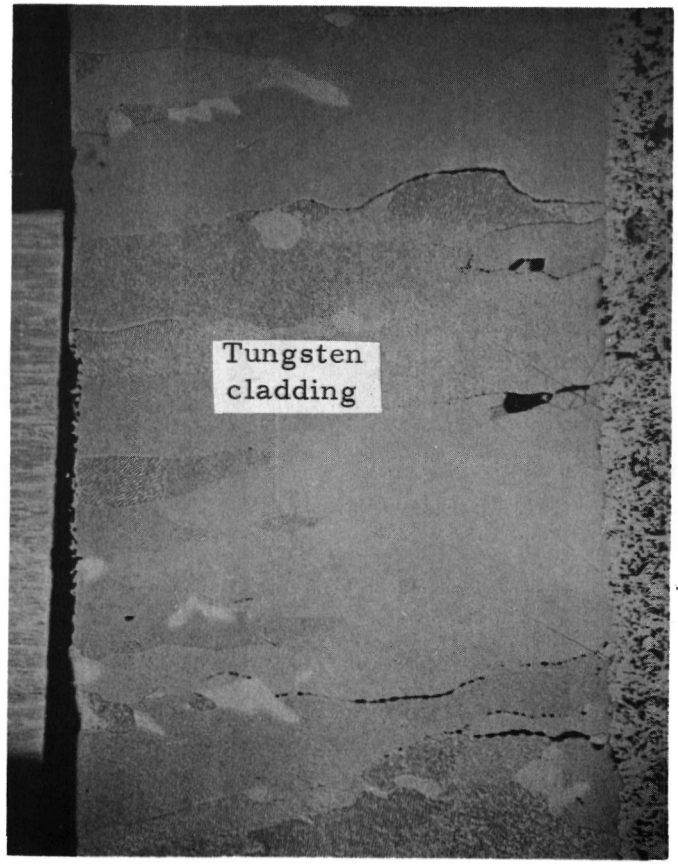

(b) Cladding facing the tungsten centering pin

(c) Left corner below the region shown in (b)

Fig. 31. Microstructures of cladding near the bottom region of V-2C fuel pin (75X) (Sheet 2 of 2)

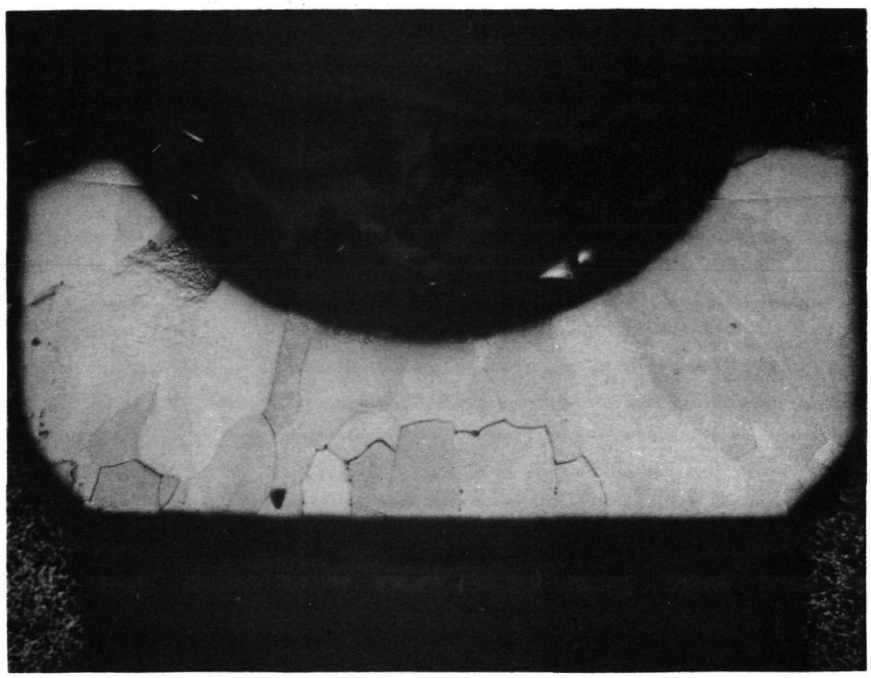

Fig. 32. Macroscopic appearance of end of tungsten thermocouple well of V-2C fuel pin (25X)

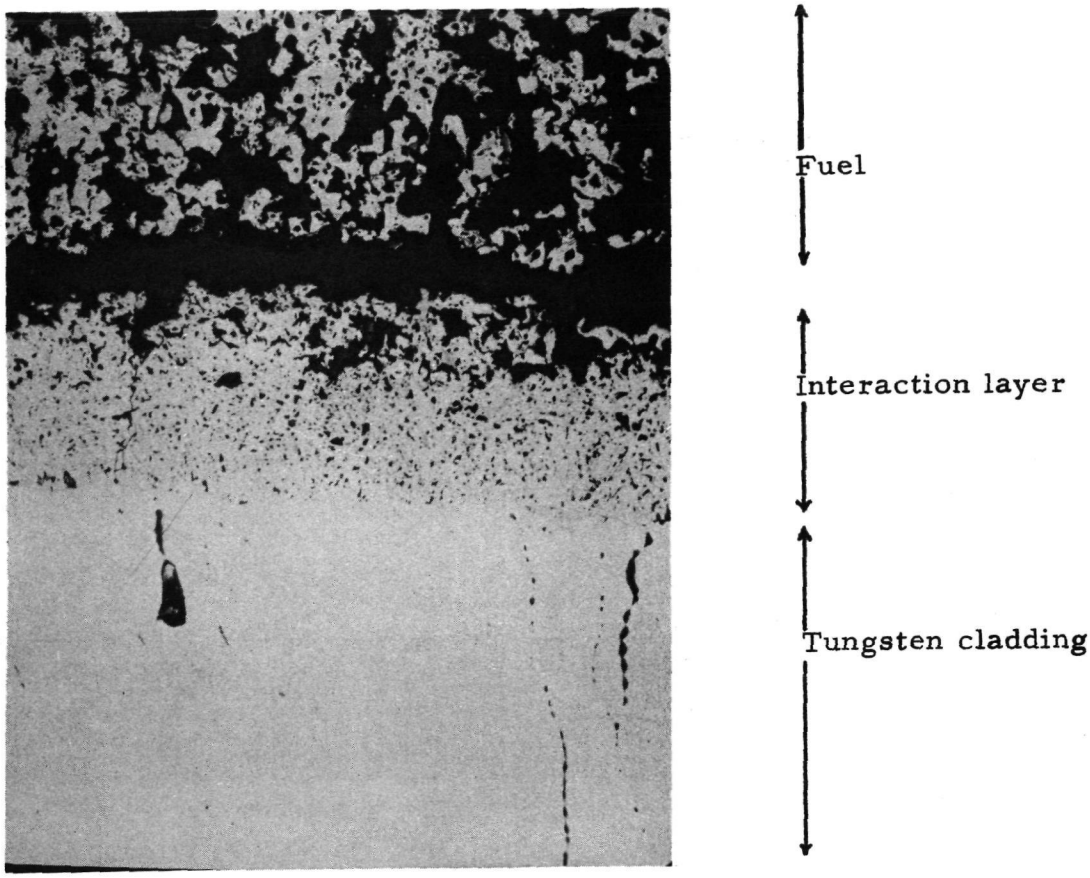

(a) Fuel-cladding interface

Fig. 33. Microstructures of fuel-tungsten interaction layers in Sample V-2C-1T (100X) (Sheet 1 of 2)

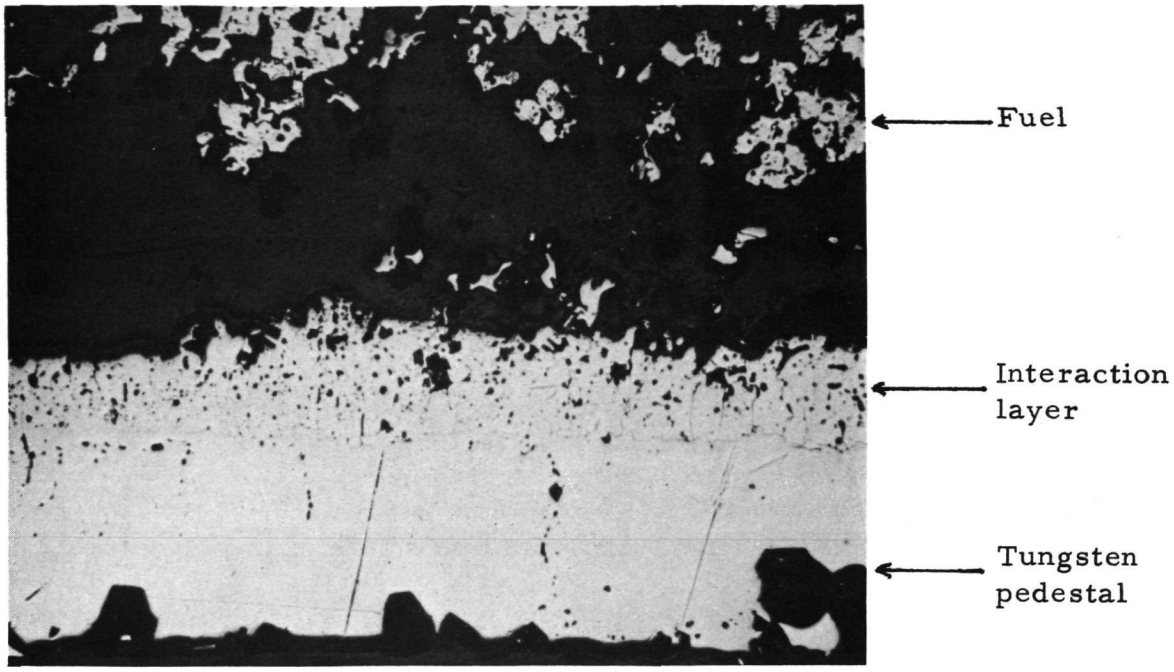

(b) Fuel-pedestal interface

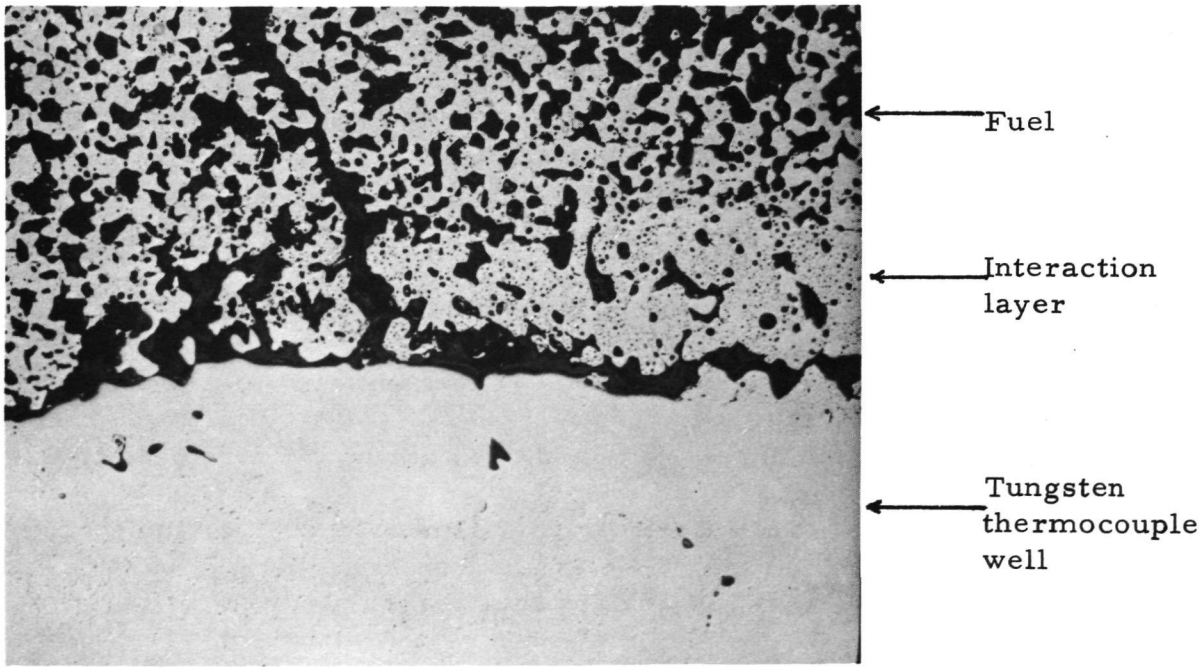

(c) Fuel-thermocouple well interface

Fig. 33. Microstructures of fuel-tungsten interaction layers in Sample V-2C-1T (100X) (Sheet 2 of 2)

6.2. V-2D Fuel Pin

(1) Fuel material

Like the 90UC-10ZrC fuel material in V-2C fuel pin, the microstructures of irradiated 50UC-50ZrC fuel material in V-2D fuel pin are different from that of the unirradiated fuel material. The elongated fine porosities in the unirradiated fuel material are replaced by small fission gas bubbles and larger pores of more "equiaxial" shapes. This is illustrated in Figs. 34(a) and (b). Figure 34(a) shows the pore structures of the 50UC-50ZrC fuel material in Sample V-2D-2B near the bulge side of the cladding, while Fig. 34(b) represents the pore structures of the 50UC-50ZrC fuel material before its irradiation in V-2D fuel pin. The pore size, in the irradiated fuel material, however, is much smaller than that in the irradiated 90UC-10ZrC fuel material in V-2C fuel pin (compare Fig. 34(a) with Fig. 19(a)). This is probably because the 50UC-50ZrC is more refractory and thus less sinterable than 90UC-10ZrC. A good part of the fine pores is therefore retained. The 50UC-50ZrC is also mechanically stronger than 90UC-10ZrC; therefore the pores will expand less than that in 90UC-10ZrC when they are closed and filled with fission gas. The fact that 85% of the fission gas generated was released indicates that a large part of these pores remained open during the irradiation. Quantitative metallographical evaluation yielded a density of 60% for the irradiated fuel material, as compared to 75% for the unirradiated fuel material.

Figures 35(a), (b), and (c) compare the microstructures of the irradiated 50UC-50ZrC fuel materials in Samples V-2D-3B, V-2D-4B, and V-2D-5B. It appears that the pores are bigger in samples exhibiting more

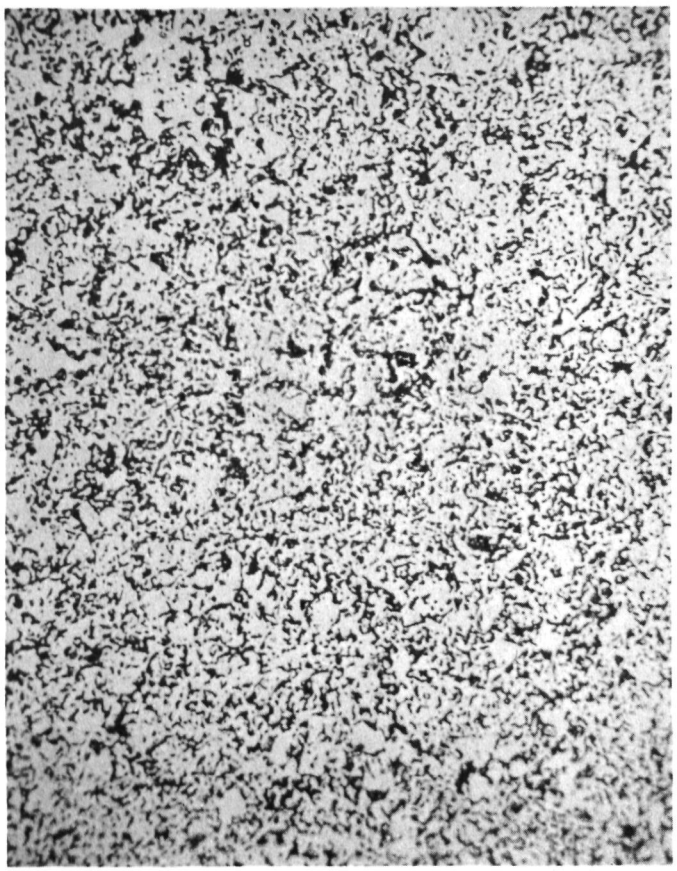

(a) Unirradiated

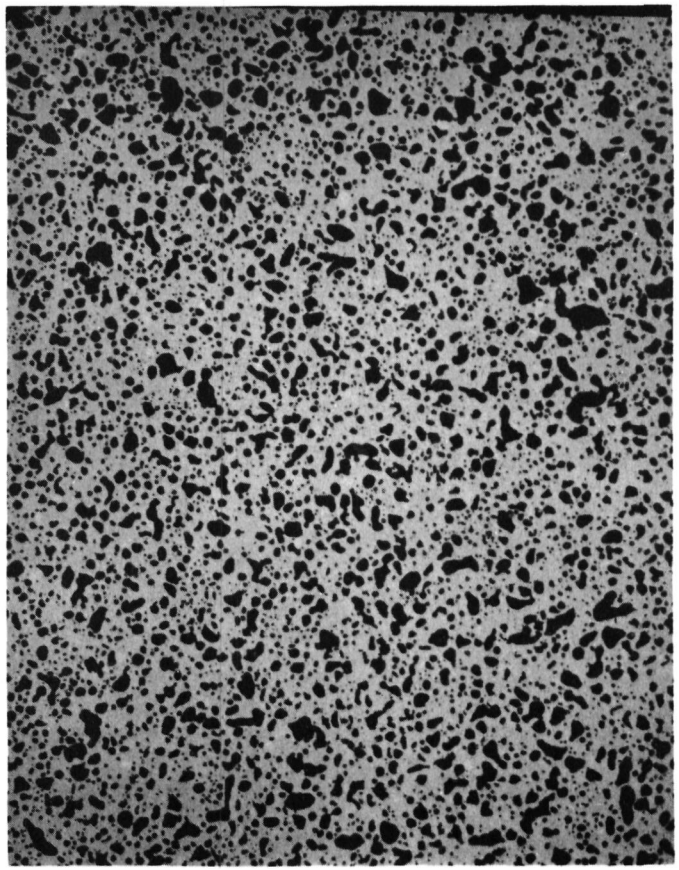

(b) Irradiated, near bulge side of cladding

Fig. 34. Comparison of the microstructures of irradiated and unirradiated 50UC-50ZrC fuel materials of Sample V-2D 2B at 200X magnification

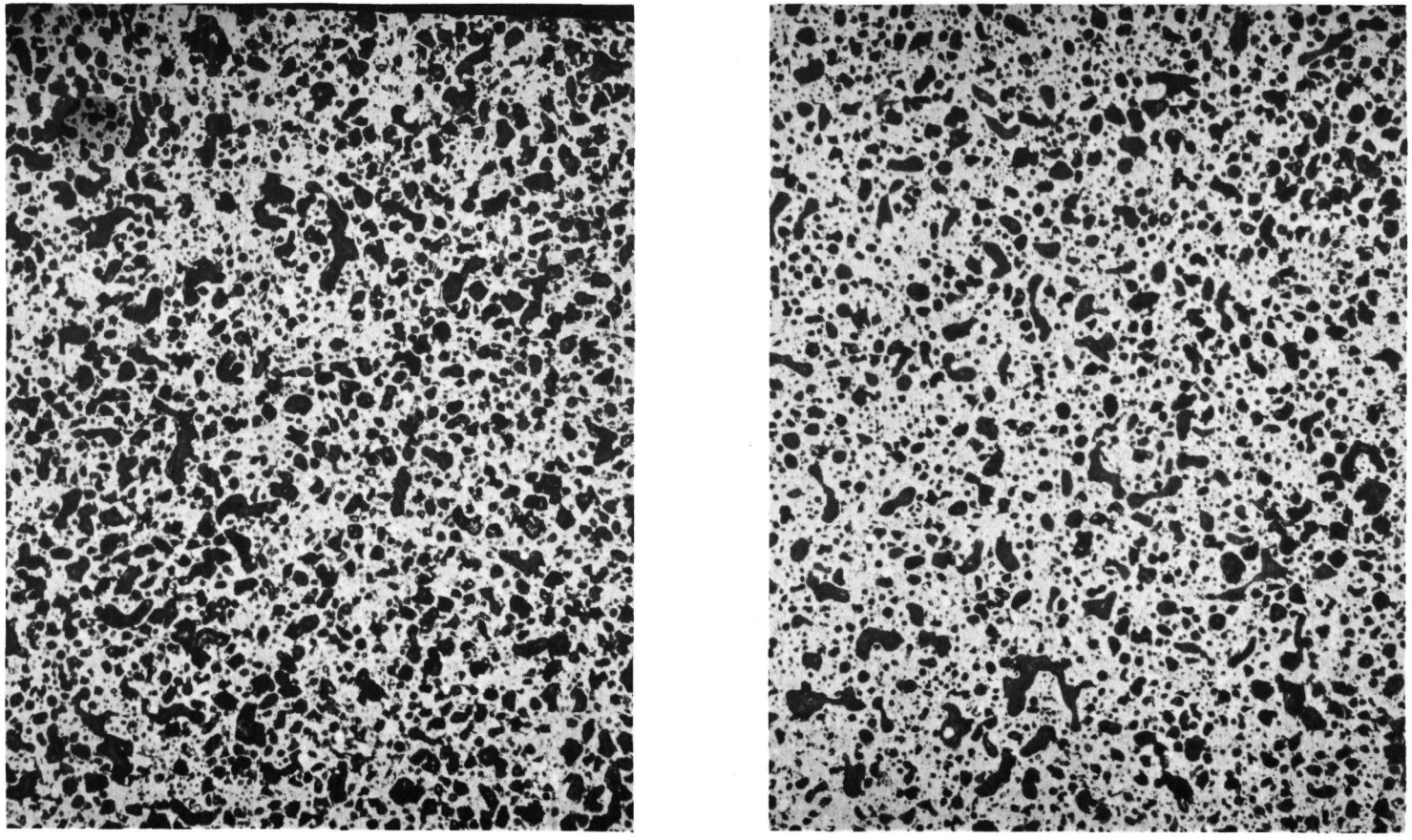

(a) V-2D-3B

(b) V-2D-4B

Fig. 35. Microstructures of irradiated 50UC-50ZrC fuel materials in Samples V-2D-3B, V-2D-4B and V-2D-5B near the bulge side of the cladding (200X) (Sheet 1 of 2)

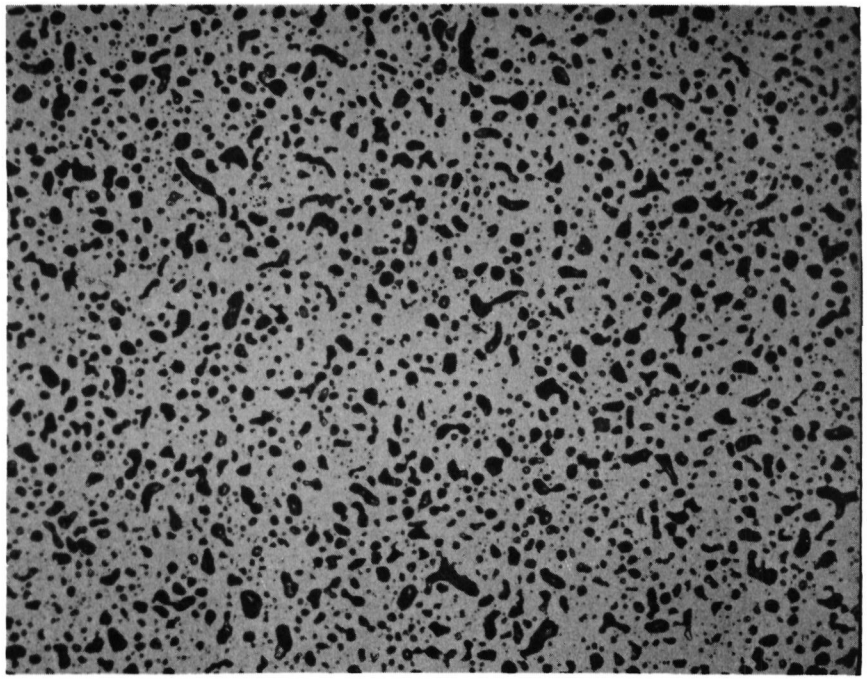

(c) V-2D-5B

Fig. 35. Microstructures of irradiated 50UC-50ZrC fuel materials in Samples V-2D-3B, V 2D-4B, and V-2D-5B near the bulge side of the cladding (200X) (Sheet 2 of 2)

cladding expansion. The densities deduced by quantitative metallography are 50%, 60%, and 70% for the fuel materials in V-2D 3B, V 2D-4B, and V-2D 5B respectively. For each of these samples, and for Sample V-2D-2B, no significant difference in pore structures of the fuel material was observed at various circumferential and radial positions. Figure 36 shows the etched microstructures of the 50UC-50ZrC fuel material in Sample V-2D-4B. The composition of the dispersions in the etched fuel sample will be discussed in a latter section of this report.

It is interesting to see that for all the samples examined, no significant deformation of the fission gas venting holes in the fuel pellets occurred even though fuel swelling and cladding expansion were observed. This implies that 50UC-50ZrC is stronger than tungsten at the irradiation temperature so that when the fuel material swelled by fission gas pressure, the tungsten cladding, rather than the fission gas venting holes, was deformed.

(2) Tungsten cladding

In the region where severe deformation and cracking occurred, the tungsten cladding exhibited excessive grain growth and grain boundary void formation. Figures 37(a) through (f) illustrate the microstructures of the tungsten cladding near the cracks in Samples V-2D 2B, V-2D-3B, V-2D-4B, and V-2D-5B. No excessive grain growth was observed near the cracks of the cladding in the 90UC-10ZrC fueled samples in V-2C fuel pin. This implies that the cladding was subjected to higher stress in the 50UC-50ZrC fueled samples, presumably because the 50UC-50ZrC fuel material is

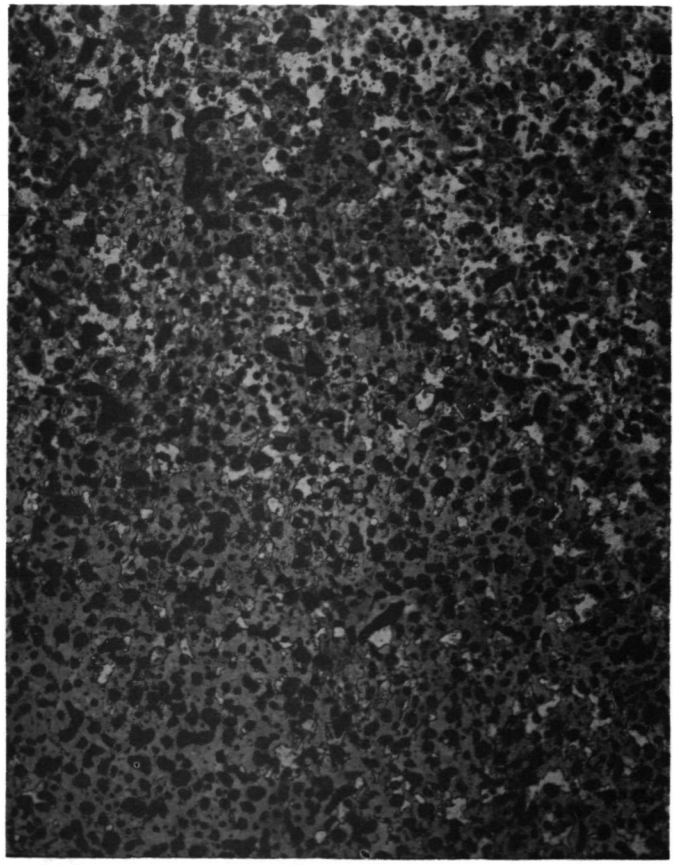

Fig. 36. Etched microstructures of irradiated 50UC-50ZrC fuel material in Sample V-2D-4B near the bulge side of the cladding (200X)

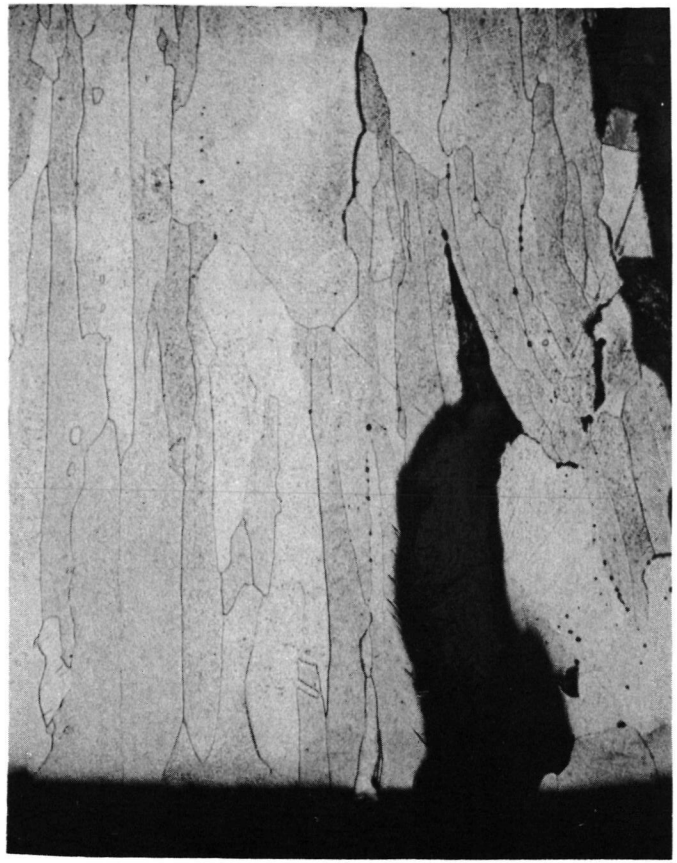

(a) At the cracked region of Sample V-2D-2B

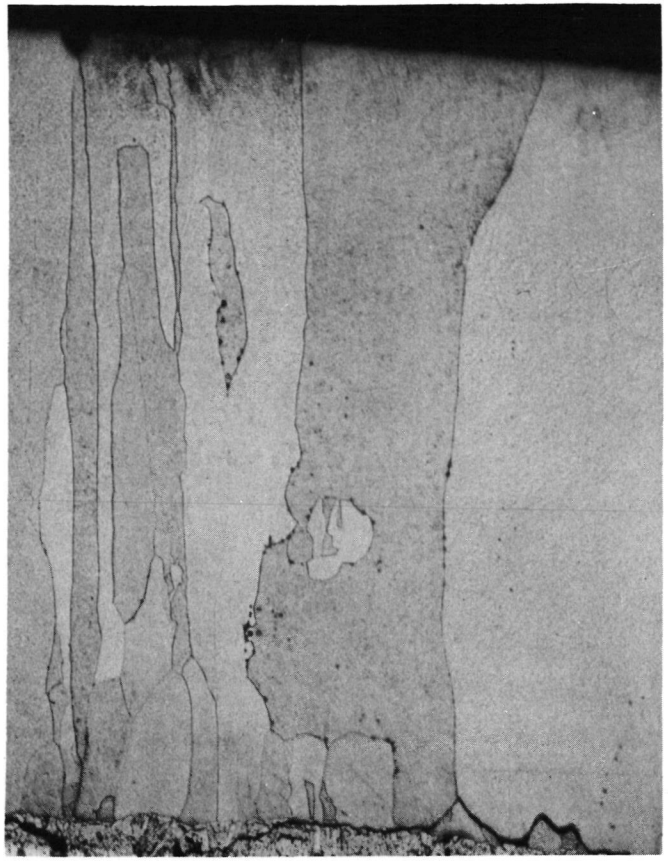

(b) Near the cracked region of Sample V-2D-2B

Fig. 37. Microstructures of tungsten claddings at and near the cracked regions in Samples V-2D-2B, V-2D-3B, V-2D-4B, and V-2D-5B. Note grain growth in cladding and grain boundary voids (100X) (Sheet 1 of 3)

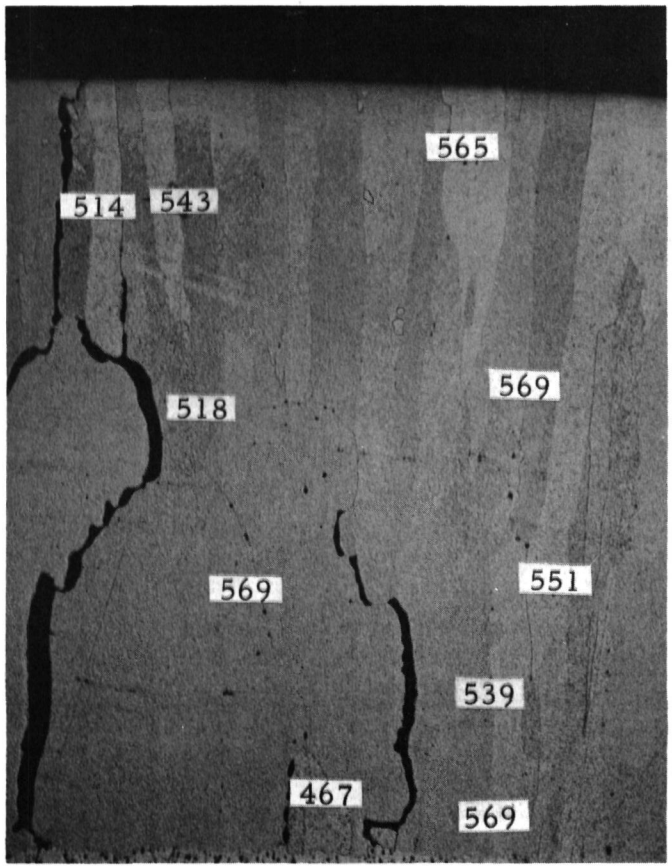

(c) At the cracked region of Sample V-2D-3B

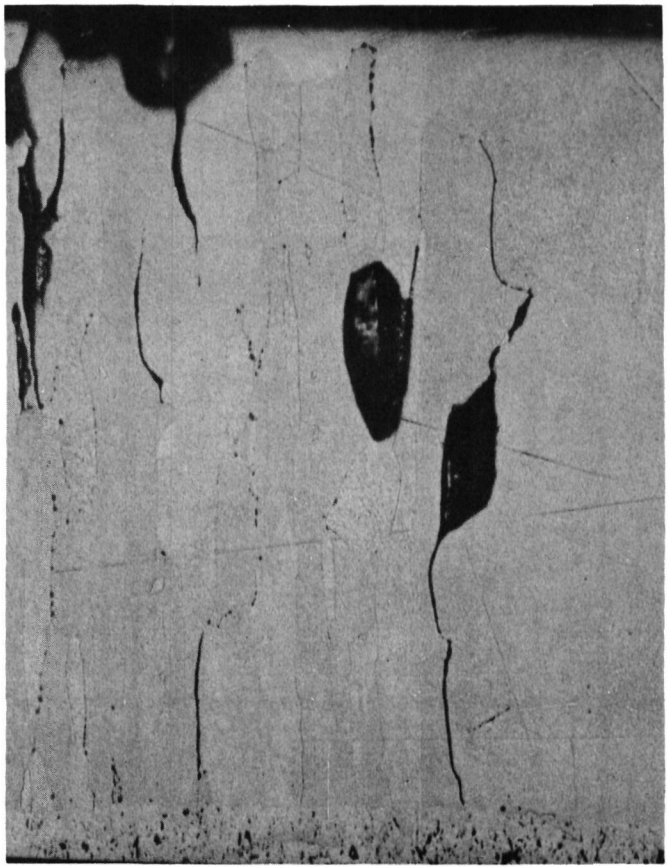

(d) At the cracked region of Sample V-2D-5B

Fig. 37. Microstructures of tungsten claddings at and near the cracked regions in Samples V-2D-2B, V-2D-3B, V-2D-4B, and V-2D-5B. Note grain growth in cladding and grain boundary voids (100X) (Sheet 2 of 3)

Numbers indicated are Knoop hardness numbers

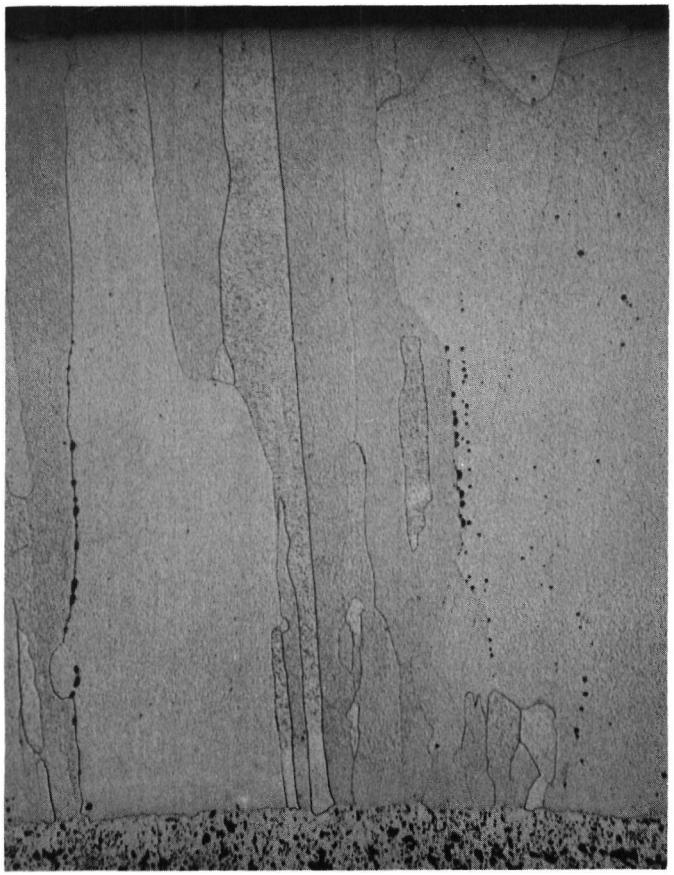

(e) At the cracked region of Sample V-2D-4B

(f) Near the cracked region of Sample V-2D-4B

Fig. 37. Microstructures of tungsten claddings at and near the cracked regions in Samples V-2D-2B, V-2D-3B, V-2D-4B, and V-2D-5B. Note grain growth in cladding and grain boundary voids (100X) (Sheet 3 of 3)

mechanically stronger than the 90UC-10ZrC fuel material. Microhardness measurements made near the cracks in the cladding of Sample V-2D-3B yielded values similar to that of unirradiated fluoride tungsten, indicating no grain boundary embrittlement by carbide fuel components (Fig. 37(c)).

In the region away from the cracked areas of Samples V-2D-2B and V-2D-5B which show less cladding expansion, the claddings have normal columnar grain structures. The microhardness values obtained are close to that of normal fluoride tungsten. (Figures 38(a) and (b)).

(3) Tungsten thermocouple well

The tungsten thermocouple well samples examined showed various degrees of grain growth and grain boundary voids. Generally speaking, samples from regions where no excessive fuel swelling and cladding deformation occurred (e. g. Sample V-2D-5B) showed less grain growth and grain boundary voids than samples from regions where large amounts of fuel swelling and cladding deformation were observed (e. g. Sample V-2D-3B). This is borne out by Figs. 39(a) through (d) which represent the microstructures of the tungsten thermocouple well in Samples V-2D-2B, V-2D-3B, V-2D-4B, and V-2D-5B respectively. The microhardness numbers obtained do not differ significantly from that of unirradiated tungsten except at grain boundaries containing voids, where slightly lower values were observed.

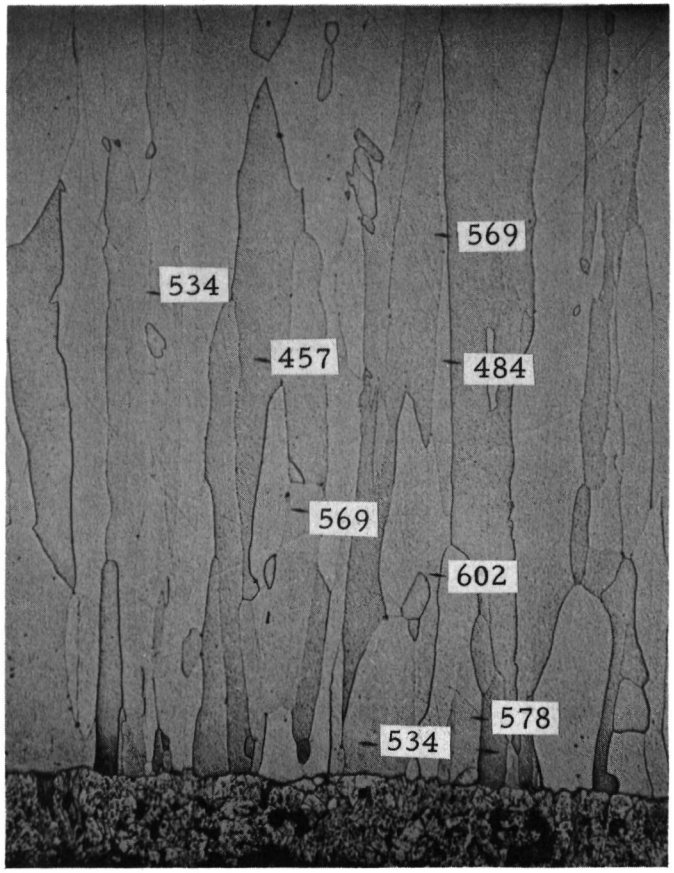

(a) Sample V-2D-2B
180° from cracked region

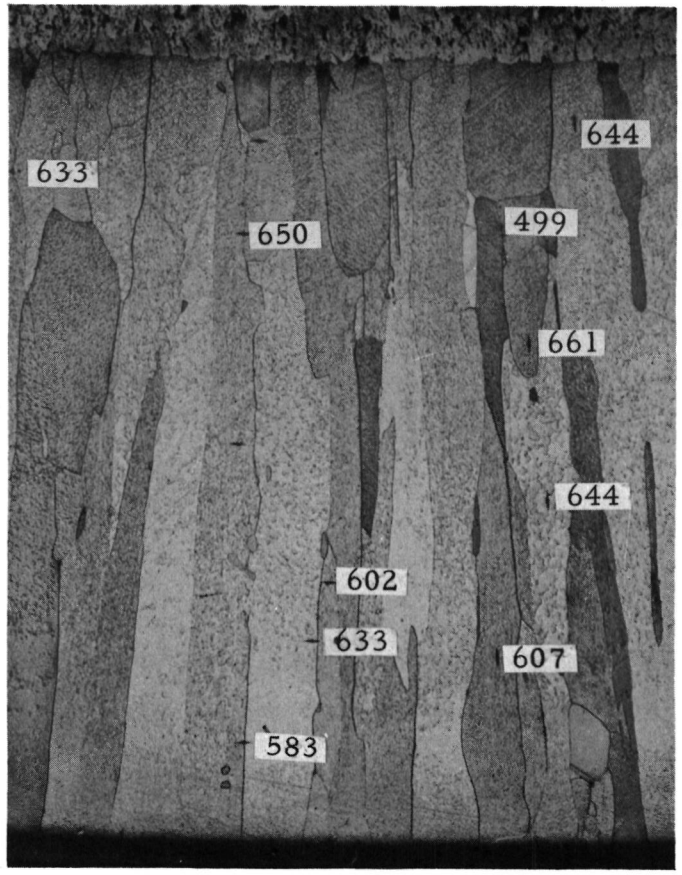

(b) Sample V-2D-5B
180° from cracked region

Fig. 38. Microstructures of tungsten claddings away from the cracked regions of Samples V-2D-2B and V-2D-5B. Note lack of excessive grain growth and grain boundary voids. (100X) Numbers indicated are Knoop hardness numbers

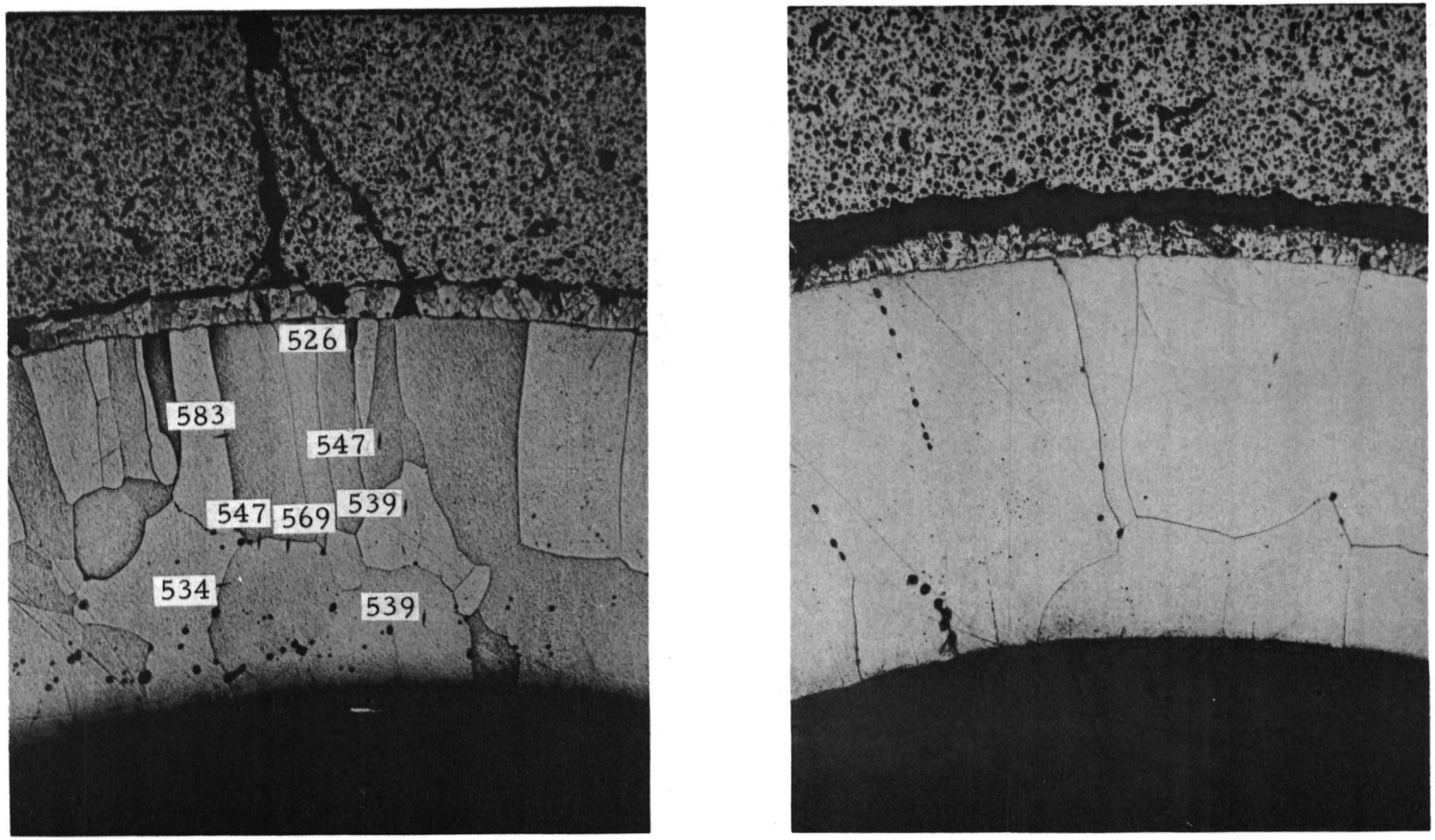

(a) Sample V-2D-2B

(b) Sample V-2D-3B

Fig. 39. Microstructures of tungsten thermocouple wells from various regions of V-2D fuel pin (100X) Numbers indicated are Knoop hardness numbers (Sheet 1 of 2)

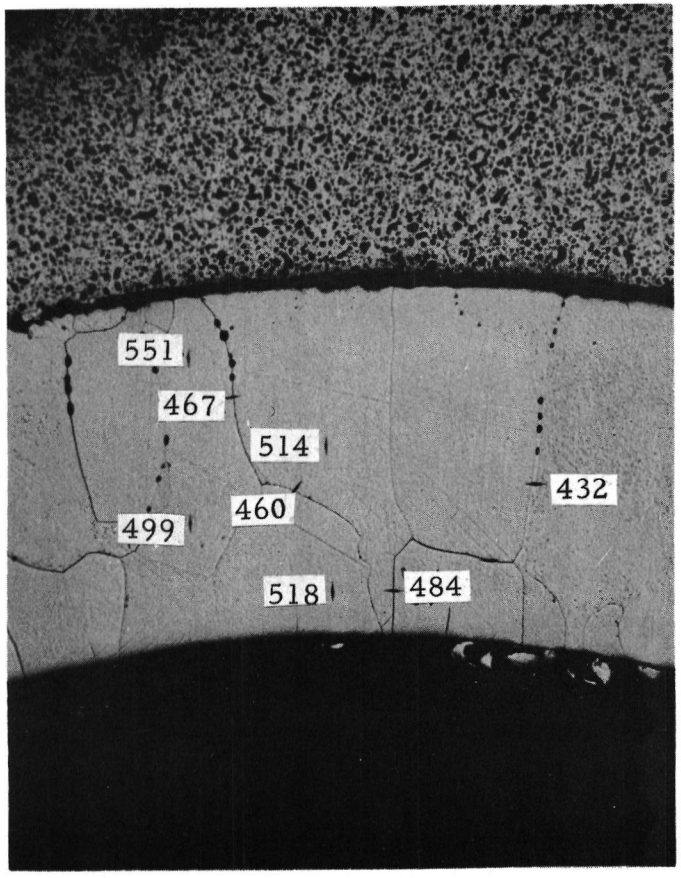

(c) Sample V-2D-4B

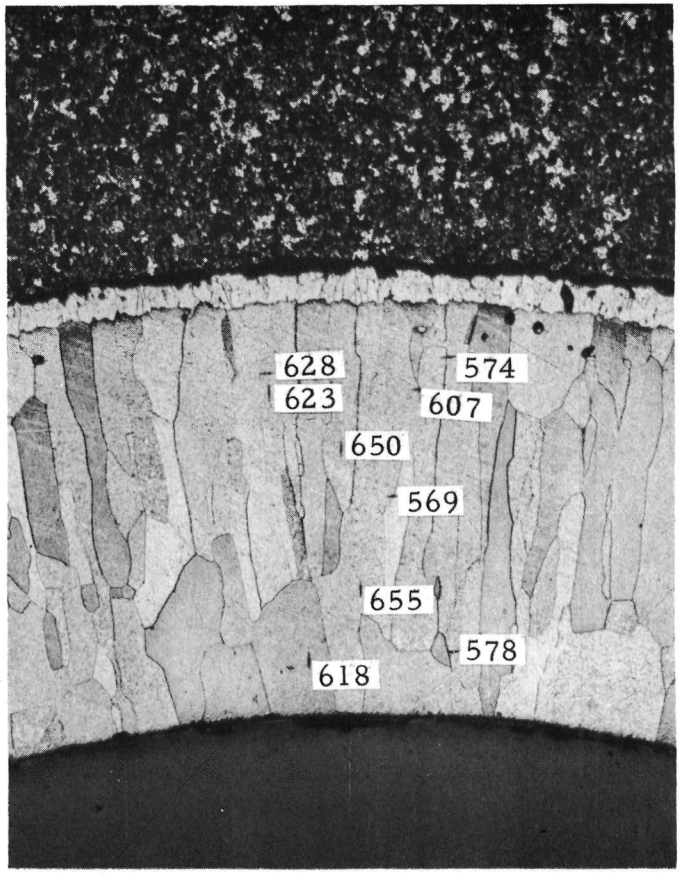

(d) Sample V-2D-5B

Fig. 39. Microstructures of tungsten thermocouple wells from various regions of V-2D fuel pin (100X) Numbers indicated are Knoop hardness numbers (Sheet 2 of 2)

(4) Fuel-tungsten interaction layer

The microstructures of the fuel-thermocouple well interaction layer in V-2D fuel pin have been shown in Fig. 39. The layer formed is compact and adheres to the tungsten thermocouple well. This is different from that formed in the V-2C fuel pin (see Fig. 25). The thickness of such interaction layers in V-2D fuel pin does not vary significantly with axial positions. For each axial location, the thickness varies between .013 to .051 mm (0.5 to 2 mils) with circumferential positions and is usually higher at locations about 180° from the bulge of the fuel pin. This is much less than the thickness of the fuel-thermocouple well interaction layer in V-2C fuel pin. The composition of the fuel-thermocouple well interaction layer will be discussed in a latter section of this report.

The fuel-cladding interaction layer, as determined from photomicrographs taken of the fuel-cladding interface at various locations on V-2D fuel pin, varies very little with axial and circumferential positions. The thickness range of .10 to .15 mm (4 to 6 mils) observed is much less than that observed for V-2C fuel pin. Figure 40 shows the typical microstructures of such fuel-cladding interaction layers. The composition of such interaction layers will be discussed in a latter section of this report.

(5) Fuel pin bottom

Sample No. 1 (see Fig. 14(a)), which is located at the bottom of V-2D fuel pin, was sectioned longitudinally along the cylindrical axis of the

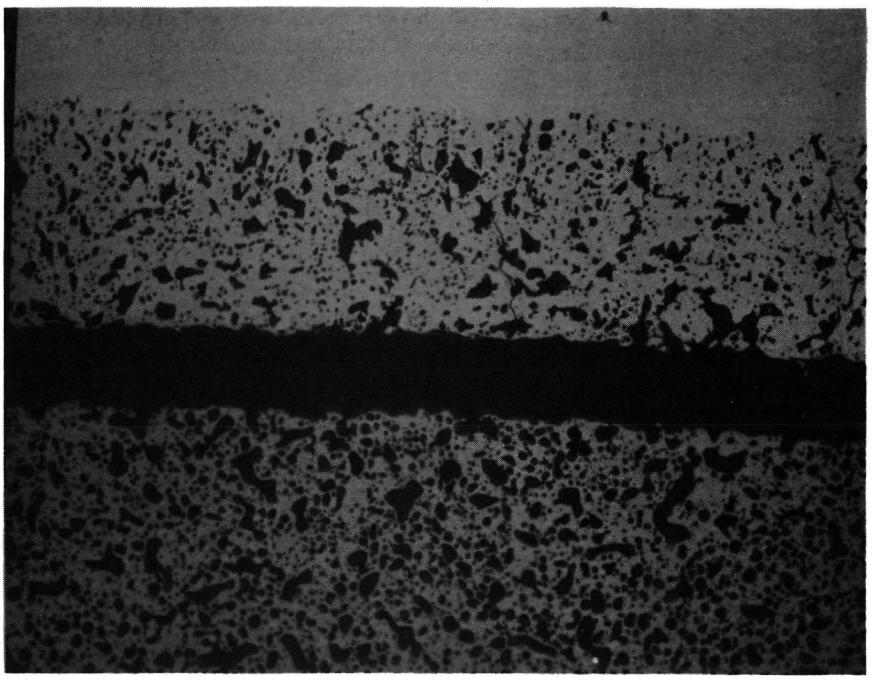

Fig. 40. Typical microstructures of the interaction layer between 50UC-50ZrC and tungsten cladding. Sample V-2D-2B 180° from bulge side of fuel pin (200X)

fuel pin into two halves. Figure 41 shows the appearance of the sectioned surface.

No deformation of the bottom of the tungsten fuel pin and the bottom of the tungsten thermocouple well can be detected. The tungsten pedestal for the fuel pellets was pushed downward at its central region by fuel swelling. Some extrusion of fuel material around the corner of the thermocouple well into the central fuel cavity has occurred. The annular fission gas venting groove located at the bottom of the fuel pellet, however, remained open and showed only slight change in shape.

Figures 42(a), (b), and (c) show the microstructures of the 50UC-50ZrC fuel materials near the cladding, near the thermocouple well, and near the fuel pedestal respectively. The estimated densities by using quantitative metallography techniques are 60%, 60%, and 65%. Figure 43 shows the etched fuel structures and the dispersion phases. These fuel structures are similar to that in other V-2D samples.

The cladding of Sample V-2D-1T has normal grain structures of fluoride tungsten. No grain boundary voids can be detected either at the bottom or at the corner of the cladding. (Figures 44(a) and (b)).

Figure 45 shows the appearance of the end of the tungsten thermocouple well of V-2D fuel pin. No excessive grain growth has occurred. A crack, however, has developed above the right corner.

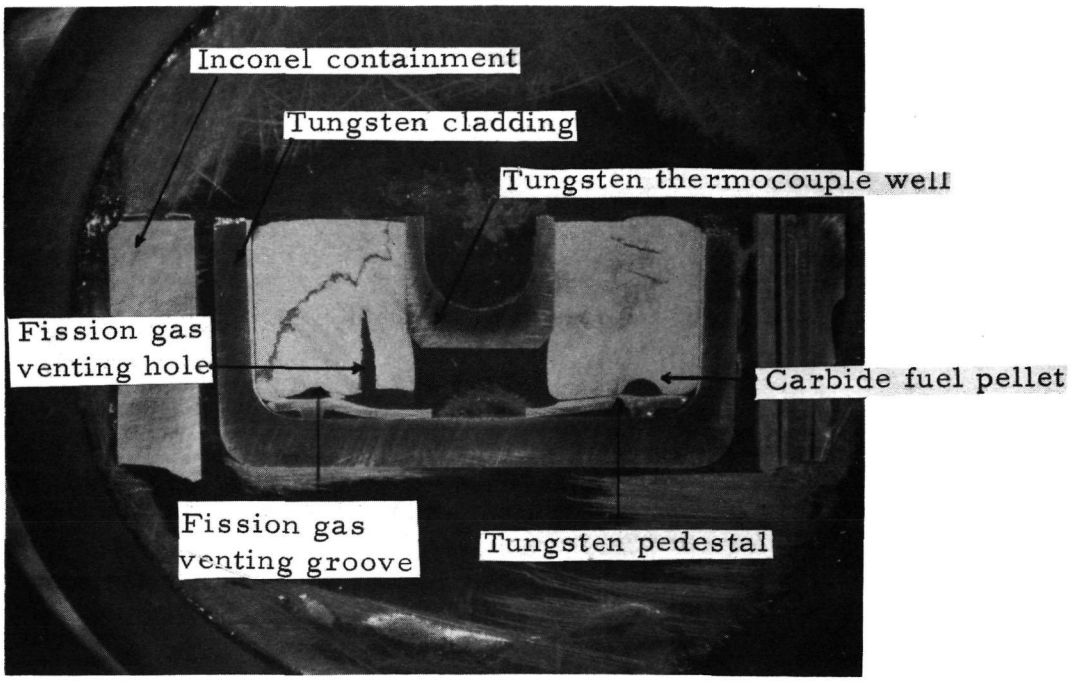

Fig. 41. Macroscopic appearance of the longitudinal cross section of Sample No. 1 of V-2D fuel pin. Designated as Sample V-2D-1T (4.3X)

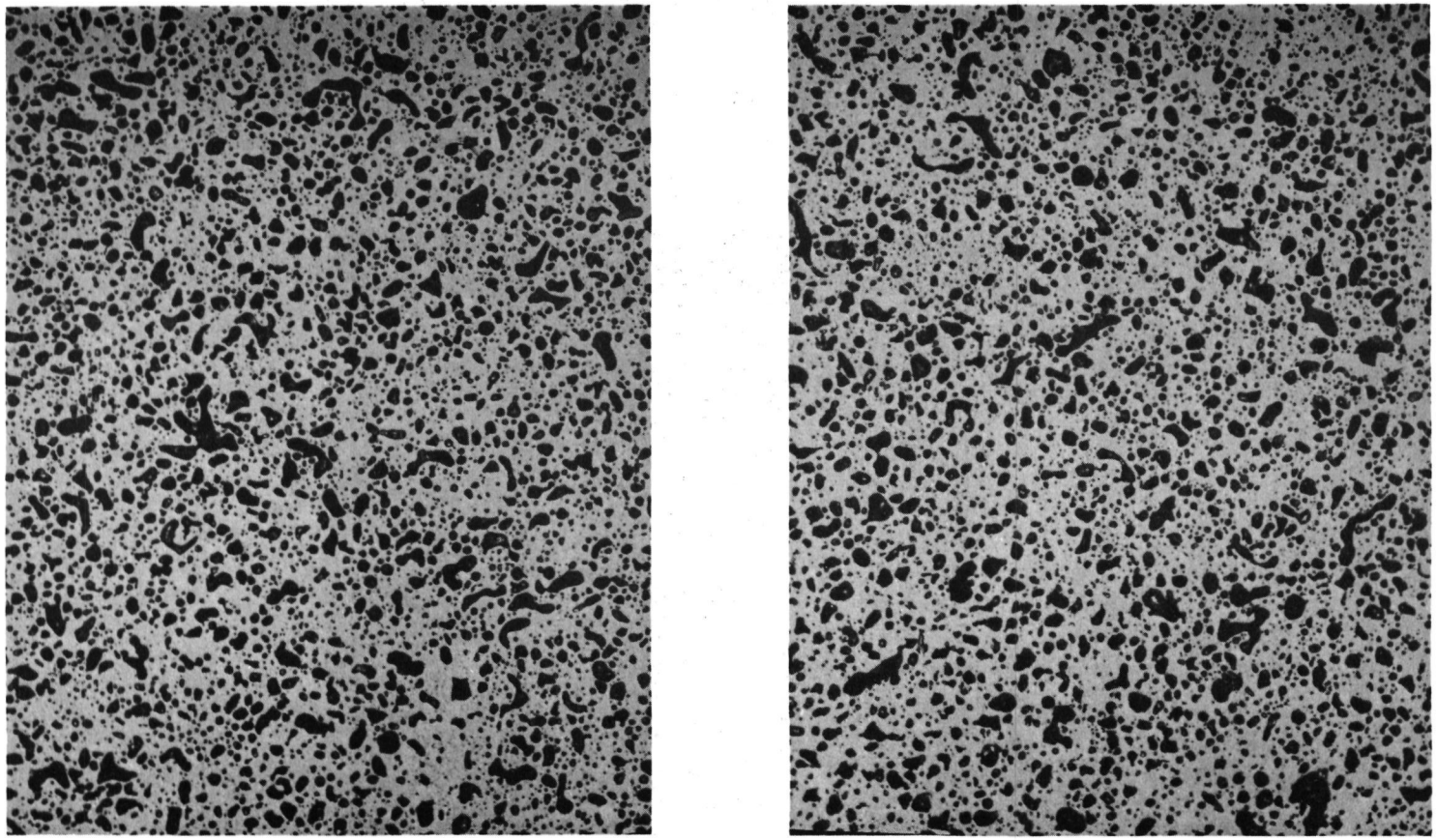

(a) Near cladding

(b) Near thermocouple well

Fig. 42. Microstructures of 50UC-50ZrC fuel material in Sample V-2D-1T (200X) (Sheet 1 of 2)

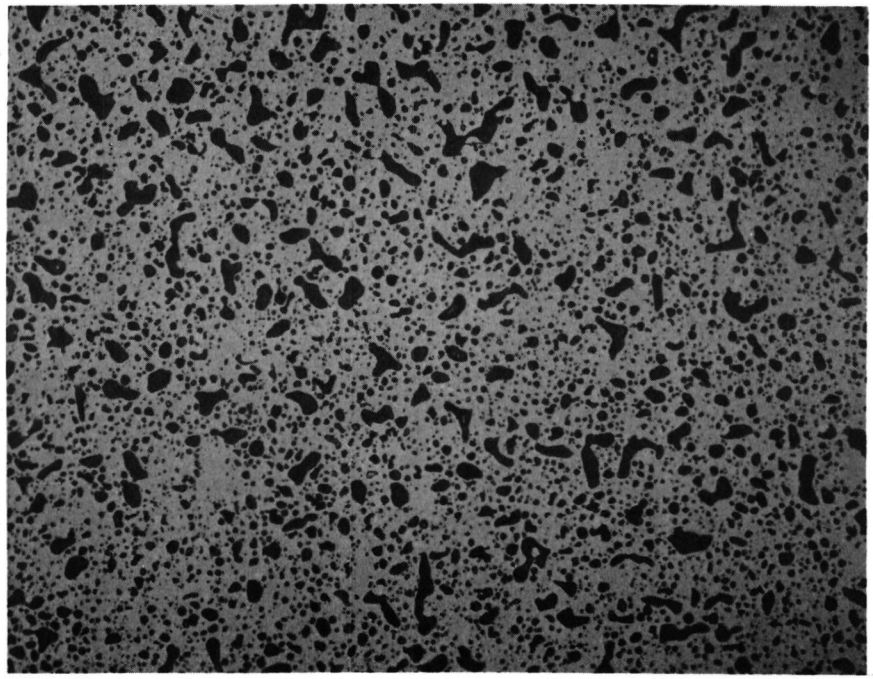

(c) Near fuel pedestal

Fig. 42. Microstructures of 50UC-50ZrC fuel material in Sample V-2D-1T (200X) (Sheet 2 of 2)

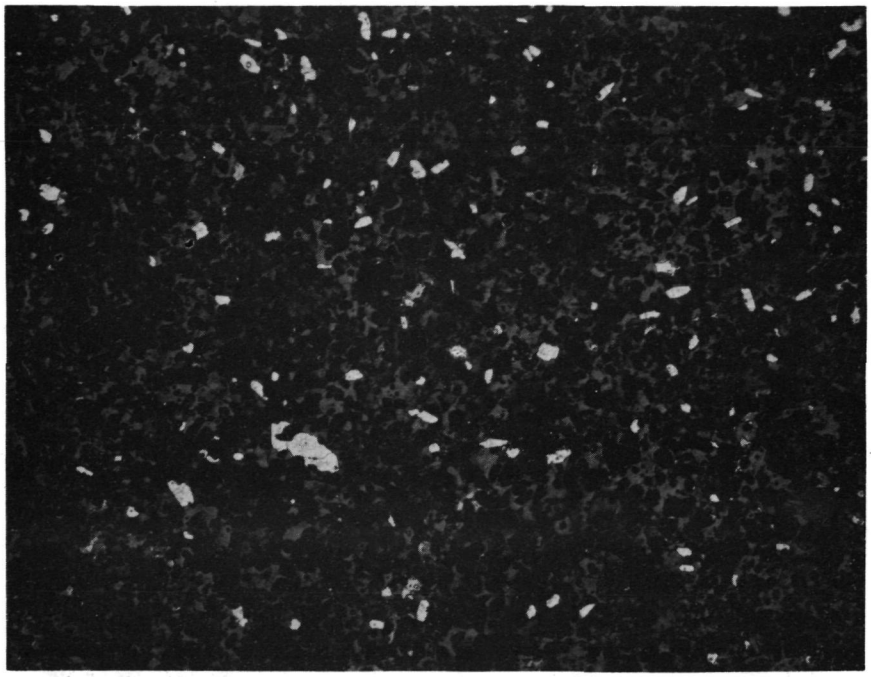

Fig. 43. Etched 50UC-50ZrC fuel structures in Sample V-2D-1T near the fuel pedestal (200X)

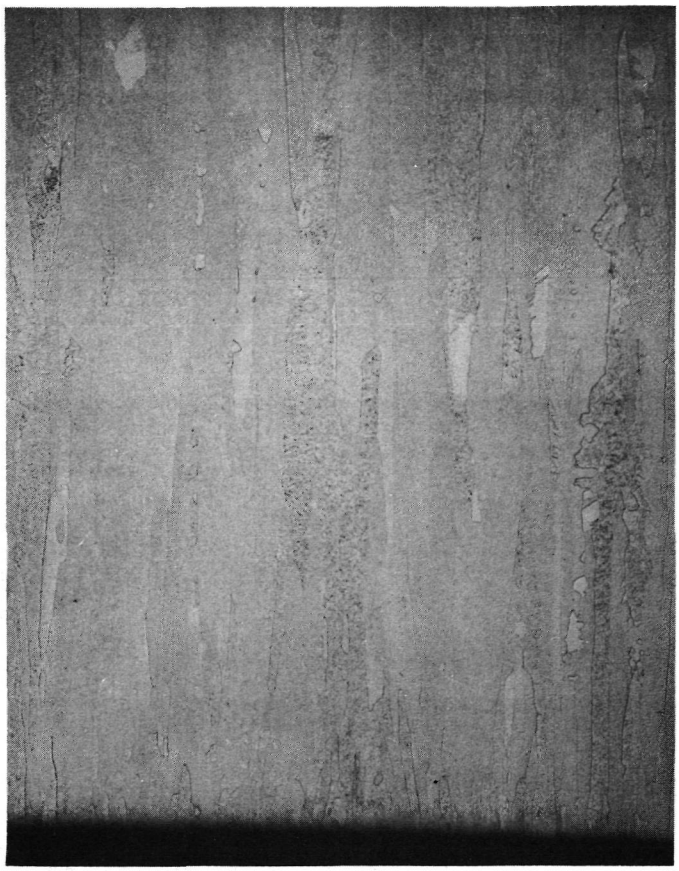

(a) Bottom

(b) Left corner

Fig. 44. Microstructures of the cladding in Sample V-2D-1T (75X)

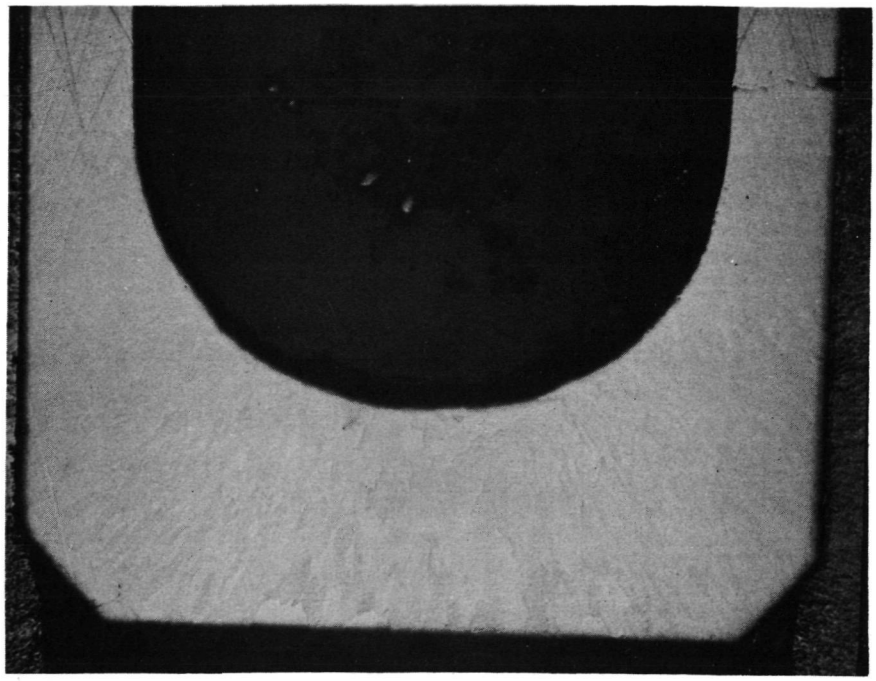

Fig. 45. Appearance of the end of the tungsten thermocouple well in V-2D fuel pin (25X)

Figures 46(a), (b), and (c) illustrate the microstructures of the fuel-tungsten interaction layers at the fuel-cladding, the fuel-thermocouple well, and the fuel-pedestal interfaces respectively. The thicknesses of these interaction layers, about .05 mm (2 mils) for the fuel-thermocouple well interface, and about .10 to .15 mm (4 to 6 mils) for the other two interfaces, fall into the range observed for other fuel tungsten interfaces in V-2D fuel pin.

7. ELECTRON MICROPROBE ANALYSIS OF COMPOSITIONS OF FUEL-TUNGSTEN INTERACTION LAYERS AND DISPERSION PHASES IN FUEL MATERIALS

Samples V-2C-1T and V-2D-1T were sent to the hot cell of Battelle Columbus Laboratories for the electron microprobe analysis of the compositions of the interaction layers at the fuel-cladding and the fuel-thermocouple well interfaces, and the compositions of the fuel matrix and the dispersion phases.

A Materials Analysis Corporation Model 450 Shielded Microprobe was used for the analysis. The desired quantitative analyses were conducted by performing point counts for uranium, tungsten, and zirconium in the areas of interest. The MAGIC computer program (Colby, J. W., Bell Telephone Laboratory, Allentown, Pennsylvania) was used to correct the raw point-counting data input for deadtime, background, absorption, and atomic number. Visual displays of relative composition differences for the elements of interest were obtained by rate meter X-ray imaging. Evidence of contaminant elements was sought by two-theta spectral scans of the suspect areas.

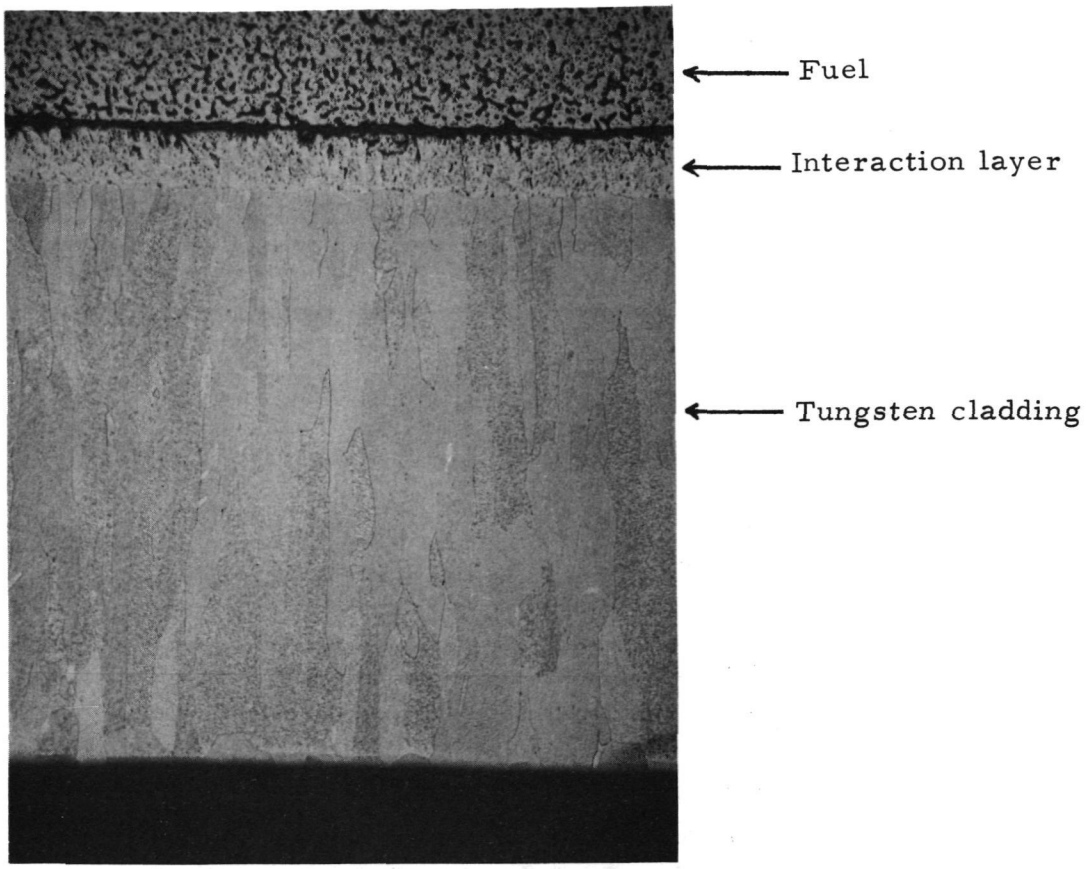

(a) Fuel-cladding interaction layer (75X)

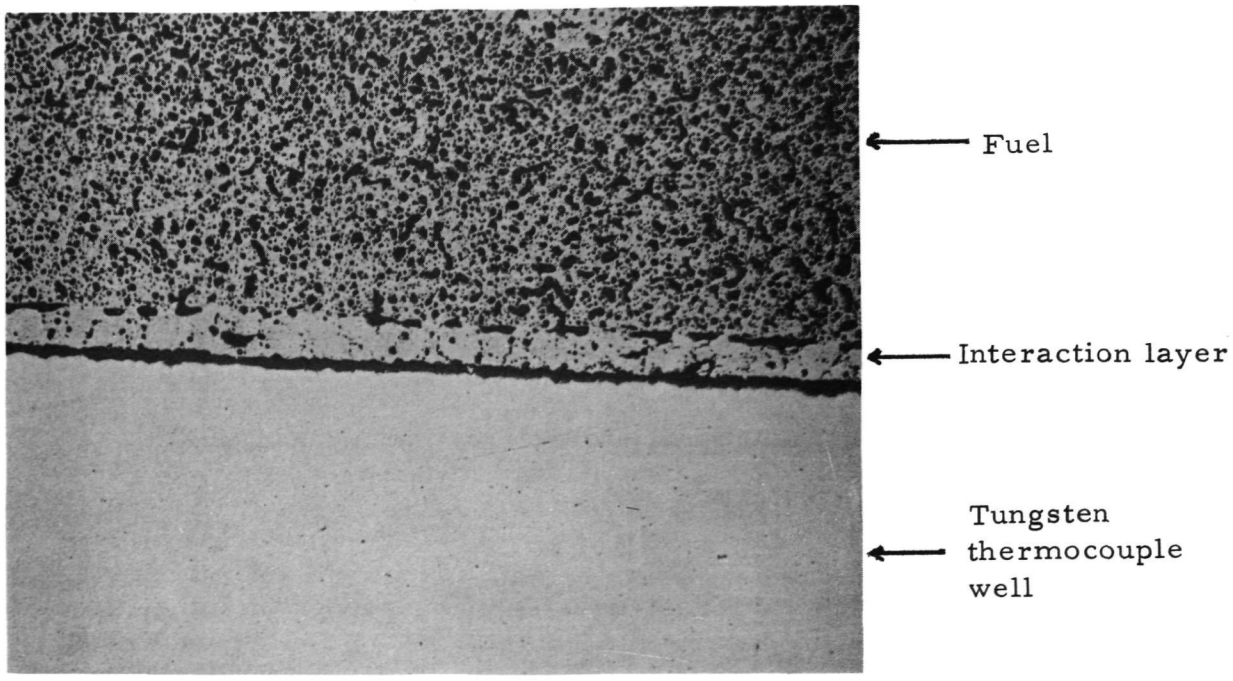

(b) Fuel-thermocouple well interaction layer (100X)

Fig. 46. Microstructures of fuel-tungsten interaction layers in Sample V-2D-1T (Sheet 1 of 2)

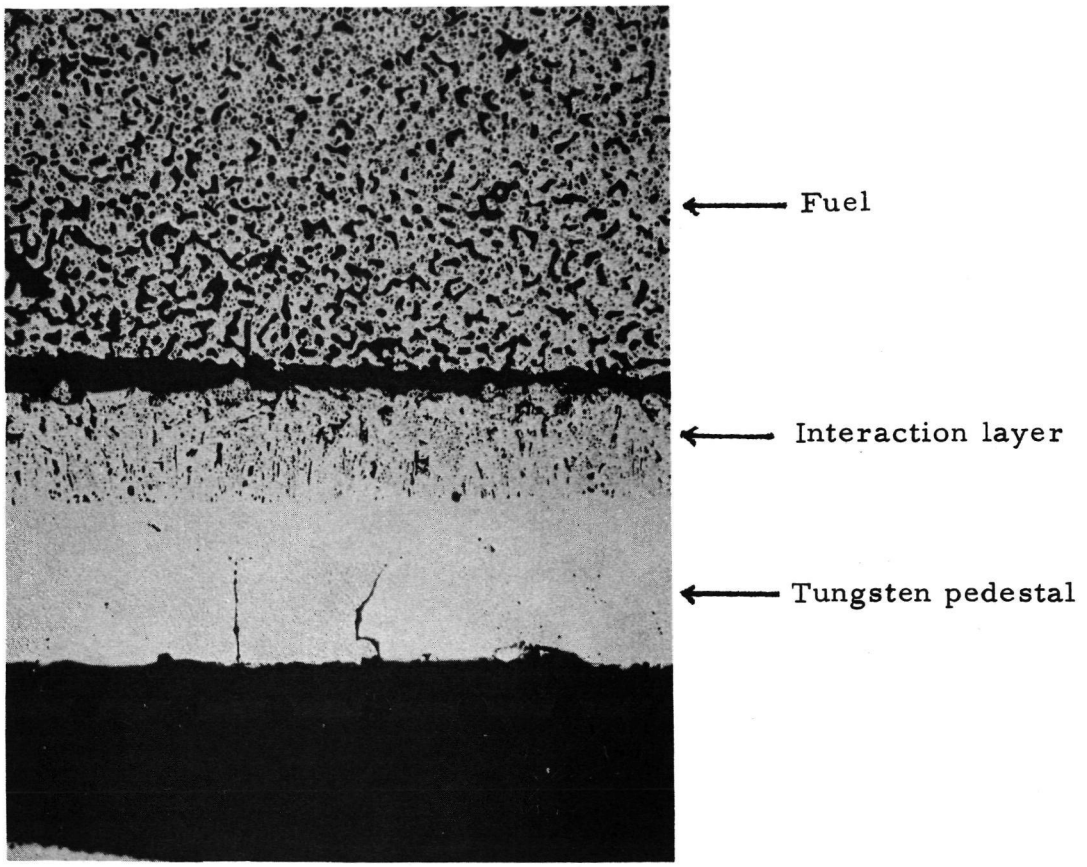

(c) Fuel-pedestal interaction layer (100X)

Fig. 46. Microstructures of fuel-tungsten interaction layers in Sample V-2D-1T (Sheet 2 of 2)

The interaction layers at the fuel-cladding interface and the fuel-thermocouple well interface of Sample V-2C-1T are similar in composition. They contain uranium and tungsten in ratio similar to that of UWC_2 but no zirconium. The fuel matrix is essentially of the normal composition of 90UC-10ZrC containing a few percent of dissolved tungsten. Some of the dispersions in the fuel body are the UWC_2 phase while others contain more than 90% of tungsten and a few percent uranium. The tungsten cladding in contact with the tungsten centering pin welded to the Inconel containment contain only tungsten and no Inconel constituents.

The interaction layer at the fuel-cladding interface of V-2D-1T is essentially identical to that at the fuel-thermocouple well interface. Both contain uranium and tungsten in ratio similar to that of UWC_2, and from a few tenths of a percent to one percent zirconium. The fuel matrix consists of 50UC-50ZrC containing 2 to 3% of dissolved tungsten. The dispersion phases contain various amounts of uranium (9.6 to 54.0%), zirconium (1.8 to 12.9%), and tungsten (29.8 to 79.7%). Since the dispersion particles in 50UC-50ZrC are small and the counting results may be affected by the contributions from the fuel matrix, the data are only of qualitative significance.

8. DETERMINATION OF RADIAL DISTRIBUTION OF FUEL BURNUP

The radial distribution of fuel burnup in Samples V-2C-2B, V-2C-3B, V-2C-4B, and V-2C-5B of the V-2C fuel pin, and Samples V-2D-2B, V-2D-3B,

V-2D-4B, and V-2D-5B were determined by transversal gamma-scan of selected fission product activity, autoradiography of fission product distribution, and isotopic burnup analysis.

8.1 Transversal Gamma-Scan

The distributions of the gamma-activity of Zr^{95} from the bulge side of the fuel pin to the opposite side were determined for each of the fuel samples described above. The slit system used for the transversal gamma-scan was the same as that used for the axial gamma-scan in Section 3. The polished surface of the sample was moved across the length of the slit from the bulge side of the sample(or from the side in line with the bulge side of the fuel pin if the sample showed no significant cladding expansion) toward the opposite side or vice versa. The activity of the selected characteristic gamma radiation from Zr^{95} was recorded by using a 51 x 51 mm (2 x 2 inch) NaI sensor and a single channel pulse-height analyzer.

The results obtained showed that for each of the samples scanned, the Zr^{95} activity was always higher on the bulge side of the fuel pellet than on the opposite side. Typical examples on Zr^{95} scan are given in Fig. 47. This implies that the average burnup in the fuel pellet is higher on the bulge side than on the opposite side.

8.2. Autoradiography

Kodak high resolution photographic plates, wrapped in black paper, were exposed to the polished surfaces of the above-described fuel samples

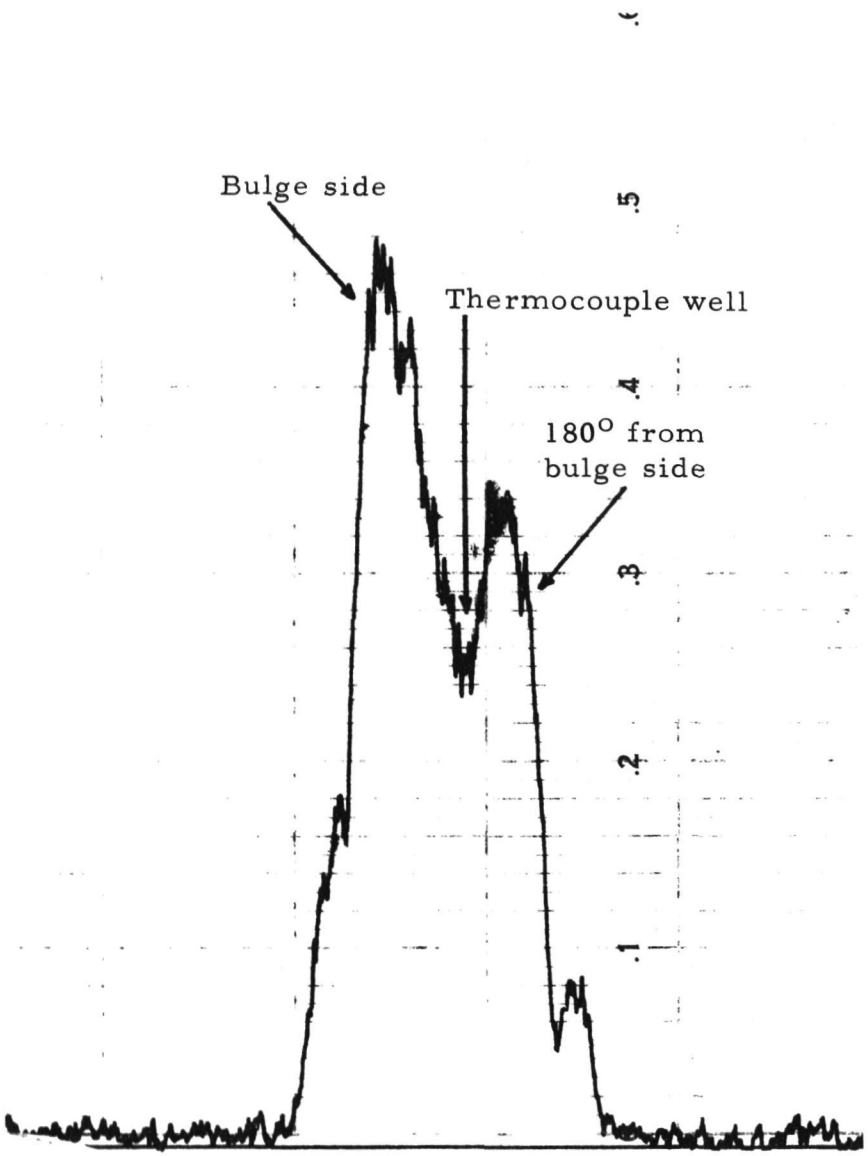

(a) Sample V-2C-3B

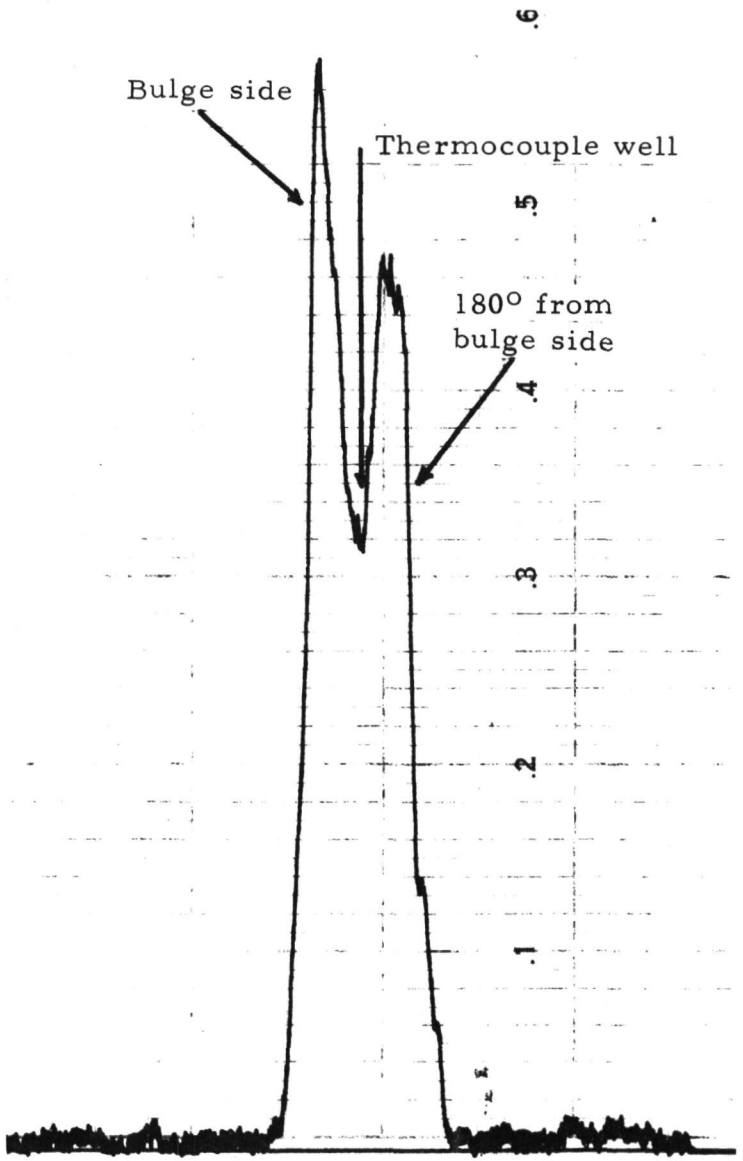

(b) Sample V-2D-3B

Fig. 47. Typical transversal gamma-scans of Zr^{95} activity in V-2C and V 2D fuel samples

from V-2C and V-2D fuel pins in hot cell for about 3 minutes. The image obtained reflects the distribution of the fission products, and thus the burnup, if the migration of the fission products was kept at a minimum during high temperature operation in the reactor.

Figure 48 illustrates the type of image obtained from these fuel samples. In addition to the image due to the fuel pellet, strong intensity was recorded from fission products migrated through the defects in the cladding and condensed on the surface of the Inconel containment. Readings taken from the various regions of these fuel pellet images with a photoelectric comparator yielded the intensity distribution maps in Fig. 49(a) (for V-2C samples) and Fig. 49(b) (for V-2D samples). Although the results are only of qualitative significance, it is clear that the burnups in these fuel samples are higher on the bulge side than on the side opposite to the bulge side.

8.3. Isotopic Burnup and Fission Product Analysis

For a quantitative comparison of the fuel burnup at the bulge side with that at the opposite side in V-2C and V-2D fuel pins, small pieces of samples were taken in pairs from each of the fuel sections studied above, one from the vicinity of the crack and bulge in the cladding and the other 180° from this location near the fuel-cladding interface. Each sample was dissolved in $HNO_3 + HClO_4$ and the solution was diluted to a specific volume from which an aliquot was taken for the burnup analysis. The uranium was separated from the aliquot by ion exchange. The solution leached from the ion exchange column was used for isotopic analysis at TRAPELO/WEST.*

*Formerly Tracer Laboratory

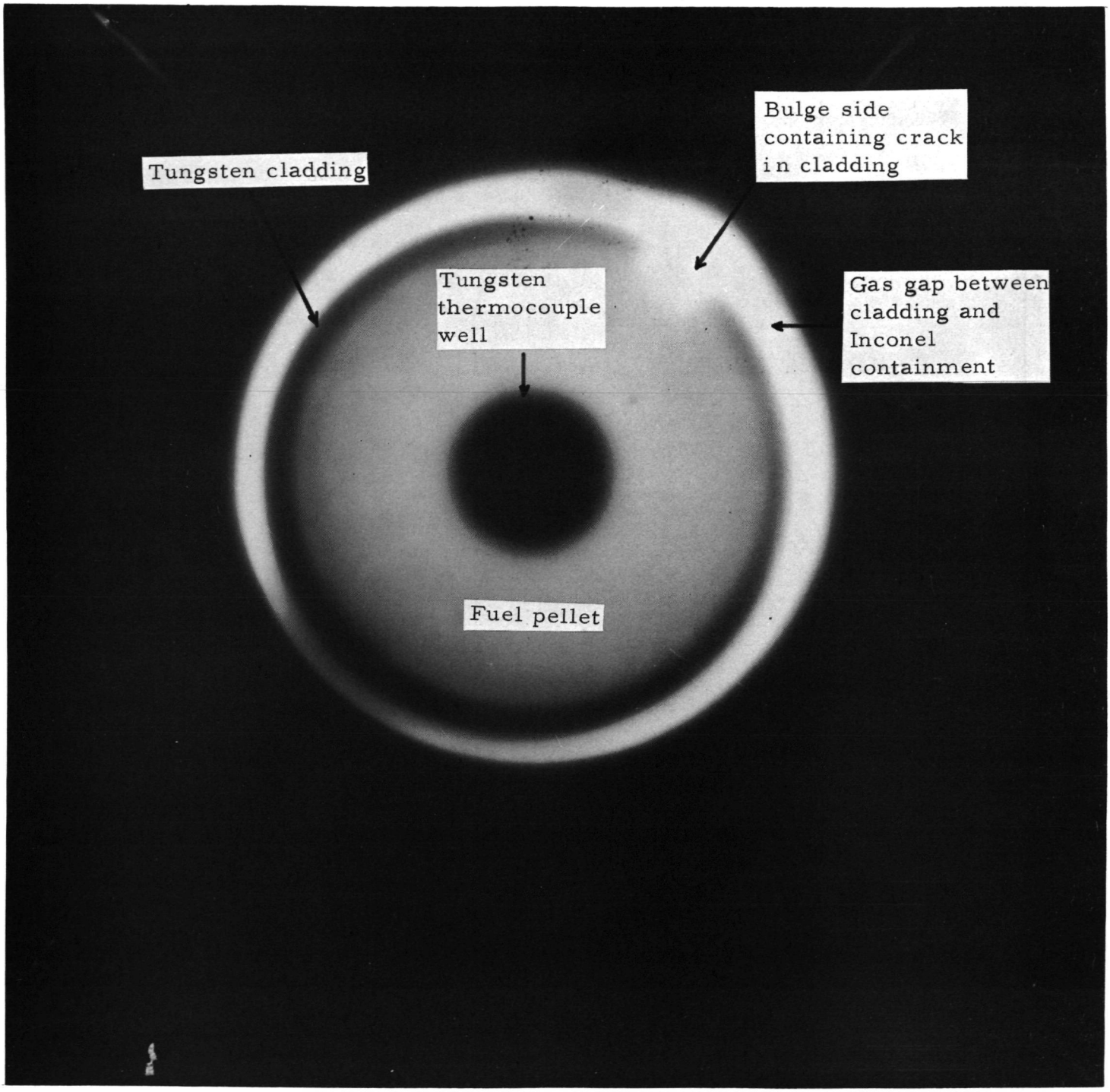

Fig. 48. Typical autoradiograph obtained from the polished surfaces of the fuel sections of V-2C and V-2D fuel pins. Sample V-2C-3B (5.6X)

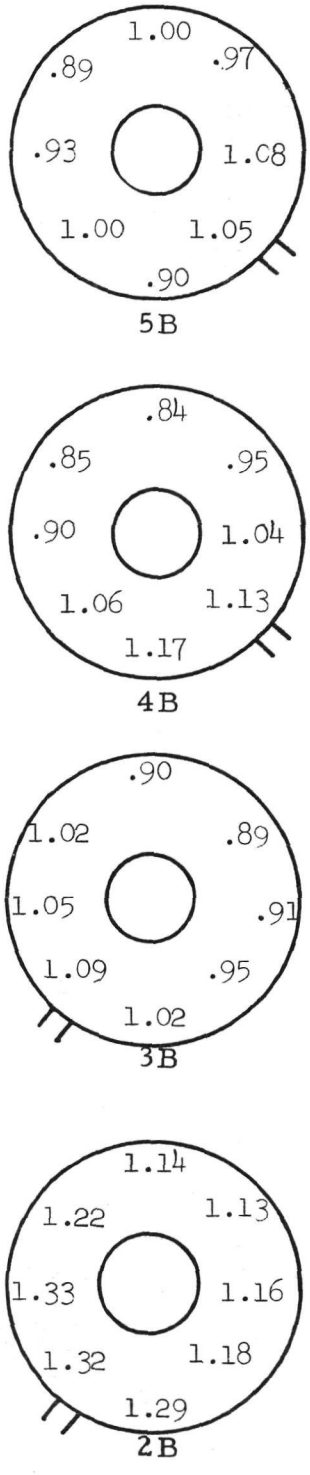

Fig. 49(a). Intensity distributions in autoradiographs taken of samples from V-2C fuel pin

// = Major crack in tungsten cladding

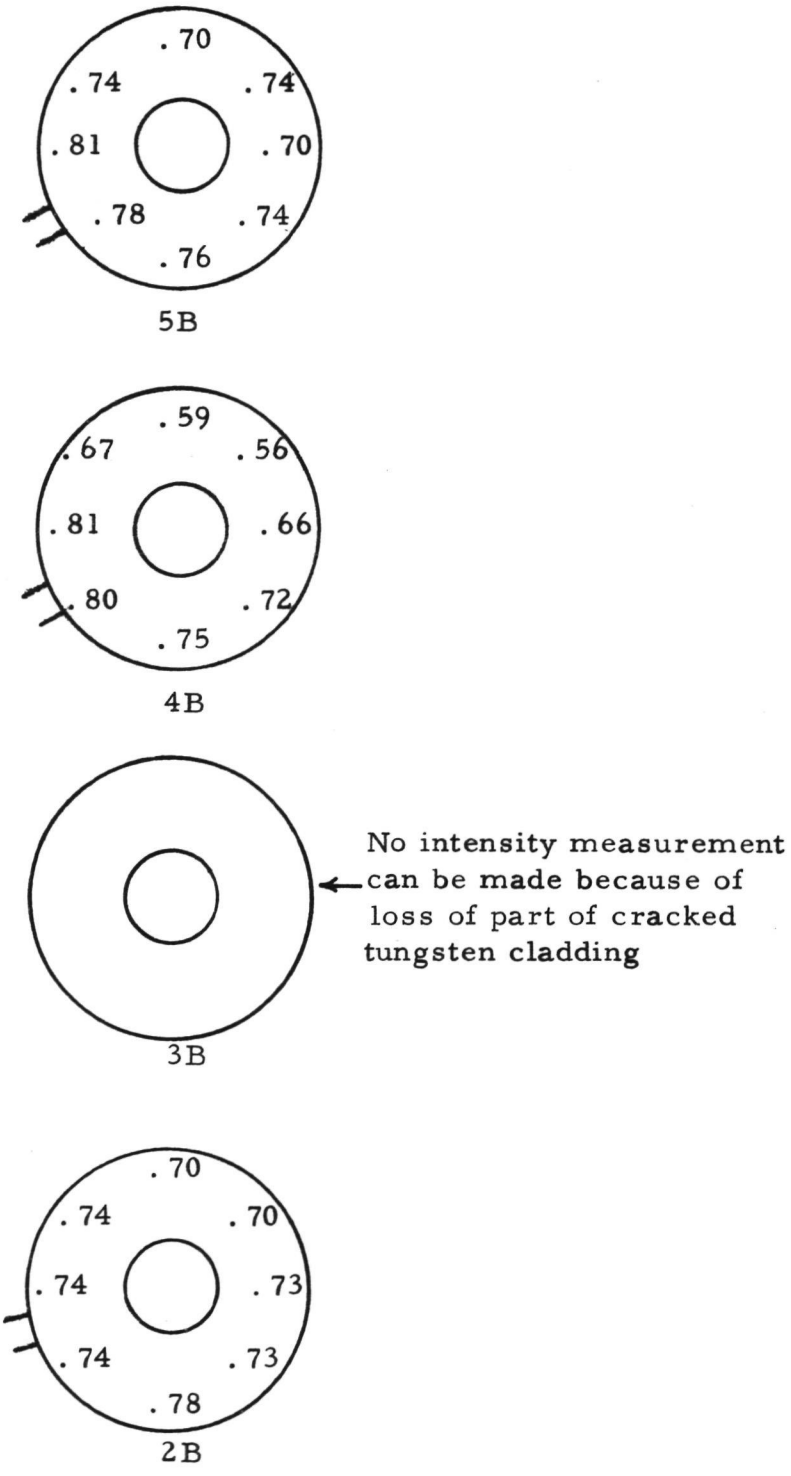

Fig. 49(b). Intensity distributions in autoradiographs taken of samples from V-2D fuel pin

// = Major crack in tungsten cladding

Unirradiated reference fuel materials from which the samples were prepared were also submitted at the same time. Burnup results were calculated from these isotopic data.

Two methods of computing the burnup were used. The first was based on the U^{236}/U^{235} ratios of the unirradiated and the irradiated samples. The second was based on the U^{235}/U^{238} ratios of the unirradiated and the irradiated samples. The calculated burnups are expressed as percentage of the total uranium atoms in the sample.

Calculation of the burnup from the U^{236}/U^{235} ratio is based on the following equation

$$B = N_5^{o} \left[\frac{R_{6/5} - R^{o}_{6/5}}{R_{6/5} + \alpha(1 + R_{6/5})}\right]$$

where

B = Burnup in atom % of total uranium

N_5^{o} = atom % of U^{235} before irradiation

$R_{6/5}$ and $R^{o}_{6/5}$ = atom ratios of U^{236} to U^{235} after and before irradiation respectively

α = U^{235} capture to fission ratio = .177 for reactor of thermalized spectrum

Calculation of the burnup from the U^{235}/U^{238} ratio is based on the following equation

$$B = N_8^{\circ} \left[(R^{\circ}_{5/8} - R_{5/8}) - (R_{6/8} - R^{\circ}_{6/8}) \right]$$

where

B = burnup in atom % of total uranium

N_8° = atom % of U^{238} before irradiation

$R^{\circ}_{5/8}$ and $R_{5/8}$ = atom ratios of U^{235} to U^{238} before and after irradiation respectively

$R_{6/8}$ and $R^{\circ}_{6/8}$ = atom ratios of U^{236} to U^{238} after and before irradiation respectively

Since the change in the ratio $R_{6/5}$ is always greater than the change in the corresponding ratio $R_{5/8}$, the method based on the change in U^{236} to U^{235} ratio is more sensitive and also independent of U^{238} contamination. However, the $R_{6/5}$ results depend upon the α factor which is subjected to uncertainties in cross sections or neutron energies.

The calculated results on V-2C and V-2D samples by these two methods are shown in Table 4 and Table 5. These results indicate the following:

(1) The bulge side of each sample studied has a higher burnup than the side 180° from it, indicating that the bulge was due to the higher burnup there.

(2) The burnup differentials vary from a factor of about 2 to a

TABLE 4

BURNUP RESULTS OF SAMPLES FROM V-2C CAPSULE

(in atom % of total uranium in sample)

Sample	U^{236}/U^{235} Method			U^{235}/U^{238} Method		
	Bulge Zone	180° From Bulge Zone	Ratio	Bulge Zone	180° From Bulge Zone	Ratio
2B	2.20	1.57	1.40	2.61	1.87	1.40
3B	1.93	1.36	1.42	1.84	1.26	1.46
4B	2.32	1.18	1.97	2.45	1.13	2.17
5B*	1.85	1.44	1.29	2.17	1.81	1.20

*Sample 5B shows no bulge. It was taken from the area in line with the bulge sides of Sample 3B and Sample 4B.

TABLE 5

BURNUP RESULTS OF SAMPLES FROM V-2D CAPSULE
(in atom % of total uranium in sample)

	U^{236}/U^{235} Method			U^{235}/U^{238} Method		
	Bulge Zone	180° From Bulge Zone	Ratio	Bulge Zone	180° From Bulge Zone	Ratio
2B	2.56	1.91	1.34	3.07	2.12	1.45
3B	2.25	1.75	1.29	2.47	1.81	1.37
4B	2.56	1.50	1.71	2.38	1.53	1.56
5B*	2.32	1.88	1.23	2.16	1.68	1.29

*Sample 5B shows no bulge. It was taken from the area in line with the bulge sides of Sample 3B and Sample 4B.

factor of about 1.3 for samples taken from V-2C fuel pin. Sample V-2C-5B shows the least burnup differential and also no bulge in cladding. The burnup differentials for samples taken from V-2D fuel pin vary from a factor of about 1.7 to a factor of about 1.2. Here again, Sample V-2D-5B shows the least burnup differential and also no bulge in cladding. The difference in the burnup differentials of these two capsules is probably due to the fact that they were located at different radial positions in the V-tube during irradiation.

(3) The average burnups for the samples shown in Table 4 are slightly higher than the 1.5% deduced from thermal data for V-2C fuel pin (see Table 1). Similarly, the average burnups for the samples shown in Table 5 are slightly higher than the 1.7% deduced from the thermal data for V-2D fuel pin. This is because the burnups shown in Table 4 and Table 5 represent the burnups near the fuel-cladding interface. The burnups in the central region of the carbide fuel pellet are expected to be lower because of self-shielding. The isotopic burnup data are therefore not inconsistent with respect to the average burnups deduced from calorimetric means.

In addition to isotopic burnup analysis, the solutions obtained by dissolving the fuel sample pieces in HNO_3 + $HClO_4$ were analyzed for their uranium, Ce^{144}, Cs^{137}, Zr^{95} and Sr^{90}* contents. The results were used in conjunction with the burnup results in Table 4 and Table 5 and the

*Only for samples V-2C-3B, V-2C-5B, V-2D-3B, and V-2D-5B

irradiation history of V-2C and V-2D capsules to calculate the fractional retention of these fission products in the fuel material next to the fuel-cladding interface. The results are shown in Table 6. It can be seen that the retention of Ce^{144} and Cs^{137} in 50UC-50ZrC is much lower than that in 90UC-10ZrC. The retention of Zr^{95} is much higher than Ce^{144} and Cs^{137} in all the samples studied. This is consistent with the fact that zirconium forms a stable carbide and therefore is less liable to loss by vaporization. For each fuel sample, the retention of Ce^{144}, Cs^{137} and Sr^{90} is in general lower at the bulge side of the sample where cracks are present in the tungsten cladding than at the side 180° from the bulge. Gamma-scan of the gas gap region between the tungsten cladding and the Inconel containment showed the presence of Ce^{144} and Cs^{137} in the condensate on the Inconel surface and the activities were the highest at the location facing the crack in the cladding and the lowest at the location 180° away from the crack. This is also borne out by the autoradiograph of Sample V-2C-3B shown in Figure 48.

TABLE 6

FRACTIONAL RETENTION OF SOME FISSION PRODUCTS IN V-2C AND V-2D FUEL SAMPLES

Sample	Isotope	V-2C (90UC-10ZrC)		V-2D (50UC-50ZrC)	
		Bulged Side	180° From Bulged Side	Bulged Side	180° From Bulged Side
2B	Ce-144	0.212	0.507	0.085	0.084
	Cs-137	0.115	0.564	0.055	0.094
	Zr-95	0.859	0.932	0.805	0.918
3B	Ce-144	0.200	0.604	0.065	0.075
	Cs-137	0.154	0.430	0.046	0.076
	Zr-95	0.850	0.898	0.817	0.939
	Sr-90	0.138	0.434	0.008	0.014
4B	Ce-144	0.339	0.705	0.056	0.107
	Cs 137	0.216	0.765	0.083	0.100
	Zr-95	0.892	0.910	0.855	0.929
5B	Ce-144	0.468	0.675	0.060	0.084
	Cs-137	0.354	0.591	0.052	0.061
	Zr-95	0.910	0.958	0.980	0.978
	Sr-90	0.142	0.253	0.012	0.021

9. SUMMARY OF RESULTS

Two tungsten clad UC-ZrC fueled capsules were examined in the Gulf hot lab facility following irradiation in the NASA Plum Brook Reactor. One capsule (V-2C) contained 90% UC-10% ZrC + 4 wt% W (designated as 90-10); the other (V-2D) contained 50% UC-50% ZrC + 4 wt% W (designated as 50-50). The fuel pin in each capsule had a 16 mm (0.625 inch) diameter and was clad with 1 mm (0.040 inch) thick fluoride tungsten. The 90-10 fuel pin was irradiated to a fuel burnup of 3×10^{20} fission/cm^3 (1.5 a/o)* in 11,089 hours at a maximum clad temperature of 1930°K. The 50-50 fuel pin was irradiated to a burnup of 2.1×10^{20} fission/cm^3 (1.7 a/o) in 12,030 hours at a maximum clad temperature of 1925°K. Irradiation was terminated for each capsule when excessive clad deformation was observed via neutron radiographs. The deformation was non-uniform, occurring as a bulge on one side of each fuel pin.

Clad deformation, interaction layer thickness, and burnup (all obtained by hot cell examination) together with fuel and clad temperature are summarized as a function of axial position in Figs. 50 and 51. Locations of the fuel samples examined in the hot cell are noted along with abscissa. Maximum clad diametral deformation of the 90-10 fuel pin was 0.63 mm (0.025 inch) on the bulge side and 0.25 mm (0.010 inch) 90° from the bulge (fuel temperature was 2035°K here). Corresponding deformations for the 50-50 fuel pin

---

*Determined by calorimetric means using capsule thermocouples. The volume (cm^3) is the annular space occupied by the fuel.

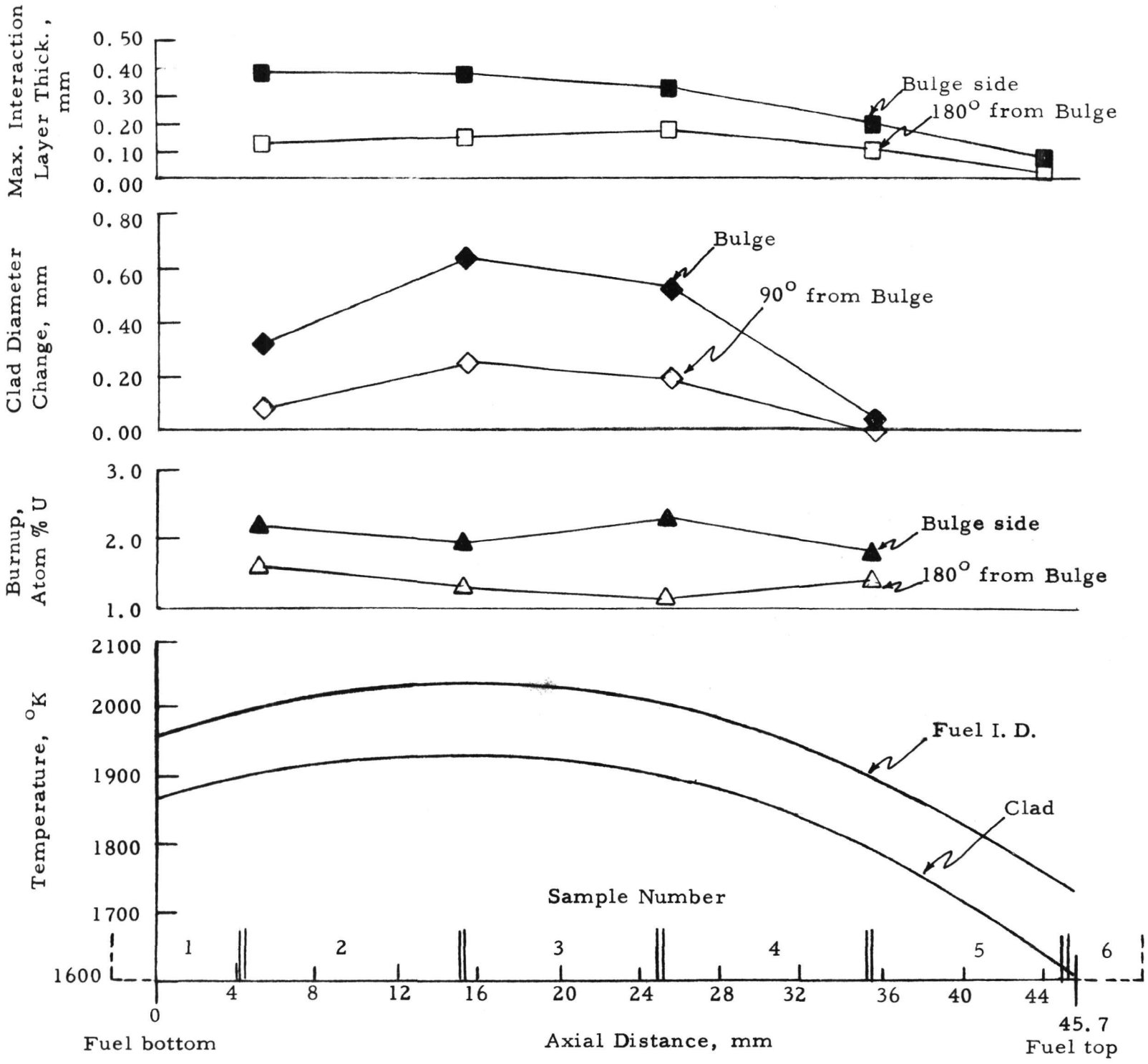

Fig. 50. Summary of V-2C (90-10) fuel pin hot cell examination data

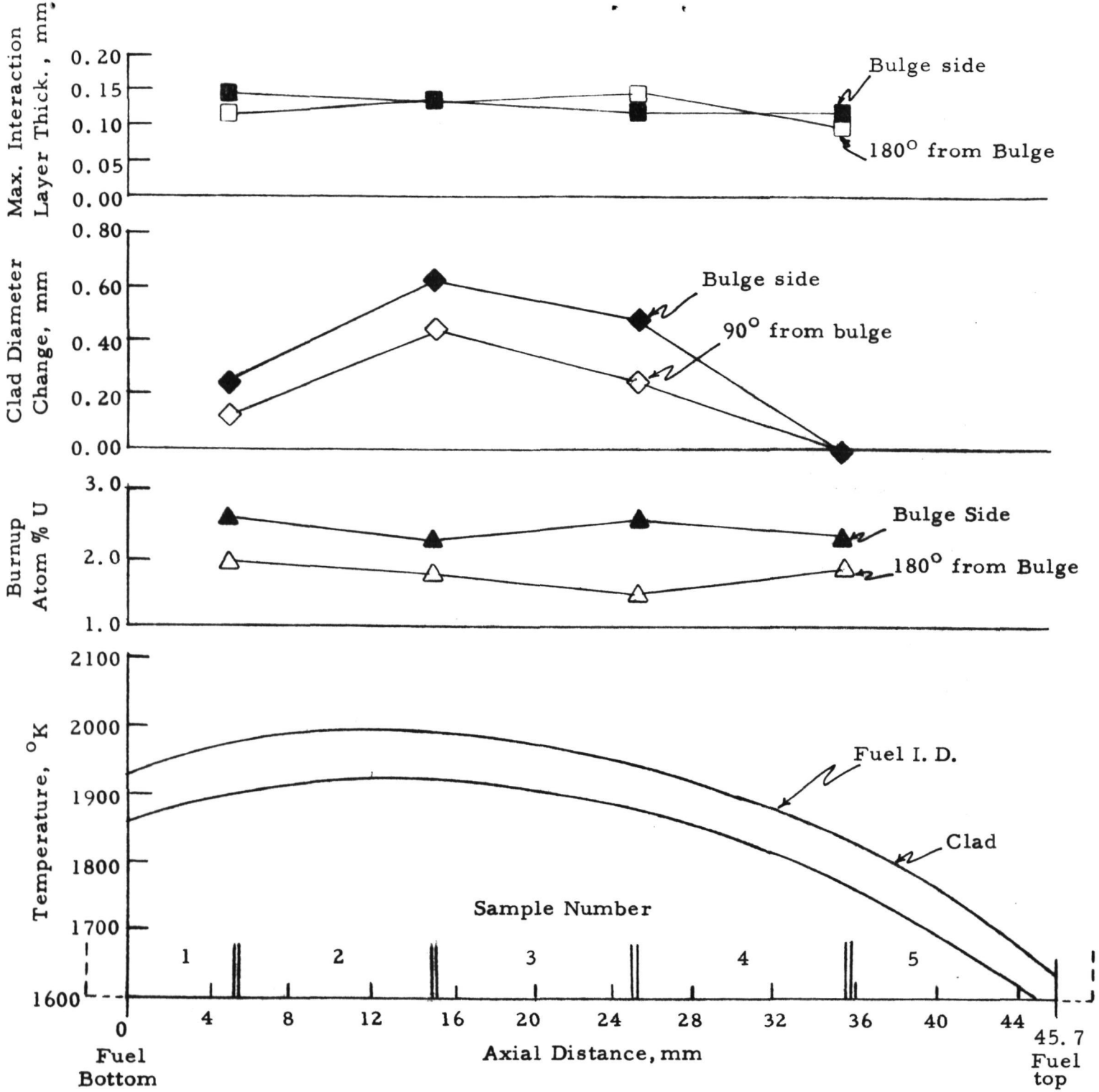

Fig. 51. Summary of V-2D (50-50) fuel pin hot cell examination data

were 0.63 mm (0.025 inch) and 0.43 mm (0.017 inch). In the vicinity of the bulge of each pin the burnup was up to 100% higher than 180° from the bulge; and the bulge was located toward the test reactor core during irradiation.

The fuel-clad interaction layer (composition similar to UWC_2) had a maximum thickness of 0.38 mm (0.15 inch) for the 90-10 fuel pin and 0.15 mm (0.006 inch) for the 50-50 pin. The layer thickness was temperature dependent for the 90-10 specimen, reducing to about 0.15 mm (0.006 inch) at a fuel temperature of 1825°K, but was essentially constant for the 50-50 specimen.

At fuel temperatures below about 1850°K there was essentially no clad deformation. The maximum clad deformation and interaction layer thickness both occurred in the region of maximum fuel temperature and towards the bulge (core) side of the fuel pins.

Fission gas release was found to be 66% for the 90-10 fuel and 85% for the 50-50 fuel. Due to fuel swelling, the fission gas venting holes, which were machined in the fuel, deformed by different amounts. The holes in the 90-10 fuel underwent substantially more deformation than those in the 50-50 fuel at similar temperatures.

10. CONCLUDING REMARKS

In applying the information generated in V-2C and V-2D fuel pin irradiation to the prediction of the irradiation behavior of a fueled prototypical emitter in a thermionic reactor core, one has to bear in mind the difference in the configuration and the operating conditions of these

fuel-cladding systems. Table 7 compares the configuration and the operating conditions of V-2C fuel pin with that for the fueled emitter in a 120 eKw thermionic reactor core for electrical propulsion application. The V-2C fuel pin contains the same fuel material (90UC-10ZrC + 4 wt% W) as that in the prototypical emitter and has attained in 11,089 hours the burnup equivalent to that for 40,000 hour operation of the reactor. However, from the point of view of cladding dimensional stability, the V-2C fuel pin design is more conservative than the fueled prototypical emitter with respect to specific cladding thickness (i. e., cladding thickness per unit diameter) for restraining fuel swelling, and the specific surface area (i. e., geometric surface area per unit fuel volume) for releasing fission gas. On the other hand, the high fission power density (about a factor of four higher than that in the fueled prototypical emitter) and the lack of a central void for accommodating fuel swelling, tend to offset these advantages. A more detailed analysis is needed to determine the net effect of such variations in configuration and operating conditions on emitter dimensional stability.

It was observed that there was no significant change in the size of the fission gas venting holes and the dimension of the cladding in Samples V-2C-5B and V-2D-5B, both of which were operated at fuel I. D. temperatures of 1885 and 1820^{o}K respectively. This implies that the amount of swelling of the fuel material was small under these conditions. Since no significant cladding deformation is expected when the fuel swelling is small, irrespective of the diameter of the emitter, it should therefore be possible to keep the cladding

TABLE 7

COMPARISON OF FUEL-CLADDING CONFIGURATION AND OPERATING PARAMETERS OF V-2C FUEL PIN WITH THAT FOR THE PROTOTYPICAL EMITTERS IN A 120 eKw THERMIONIC REACTOR

	V-2C Fuel Pin	Prototypical Emitter
Cladding diameter	0.625 inch	1.100 inch
Cladding thickness	40 mils	40 mils
Fuel length	1.8 inch	2.0 inch
Geometric area per unit fuel volume	5.70 to 6.91 cm^2/c.c.	~ 1 cm^2/c.c.
Central fission gas venting void in fuel body	No	Yes
Fission gas venting holes and grooves in fuel body	Yes	No
Operating temperature	1761-1973°K	1805-1880°K beginning of life
Fission power density	260 W/c.c.	51-71 W/c.c. beginning of life
Burnup	3.0×10^{20} fission/c.c.	$6\text{-}8 \times 10^{19}$ fission/c.c. in 10,000 hours

expansion of a prototypical emitter to a minimum if the fuel body has a specific surface area of at least 6.91 cm^2/cc. and the maximum fuel temperature is kept below 1850°K. The lowering of the fission power density from 260 W/cc to 60-80 W/cc and the incorporation of a central void in the fuel body to accommodate some fuel swelling should further improve the situation. Irradiation of prototypical emitters should be planned to evaluate these possibilities. To minimize nonuniform radial distribution of fission power density due to self shielding, it is highly desirable to use fuel of low enrichment or to irradiate the capsule in a fast neutron environment.

If the 90UC-10ZrC fueled prototypical emitter is to operate at a maximum fuel temperature of 1873°K, the cladding temperature is estimated to be no more than 1750°K. It is therefore necessary to improve the thermionic performance at low emitter temperatures (circa 1750°K) to meet the design requirement for the thermionic fuel element. The use of high work function emitters for better thermionic performance, equiaxial tungsten barrier for minimizing fuel transport effects on electrode work functions, and rhenium coated niobium collector for absorbing the deposited fuel components and thus maintaining a clean collector surface, are currently under investigation. The operation of fueled emitter at lower temperature should help to minimize fuel-cladding interaction. The results obtained on V-2C fuel pin showed that the loss of tungsten cladding thickness at a fuel temperature of 1860°K amounted to about 0.10 mm (0.004 inch) in 11,089 hours for a 90UC-10ZrC fuel of C/U = 1.04.

While the irradiation of V-2C and V-2D fuel pins was carried out with the fuel in an inert gas (argon) of about a few hundred torr pressure, the fuel in a prototypical emitter in a thermionic fuel element operates in a low pressure (~ 20 torr) inert gas environment. Difficulty in the transfer of heat from the fuel to the cladding causes the temperature of the fuel body to rise to such an extent that appreciable fuel sintering and vaporization occur. The loss of open porosity due to sintering is detrimental to the dimensional stability of the emitter. The differential vaporization of fuel components may change the composition of the fuel material in contact with the cladding and thus the emitter work function. Irradiation of prototypical emitters is being planned in both capsule and thermionic fuel element to study the effect of gas pressure over the fuel body on the dimensional stability and electrical performance of the emitter in the temperature range of thermionic interest.

REFEREMCES

(1) "Studies of Thermionic Materials for Space Power Applications," (U) Summary Report for the Period November 23, 1965 through September 30, 1968, page 68, NASA CR-72517, GA-8974. (C/RD)

(2) Smith, J. R. and G. L. Snyder, "Irradiation of Uranium-Carbide Fuel Forms," NASA TM X52696, Proceedings of the Thermionic Conversion Specialists Conference, page 66, Monterey, California, October 23-24-, 1969.

(3) Smith, J. R., "Irradiation of Uranium/Zirconium Carbide Fuel to 11,000 Hours," NASA TM X52913, Proceedings of the Thermionic Conversion Specialists Conference, page 83, Miami, Florida, October 30, 1970.

APPENDIX A

FUEL AND CLAD TEMPERATURES

Use was made by NASA of a two-dimensional computer program for determining all fuel and clad temperatures presented in this report. This program, designated as STHTP,* is capable of handling two or three-dimensional geometries involving internal heat generation, constant or temperature-dependent thermal conductivity, constant contact and film coefficients and heat transfer between solids by radiation.

The as-built capsule geometry was laid out using 416 material nodes in a two-dimensional cylindrical (r, z) configuration. Gamma heat generation input was fixed since there were thermocouples included in the capsule to measure gamma heating. The fuel heat generation (fission and gamma) was then adjusted until the node temperatures at all capsule thermocouple locations agreed with the actual data within $\pm 10^{\circ}C$.

---

*Mollerus, F. S., Jr.: Steady State Heat Transfer Program (STHTP). Rep. HW-73668, Hanford Lab., General Electric Co., May 12, 1962

DISTRIBUTION LIST

1. National Aeronautics and Space Administration
400 Maryland, S. W.
Washington, D. C. 20546
Attention: James J. Lynch, Code NS-1 (1)
Carl Johnson, Code NS-1 (1)

2. National Aeronautics and Space Administration
Lewis Research Center
21000 Brookpark Road
Cleveland, Ohio 44135
Attention: Report Control, MS 5-5 (1)
Technology Utilization Office, MS 3-19 (1)
Library, MS 60-3 (1)
G. M. Ault, MS 3-13 (1)
Neal Saunders, MS 105-1 (1)
John W. R. Creagh, MS 49-2 (1)
Leonard W. Schopen, MS 500-206 (1)
Roland Breitwieser, MS 302-1 (1)
James Ward, MS 302-1 (1)
Armin F. Lietzke, MS 49-3 (1)
Vince Hlavin, MS 3-10 (1)
S. J. Kaufman, MS 49-2 (1)
P. L. Donoughe, MS 49-3 (2)
J. R. Smith, MS 49-3 (4)

3. National Aeronautics and Space Administration
Manned Spacecraft Center
Attention: Technical Information Program Division
Houston, Texas 77058
For: B. J. Bragg (1)
W. Eugene Rice (1)

4. National Aeronautics and Space Administration
Marshall Space Flight Center
Huntsville, Alabama 35812
Attention: Library
For: Robert Aden (1)

5. National Aeronautics and Space Administration
Scientific and Technical Information Facility
P. O. Box 33
College Park, Maryland 20740
Attention: NASA Representative (10 copies with DRA)

6. National Aeronautics and Space Administration
Ames Research Center
Moffett Field, California 94035
Attention: Library (1)

7. National Aeronautics and Space Administration
Goddard Space Flight Center
Greenbelt, Maryland 20771
Attention: Library (1)
Joseph Epstein (1)

8. National Aeronautics and Space Administration
Langley Research Center
Langley Field, Virginia 23365
Attention: Library (1)

9. Aerojet General Nucleonics
San Ramon, California 94583
Attention: Library (1)

10. Aerospace Corporation
P. O. Box 95085
Los Angeles, California 90045
Attention: Library (1)

11. Air Force Cambridge Research Laboratories
L. G. Hanscom Field
Bedford, Massachusetts 01731
Attention: CRZAP (1)

12. Air Force Weapons Laboratory
Kirtland Air Force Base
New Mexico 87117
Attention: Library (1)

13. Babcock and Wilcox Company
1201 Kemper Street
Lynchburg, Virginia 24501
Attention: Library (1)

14. Battelle Memorial Institute
505 King Avenue
Columbus, Ohio 43201
Attention: Don Kizer (1)
Don Keller (1)

15. The Boeing Company
P. O. Box 3707
Seattle, Washington 98101
Attention: Library (1)

16. Electro-Optical Systems, Inc.
300 North Halstead Street
Pasadena, California 91107
Attention: A. Jensen (1)

17. Fairchild-Hiller
Republic Aviation Division
Farmingdale, L. I., New York 11735
Attention: Alfred Schock (1)

18. General Electric Company
Research Laboratory
Schenectady, New York 12300
Attention: Volney C. Wilson (1)

19. General Electric Company
Missile and Space Division
P. O. Box 8555
Philadelphia, Pennsylvania 19101
Attention: ANSE (1)

20. General Electric Company
Knolls Atomic Power Laboratory
Schenectady, New York 12300
Attention: R. Ehrlich (1)

21. Institute for Defense Analysis
400 Army Navy Drive
Arlington, Virginia 48092
Attention: R. C. Hamilton (1)

22. McDonnell Douglas Corporation
Missile and Space Engineering
Nuclear Research (A2-260)
3000 Ocean Park Boulevard
Santa Monica, California 90405
Attention: Library (1)

23. Jet Propulsion Laboratory
California Institute of Technology
4800 Oak Grove Drive
Pasadena, California 91103
Attention: Peter Rouklove (1)
J. Mondt (1)
V. Truscello (1)

24. Lockheed Missile and Space Division
Lockheed Aircraft Corporation
Sunnyvale, California 94086
Attention: H. H. Greenfield (1)

25. Los Alamos Scientific Laboratory
P. O. Box 1663
Los Alamos, New Mexico 87544
Attention: W. A. Ranken (1)

26. Naval Ship Systems Command
Department of the Navy
Washington, D. C. 20360
Attention: E. P. Lewis, Code 08 (1)

27. North American Rockwell Corporation
Atomics International Division
P. O. Box 309
Canoga Park, California 91305
Attention: Robert C. Allen (1)
Charles E. Smith (1)

28. North American Rockwell Corporation
S&ID Division
12214 Lakewood Boulevard
Downey, California 90241
Attention: C. L. Gould (1)

29. Oak Ridge National Laboratory
Oak Ridge, Tennessee 37831
Attention: Library
For: A. C. Schaffhauser (1)

30. Office of Naval Research
Power Branch
Department of the Navy
Washington, D. C. 20325
Attention: Cmdr. Ollie J. Loper (1)

31. Radiation Effects Information Center
Battelle Memorial Institute
505 King Avenue
Columbus, Ohio 43201
Attention: R. E. Bowman (1)

32. Radio Corporation of America
David Sarnoff Research Center
Princeton, New Jersey 08640
Attention: Paul Rappaport (1)

33. The Rand Corporation
1700 Main Street
Santa Monica, California 90401
Attention: Ben Pinkel (1)

34. Space Systems Division (SSTRE)
AF Unit Post Office
Los Angeles, California 90045
Attention: Major W. Iller (1)

35. Thermo Electron Corporation
85 First Avenue
Waltham, Massachusetts 02154
Attention: George Hatsopoulous (1)
Robert Howard (1)

36. TRW Inc.
TRW Systems Group
One Space Park
Redondo Beach, California 90278
Attention: Library (1)

37. U. S. Army Erdl
Fort Monmouth, New Jersey 07703
Attention: Emil Kittl (1)

38. U. S. Atomic Energy Commission
Space Nuclear Systems Division, F309
Reactor Power Systems Branch
Washington, D. C. 20545
Attention: D. S. Beard (1)

39. U. S. Atomic Energy Commission
Technical Reports Library
Washington, D. C. 20545
Attention: J. M. O'Leary (3)

40. U. S. Atomic Energy Commission
Division of Technical Information Extension
P. O. Box 62
Oak Ridge, Tennessee 37831 (3)

41. Varian Associates
611 Hansen Way
Palo Alto, California 94304
Attention: Ira Weismann (1)

42. Westinghouse Electric Corporation
Astronuclear Laboratory
Attention: Document Custodian
P. O. Box 10864
Pittsburgh, Pennsylvania 15236
For: Carrol Sinclair (1)